CONTRACT REPORT ARBRL-CR-00503

TWO-DIMENSIONAL, TWO-PHASE MODELING OF MULTI-INCREMENT BAGGED ARTILLERY CHARGES

Prepared by

Paul Gough Associates, Inc.
P.O. Box 1614
Portsmouth, NH 03801

February 1983

US ARMY ARMAMENT RESEARCH AND DEVELOPMENT COMMAND
BALLISTIC RESEARCH LABORATORY
ABERDEEN PROVING GROUND, MARYLAND

Destroy this report when it is no longer needed.
Do not return it to the originator.

Secondary distribution of this report is prohibited.

Additional copies of this report may be obtained from the National Technical Information Service, U. S. Department of Commerce, Springfield, Virginia 22161.

The findings in this report are not to be construed as an official Department of the Army position, unless so designated by other authorized documents.

The use of trade names or manufacturers' names in this report does not constitute indorsement of any commercial product.

REPORT DOCUMENTATION PAGE

READ INSTRUCTIONS BEFORE COMPLETING FORM

1. REPORT NUMBER: CONTRACT REPORT ARBRL-CR-00503
2. GOVT ACCESSION NO.:
3. RECIPIENT'S CATALOG NUMBER:

4. TITLE (and Subtitle): TWO-DIMENSIONAL, TWO-PHASE MODELING OF MULTI-INCREMENT BAGGED ARTILLERY CHARGES

5. TYPE OF REPORT & PERIOD COVERED: Task III Final Report November 1981 - May 1982

6. PERFORMING ORG. REPORT NUMBER: PGA-TR-82-5

7. AUTHOR(s): Paul S. Gough

8. CONTRACT OR GRANT NUMBER(s): DAAK11-81-C-0004

9. PERFORMING ORGANIZATION NAME AND ADDRESS:
Paul Gough Associates, Inc.
P.O. Box 1614
Portsmouth, NH 03801

10. PROGRAM ELEMENT, PROJECT, TASK AREA & WORK UNIT NUMBERS: 1L161102AH43

11. CONTROLLING OFFICE NAME AND ADDRESS:
US Army Armament Research & Development Command
US Army Ballistic Research Laboratory (DRDAR-BL)
Aberdeen Proving Ground, MD 21005

12. REPORT DATE: February 1983

13. NUMBER OF PAGES: 205

14. MONITORING AGENCY NAME & ADDRESS (if different from Controlling Office):

15. SECURITY CLASS. (of this report): UNCLASSIFIED

15a. DECLASSIFICATION/DOWNGRADING SCHEDULE:

16. DISTRIBUTION STATEMENT (of this Report)

Approved for public release; distribution unlimited.

17. DISTRIBUTION STATEMENT (of the abstract entered in Block 20, if different from Report)

18. SUPPLEMENTARY NOTES

19. KEY WORDS (Continue on reverse side if necessary and identify by block number)

Interior Ballistics
Two-Phase Flow
Flamespread
Computer Code
TDNOVA
Solid Propellant Gun

20. ABSTRACT (Continue on reverse side if necessary and identify by block number) mb

This report describes an extension to TDNOVA, a code whose purpose is the digital simulation of convective flamespreading through bagged artillery charges. TDNOVA is based on the numerical solution of the axisymmetric, two-dimensional equations which govern the macroscopic aspects of the flow of a two-phase, heterogeneous mixture. Of principal interest are the interplay among the venting characteristics of the ignition system, the properties of the bag and the distribution of ullage during the period (cont'd on back)

of flamespreading, and the consequences of the path of flamespreading in respect to the structure of the longitudinal pressure field throughout the entire interior ballistic cycle.

Previously, TDNOVA was restricted to simulations of a single-increment charge. Here an extension of the code is described to permit simulations of multi-increment bagged charges subject to the assumptions that the increments are assembled end-to-end and are of comparable, but not necessarily identical, diameters. Each increment is assumed to be contained in a separate bag. Within the macroscopic formulation all the substrates of each bag, including basepad igniters, centercore tubes, salt bags, foil liners and talc additives, are viewed as attributes of the boundary of the enclosed main charge increment. The properties of the bag may be specified as time-dependent surface distributions of mass flux, exothermic or endothermic, of mechanical strength and of gas-phase permeability. Mathematically, these properties are embedded in the finite jump conditions which describe the balance of mass, momentum and energy at a macroscopic discontinuity in two-phase flow. Each increment may also contain a centercore igniter charge which is modeled as a quasi-one-dimensional, two-phase flow.

Each main charge increment is always modeled as a two-dimensional, two-phase flow at least until flamespreading and bag rupture are complete for all increments and the radial pressure gradients have vanished to within some user-selectable tolerance. Subsequently, the user may elect to complete the solution by means of a quasi-two-dimensional representation in which only the axial structure of each region is modeled on a continuum basis but which preserves the separate identity of the coaxial flows defined by the centercore igniter, the main charge and the external annular ullage between the mixture and the tube wall.

The ullage is always modeled as an inviscid, compressible single-phase flow. The ullage is divided into several subregions predicated on the configuration of the propelling charge. Each such region may be lumped parameter, quasi-one-dimensional, or fully two-dimensional in accordance with its dimensions and certain user-selectable length criteria.

The governing equations are solved by means of an explicit two-step marching scheme at all interior mesh points. Characteristic forms are used at both the external boundaries and the internal boundaries between computational regions. A time-dependent, equipotential algorithm is used to define the mesh in all two-dimensional regions.

The extended method is illustrated by reference to a complete solution for a hypothetical 155-mm propelling charge which consists of two identical increments, each having a basepad, a centercore igniter and a lead foil liner.

Table of Contents

Table of Contents (continued)

List of Illustrations

List of Illustrations (continued)

1.0 INTRODUCTION

We have previously reported details of the development of TDNOVA, a code whose principal purpose is the digital simulation of the interior ballistics of bagged artillery charges.[1,2] TDNOVA is based on a numerical solution of the balance equations which describe the macroscopic aspects of unsteady, two-dimensional, two-phase reacting flow. In Reference 1 we established an overall approach to the model and demonstrated the capability to perform two-dimensional simulations of convective flamespreading in an irregularly shaped container. In Reference 2 we described the development of the code to a point which permitted a simulation of the complete interior ballistic cycle of a typical single bag artillery charge, taking into account the two-dimensional details of the gun chamber and projectile base, the distribution of ullage around the bag and the influence of the bag itself.

In the present report we describe the extension of the code to treat multi-increment charges, each increment being separately bagged, and taking into account, on a time-dependent basis, the possibility of ullage between increments. As in the previous version of the code,[2] a fully two-dimensional treatment of the propelling charge is maintained until flamespreading is complete and all bags are fully ruptured. Subsequently, when the radial pressure distribution has equilibrated to within a user-selectable tolerance, the solution is continued to the point of muzzle exit by means of a quasi-two-dimensional analysis.

This introduction contains two subsections. In section 1.1 we provide the reader with a brief summary of background material for the purpose of orientation. Section 1.2 contains a brief outline of the technical approach to our objectives and summarizes the capabilities and limitations of TDNOVA in its present form.

A complete discussion of the governing equations is given in chapter 2.0. The method of solution is described in chapter 3.0. Chapter 4.0 presents a computational example. The code itself is documented in an appendix which describes the structure of the code and linkages of the subroutines. The appendix also contains a glossary of the principal FORTRAN variable names and a complete discussion of the input files.

---

[1] *Gough, P. S.*
"Two-Dimensional Convective Flamespreading in Packed Beds of Granular Propellant"
Ballistic Research Laboratory Report ARBRL-CR-00404 *July 1979* *(ADA 075326).*

[2] *Gough, P. S.*
"A Two-Dimensional Model of the Interior Ballistics of Bagged Artillery Charges"
Ballistic Research Laboratory Report ARBRL-CR-00452 *April 1981* *(ADA 100751).*

1.1 Background Information

A full discussion of background information is given in Reference 1 which will also direct the interested reader to the theoretical and experimental work which has motivated the development of TDNOVA.

The ballistic problem of interest may be described as follows. We seek to determine, by digital simulation, the manner in which flamespreading through bagged artillery charges is influenced by such elements of the design as the venting characteristics of the ignition system, the initial distribution of free-chamber volume (ullage) around the packages of propellant which constitute the charge and the impediment to gas flow due to the nature of the material in which the propellant is packaged.

Assuming for the moment that the dominant physical process in respect to the ignition of the charge is one of convective heat transfer, we seek answers to the following questions. If the ignition stimulus is localized, what are the consequences of local pressure buildup prior to the ignition of the rest of the propellant? To what extent are the nonuniformities of pressure during flamespreading alleviated by the presence of ullage around the charge? If the flow channel created by ullage around the bag is important in respect to relaxing the nonuniform character of the pressure field, how strong should the propellant container be in order to preserve the ullage during flamespreading? How does the permeability to the gas-phase of the container material impede convective heating of the propellant? If the propelling charge is to be ignited by a multistage ignition train consisting of a basepad and a centercore tube containing an ignition charge, how does the flamespread through the centercore igniter charge compete with that through the main charge? How strong should the centercore tube be? If the ends of the containers are impermeable and the ignition is localized, will the containers be blown apart from one another? If so, what magnitude of velocity is to be expected and is there a possibility of grain fracture due to impacts of the containers against the projectile? If there is axially distributed ullage--at the ends of the charge or between increments--how does it influence the path of flamespreading, the development of nonuniformity of pressure, and the velocity acquired by the grains during the process of flamespreading?

If large nonuniformities of pressure arise during flamespreading, what will be the overall effect on the entire ballistic cycle of the gun? If longitudinal pressure oscillations are induced by the

particular choice of ignition system, container material and ullage distribution, will the superposition of this transient on the ideal pressurization history result in a higher value of maximum pressure? Are the oscillations, if they occur, damped or do they grow in time? Given an unacceptable configuration--unacceptable in the sense that there is a possibility of damage to the tube by overpressure or to the projectile due to the mechanical coupling of the ignition transient to sensitive components--can it be made acceptable by means of minor changes to the igniter properties or the container material or the distribution of ullage?

A one-dimensional, two-phase simulation has been shown to provide answers to such questions for the related but simpler problem of Navy case gun ammunition[3, 4] in which neither the container material nor radially distributed ullage need be considered. For bagged artillery ammunition, however, a multidimensional simulation is required due to the importance of the radial ullage and the influence of the bag material[5, 6] which constitutes the container.

1.2 Summary of Approach

We first define our approach in rather general terms. We then elaborate to a certain extent by discussing, in several subsections, the physical content of the model and details of the method of solution, the differences from the previous version, and the major limitations to the scope of applicability of the present version.

A general definition of our approach is as follows. We view the fluid mechanical problem as one which involves multidimensional,

---

[3] *Horst, A. W., Smith, T. C. and Mitchell, S. E. "Key Design Parameters in Controlling Gun-Environment Pressure-Wave Phenomena--Theory versus Experiment" Proc. 13th JANNAF Combustion Meeting.* 1976

[4] *Horst, A. W. and Gough, P. S. "Influence of Propellant Packaging on Performance of Navy Case Gun Ammunition" J. Ballistics, v. 1, n. 3.* 1977

[5] *Gough, P. S. "Theoretical Study of Two-Phase Flow Associated with Granular Bag Charges" Final Report, Contract DAAK11-77-C-0028.* 1978

[6] *Horst, A. W. and Gough, P. S. "Modeling Ignition and Flamespread Phenomena in Bagged Artillery Charges" Ballistic Research Laboratory Technical Report ARBRL-TR-02263 (ADA 091790).* 1980

unsteady flow of a heterogeneous mixture consisting of the granular aggregate and its products of combustion. The analysis of such a flow taking into account details whose length scale is comparable to the scale of heterogeneity is not practical. A tractable theory can be established only at a macroscopic level in which the state variables are averages, in some sense, of the microproperties of the flow.

By formal averaging of the equations which describe the micro-flow,[7,8,9] one may establish the mathematical structure of the governing equations for the macroscopic properties of heterogeneous two-phase flow. The equations so derived are assumed to apply to all regions occupied by the propellant, both in the main charge increments and in the centercore igniter as we discuss subsequently. A feature of the macroscopic approach is the introduction of a state variable which has no microscopic counterpart, namely the porosity, which, if a volume average is considered, may be defined as the fraction of a unit macroscopic volume which is occupied by the gas phase. Corresponding definitions may be made if the average is purely time-wise as in the approach of Ishii[10] and also if an ensemble average is considered as was done by Saffman.[11]

---

[7] *Gough, P. S.*
"The Flow of a Compressible Gas Through an Aggregate of Mobile, Reacting Particles"
Ph.D. Thesis, McGill University. *1974*

[8] *Gough, P. S. and Zwarts, F. J.*
"Modeling Heterogeneous Two-Phase Reacting Flow"
AIAA J. v. 17, n. 1, pp. 17-25. *1979*

[9] *Gough, P. S.*
"On the Closure and Character of the Balance Equations for Heterogeneous Two-Phase Flow"
Dynamics and Modelling of Reactive Systems, Academic Press. *1980*

[10] *Ishii, M.*
"Thermo-Fluid Dynamic Theory of Two-Phase Flow"
Eyrolles, Paris. *1975*

[11] *Saffman, P. G.*
"On the Boundary Condition at the Surface of a Porous Medium"
Stud. Appl. Math. vol. L, no. 2, p. 93. *June 1971*

Within the mixture regions defined by the main charge increments, the porosity has an initial value which is typically of the order of 0.4. In the regions of ullage, of course, the porosity is equal to 1.0. The transition from the value 0.4, in the mixture, to the value 1.0, in the ullage, occurs over a length scale comparable to the scale of heterogeneity of the mixture. Within the macroscopic formulation, therefore, the boundaries of the mixture regions are associated with a discontinuity of porosity. Moreover, the effects of the bag--the impediment it induces in respect to the flow of the gas-phase, its reactivity due to embedded exothermic and endothermic components--are perceived as localized to such an extent as to validate their representation within the finite balances of mass, momentum and energy which connect the macroscopic states on either side of the mixture boundary.

Computationally, our approach may be summarized as one in which the equations of macroscopic two-phase flow are solved on a multiply-connected time-dependent domain defined by the instantaneous configuration of the propelling charge increments. These equations are solved, simultaneously with the balance equations for the single-phase flow in the ullage, subject to the external boundary conditions defined by the fixed tube and the moving projectile, viewed as rigid, impermeable surfaces, and subject to macroscopic jump conditions which relate the state variables on each side of the internal boundaries defined by the surfaces of the propelling charge increments. Motion of the bags independently of the surface of each of the propelling charge increments is not considered. The bags are viewed as attributes of the surfaces of each of the mixture regions defined by the main charge increments.

Although the flow is actually three-dimensional, we suppose that an adequate description of the influence of the ullage may be obtained by treating the problem as though it were two-dimensional and axi-symmetric.

1.2.1 Physical Basis of Model and Method of Solution

In Figure 1.1 we illustrate schematically a propelling charge of the type which the current version of TDNOVA is intended to simulate. We show a charge consisting of three increments. Each increment is contained in a bag and consists of a main charge of granular propellant which may or may not be packed around a center-core tube in which is placed a small secondary charge whose purpose is to promote smoothness of flamespreading.

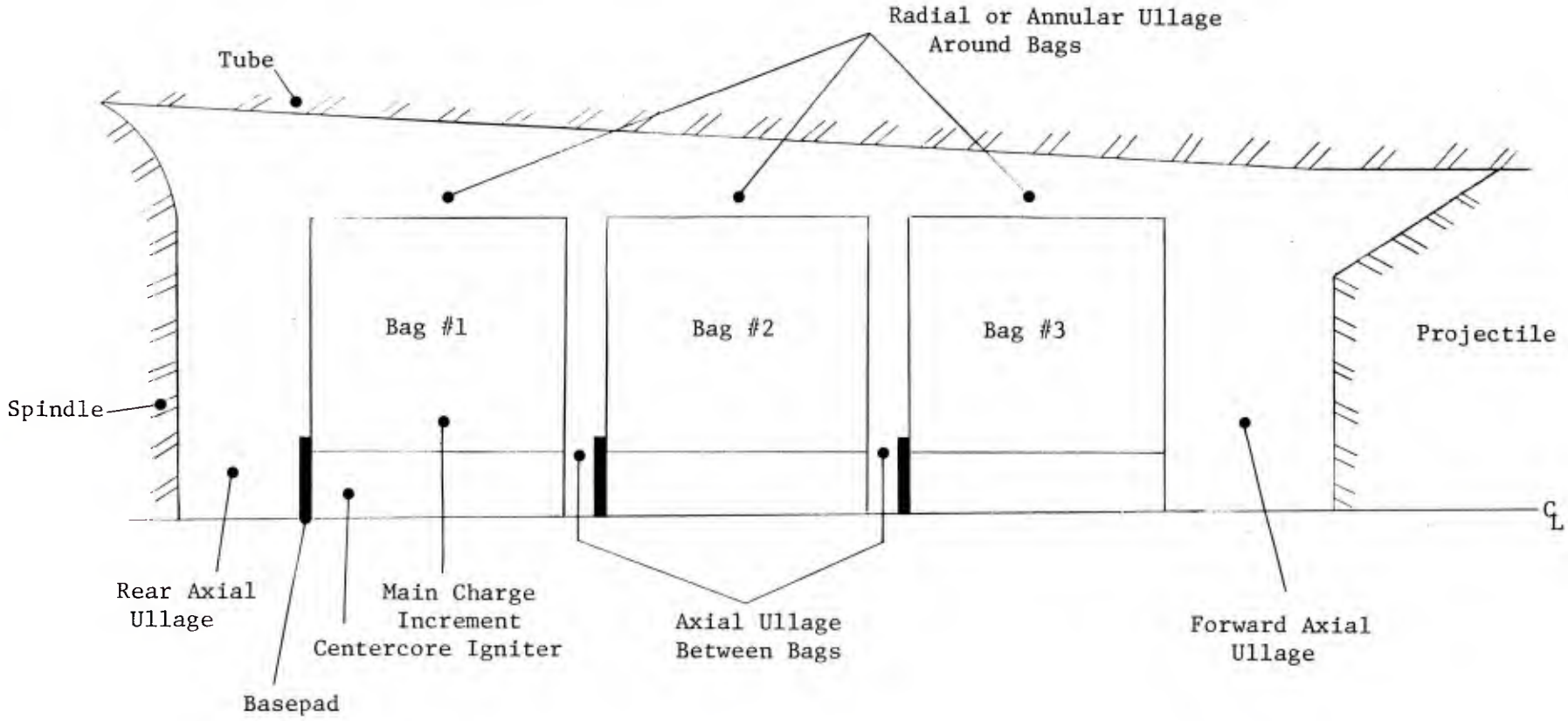

Figure 1.1 Representation of Multi-Increment Bag Charge by TDNOVA

We observe that the increments are packed end-to-end. Although TDNOVA will model the coaxial regions of two-phase flow defined by the main charge and its associated centercore igniter charge, it does not support the modeling of coaxial main charges. In respect to this point, it should be noted that whereas the main charge increments are represented as fully two-dimensional during flame-spreading, the centercore igniter charges are assumed to be sufficiently thin, in the radial direction, as to validate a quasi-one-dimensional analysis in which only the axial structure of the two-phase flow is modeled explicitly.

Figure 1.1 also illustrates the nomenclature which we adopt in regard to the free volume or ullage outside the regions occupied by the bags. We refer to the ullage between the spindle and the first increment as the rear axial ullage and, similarly, the space between the last increment and the base of the projectile is referred to as the forward axial ullage. The spaces between the increments are also referred to as axial ullage. However, the free volume between the tube wall and the exterior circumferential surfaces of the increments is called radial or annular ullage. If, in place of a centercore tube, there exists radial ullage inside the charge, we make the further distinction between outer and inner radial ullage.

Of course, the distribution of ullage varies in time. We model explicitly the motion of both phases, and the external radial ullage may eventually disappear due to the expansion of the mixture to the tube wall. Similarly, axial ullage between the bags may disappear as two mixture regions collide. Or, it may appear and increase in size as two mixture regions separate as a possible consequence, say, of the gas-dynamic forces exerted by the venting of a basepad between them.

In Figure 1.2 we illustrate in greater detail the attributes of a typical charge increment and the manner in which these attributes are represented within TDNOVA. With the obvious exception of the main propellant charge increment, each of the attributes illustrated in Figure 1.2 is to be thought of as optional.

We illustrate, in Figure 1.2(a), an increment consisting of a main charge packed around a centercore tube made of nitrocellulose. Inside the centercore tube is a small cloth bag of black powder or, possibly, of a clean burning igniter material. The bag used to contain the main charge is shown as having certain liner materials embedded in the outer circumferential surface. These liner

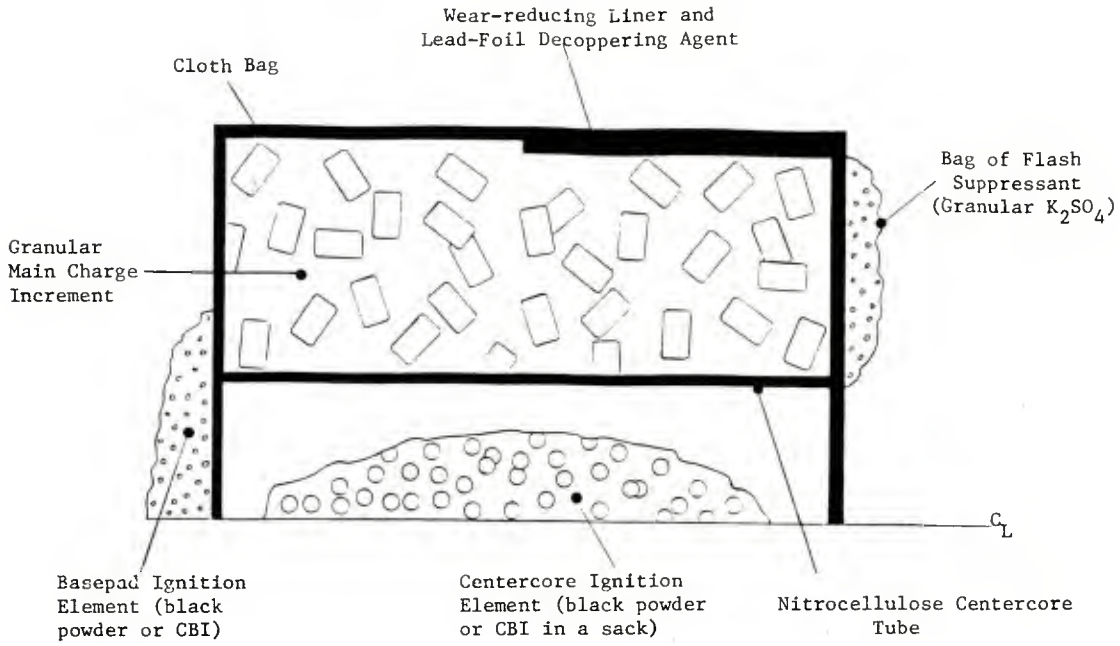

(a) Schematic Illustration of Typical Components of Bagged Artillery Charge Increment

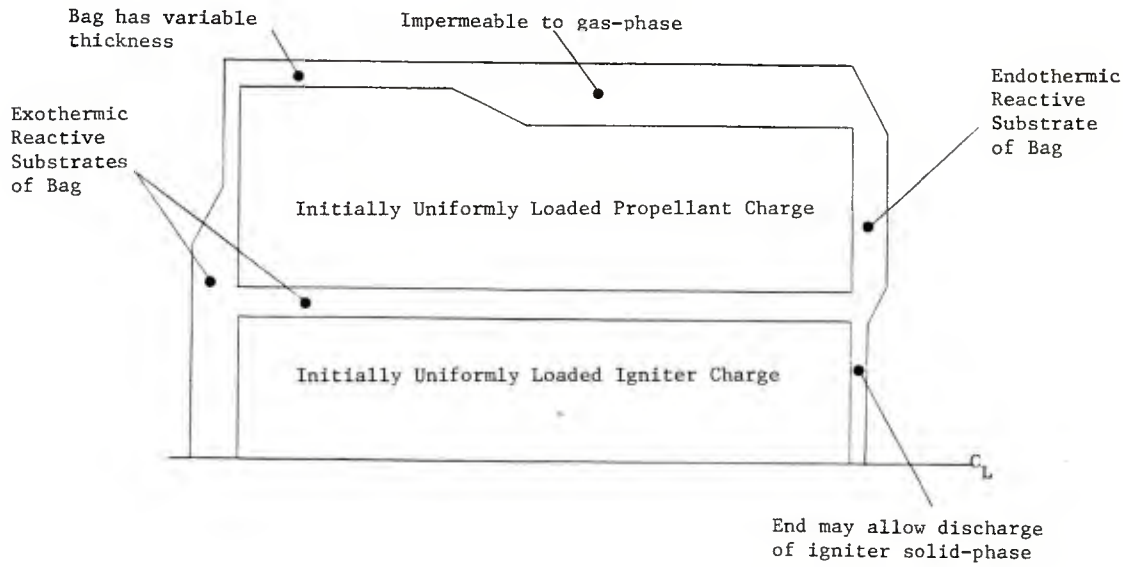

(b) Idealization of Charge Increment by TDNOVA

Figure 1.2 Charge Increment Representation by TDNOVA

materials are intended to reduce undesirable side effects of the propulsion cycle such as erosion of the tube by the hot flowing gas, and the deposition of copper on the tube wall by the rotating band of the projectile. We also illustrate a bag of flash suppressant sewn to the forward face of the bag. Its purpose is to minimize secondary combustion of the propellant gas following discharge into the atmosphere. Finally, we show a basepad sewn to the rear face of the bag.

In Figure 1.2(b) we show the corresponding idealization by TDNOVA. All the components of the bag, including the basepad, the flash suppressant, the nitrocellulose centercore tube, and the wear-reducing liner are represented as attributes of the surface of the main charge increment. The user may prescribe, in an essentially arbitrary manner, properties of exothermic or endothermic reactivity, mechanical strength, and resistance to normal gas flux, over the entire surface of each increment of the main charge. In addition, the thickness of the bag may be arbitrarily prescribed at each point on the surface. If the surface is locally reactive, the thickness will decrease at a rate consistent with the rate of mass generation. If the bag is locally impermeable and reactive, the surface flux is ascribed to the exterior of the bag and therefore induces pressurization of the ullage or of the centercore rather than the main charge increment.

Reactivity may also be ascribed to either of the ends of the centercore tube in order to model the flux due to that part of the basepad which overlaps the end of the tube. The ends of the centercore tube are always represented as permeable to the gas-phase. As an option, they may be made permeable to an efflux of the centercore igniter solid-phase.

Figure 1.3 illustrates the computational regions considered by TDNOVA. Each region defined by a main charge increment is represented as two-dimensional and two-phase at least until flamespreading and the rupture of all bags is complete and radial pressure gradients have disappeared. Centercore igniter charges are represented as quasi-one-dimensional and two-phase at all times. The ullage is divided into subregions formed by projecting the boundaries of the bags in the axial and the radial directions.

Two modes of representation are available to the user. We refer to these as the static and the dynamic mesh allocation modes. To date, complete calculations have been obtained only with the static mode.

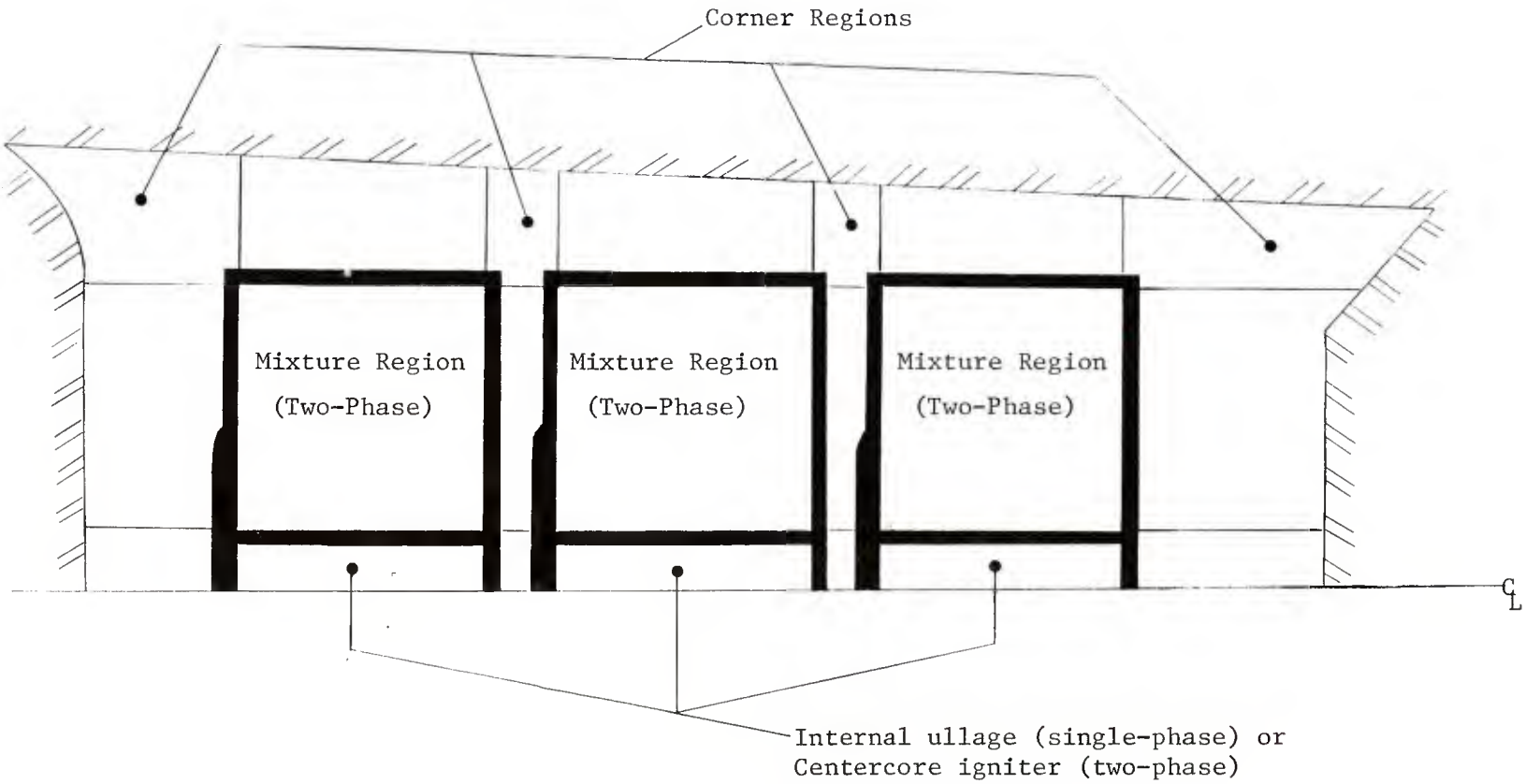

Figure 1.3 Computational Regions Considered by TDNOVA

In the dynamic mode regions of ullage may be represented as fully two-dimensional, quasi-one-dimensional or lumped parameter, in accordance with their dimensions.

In the static mode, those regions of ullage contiguous with the mixture boundaries are always treated as quasi-one-dimensional and the corner regions, which connect two or more regions of quasi-one-dimensional flow, are represented as lumped parameter. When flamespreading and bag rupture are complete and radial pressure gradients have subsided, the representation of the flow is transformed to a quasi-two-dimensional formulation in which not only the centercore igniter charges but also the main charge increments are represented as quasi-one-dimensional, two-phase flows. The regions of radial ullage remain quasi-one-dimensional, but the regions of axial ullage are subsequently treated as lumped parameter and are taken to include not only the regions which were previously contiguous with the ends of the bags but also their associated corner regions.

The regions of ullage are always modeled as containing an inviscid, compressible gas. For this reason, the static allocation mode is better-posed physically than the dynamic mode in certain respects. In the static mode we can express the pressure losses associated with the turning of the flow about the corners by means of a suitable formulation of the boundary conditions. Since the flow in the vicinity of the corners involves processes which are inherently outside the scope of the inviscid equations, an extension to multidimensional analysis of the ullage may not represent a real improvement in modeling capacity, in general, unless diffusive mechanisms are also included. One is then confronted simultaneously with an increased computational burden, due to the large number of mesh points required to resolve the structure of the flow, and the difficult theoretical task of determining the turbulence laws which apply in the highly transient interior ballistic environment.

In the regions of two-phase flow, we model the separate motion and temperature of each of the phases. In other words, the two-phase analysis does not incorporate an assumption of either mechanical or thermal equilibrium between the phases. The macroscopic equations are supported by empirical correlations which describe the interphase drag and heat transfer. Ignition of the solid-phase is taken to occur when the surface temperature, deduced from an approximate solution to the unsteady heat conduction equation, reaches a predetermined value. The subsequent combustion of the solid-phase is assumed to depend on the local average pressure according to an empirical relationship. The model also accounts for intergranular stresses when the solid-phase is sufficiently packed.

The method of solution is based on an explicit* predictor/corrector finite difference scheme at all interior mesh points. Characteristic forms are used at the boundaries. An implicit formulation of the physical boundary conditions and the characteristic relationships between gas-phase pressure and normal velocity is used to circumvent the stiffness which can arise from regions of ullage which are thin in the direction normal to the boundaries. A time-dependent equipotential mesh is used in all two-dimensional regions at all times.

1.2.2 Differences From Previous Code Version

The most significant difference from the previous version of the code[2] is, of course, the capability to treat charges consisting of more than one increment. There are several other differences, however, and we briefly summarize the more important ones.

(1) The thickness of the bag was not previously modeled.

(2) The previous version of the code supported only fixed values of the molecular weight and the specific heats of the gas-phase. In the current version each propellant increment, whether main charge or centercore igniter, may be characterized by individual values of all the properties of both the solid- and the gas-phase. Independent values of the molecular weight and the ratio of specific heats may also be ascribed to the gas generated by the reactive substrates of the bags. The code computes the variation of molecular weight and the ratio of specific heats with the changing composition of the gas.

(3) Previously the solid-phase in the centercore was required to satisfy a no-slip boundary condition at the ends of the tube. In the present version, we allow efflux of the solid-phase as an option. At bag-to-bag interfaces, transfer of the solid-phase from one tube to its neighbor is admitted.

(4) Previously an equipotential mesh was used only on the first step for the region occupied by the main charge. In the present version, all regions of two-dimensional flow have equipotential meshes at all times.

1.2.3 Code Limitations

The purpose of this concluding subsection is to remind the potential user of some of the more significant limitations to the scope of applicability of the code.

Perhaps the most important limitation to keep in mind is the fact that the code is based on a macroscopic formulation. In particular, the predicted details of the radial structure of the

*We use the term "explicit" to signify a scheme in which the spacewise derivatives are represented by means of data in current storage. The term "implicit" signifies the use of future level data to represent spacewise derivatives.

flow should be regarded with some caution as the radial dimensions of the tube are, in general, not much larger than the scale of heterogeneity of the mixture.

In respect to the details of the base of the projectile, it should be noted that the radial gap between the boattail and the tube is particularly small in most cases involving howitzer charges. In fact, the space may be smaller than the typical dimensions of a grain so that intrusion of the granular aggregate into the space around the boattail while admissible by the treatment of the aggregate as a quasi-fluid, may not be realizable in practice.

With regard to the treatment of regions of ullage according to a quasi-one-dimensional formulation, it should be kept in mind that details of the modeled velocity component are only described with any accuracy when the cross-sectional area varies slowly with respect to the nontrivial spatial coordinate and, moreover, when the curvature of the flow channel is small.

It should be kept in mind that at present no account is taken of the independent motion of the bag. It is, at all times, an attribute of the surface of the propelling charge and its influence is felt in terms of flow resistance, of mechanical constraint and of mass production due to reactive substrates.

Diffusive mechanisms are not considered in the balance equations. Accordingly, processes dependent on boundary layer development such as heat transfer to the tube cannot be modeled on a fundamental basis. The gas-phase is assumed to be in chemical equilibrium at all times and the composition of the reactants is assumed to be fixed. Changes in the overall composition of the gas-phase are due solely to the mixing of the products of combustion of the propellant to the ambient gas, without chemical reaction.

Only multi-increment charges involving end-to-end assembly of the increments may be modeled with the present version of the code. Although it is not necessary that the increments all have the same diameter, accuracy is expected to suffer if increments of significantly different diameter are considered.

We refer the reader to the previous final report[2] for a discussion of the treatment of the tangential gas-phase and solid-phase momentum equations at the boundaries of the mixture. No revisions have been incorporated in the present version of the code in respect to this particular topic.

Finally, we comment on the treatment of the centercore igniter. The igniter, which, in many cases, consists of black powder, is modeled as a quasi-one-dimensional two-phase flow. This model admits the simulation of flamespreading through the igniter as driven by a convective thermal stimulus. However, it is known that[12] at low pressure at least, flamespreading in black powder is strongly influenced by the discharge of hot molten salts which, traveling from an ignited grain to a neighboring inert grain, may represent the principal thermal stimulus. Such a process is not modeled in the code at present. Thus, a priori calculations of flamespreading through black powder cannot yet be performed.

---

[12] *Williams, F. A.*
"The Role of Black Powder in Propelling Charges"
Picatinny Arsenal Technical Report 4770. *1975*

2.0 GOVERNING EQUATIONS

Since the purpose of the present work has been the extension of TDNOVA from a single-bag to a multi-bag capability, the bulk of the effort has consisted of revisions and extensions to the code. The governing equations are virtually unchanged from those described in the previous final report.[2] We do have to consider the variation in time of the molecular weight, M_w, and the ratio of specific heats, γ, of the gas-phase due to variations in the composition of the gas. Accordingly, the following tabulation of the governing equations is included mainly for the sake of completeness of the present chapter and, to some extent, to place the governing equations for M_w and γ in context.

The order of presentation of the equations is as follows. In 2.1 we summarize all the balance equations for the various types of flow, noting the circumstances in which they are to be used. We include, in 2.1, the various formulations of the governing equations for M_w and γ which pertain to the various sets of model equations--two-dimensional, one-dimensional and lumped parameter. In section 2.2 we summarize the constitutive laws which govern the state of each of the phases as well as those which govern the microscopic interactions between them. The discussion of 2.2 is unchanged from that of the previous final report. In section 2.3 we discuss the initial and boundary conditions. While the substance of this section is unchanged from the previous final report, revisions have been included in the interests of greater clarity, particularly with reference to the influence of the bag.

2.1 Balance Equations

We refer to the previous final report[2] for details concerning the origins of the balance equations and the rationale for considering various formulations of the equations. We describe in 2.1.1 the balance equations for two-dimensional, two-phase flow which are used to model the behavior of the mixture during flamespreading and until radial pressure gradients have disappeared. In 2.1.2 we describe quasi-one-dimensional forms of the same equations with an allowance for a cross-sectional area which depends on both position and time and the incorporation of terms to describe the transverse addition or loss of gas due to exchanges with a neighboring region which may be either two-dimensional or quasi-one-dimensional. The equations of 2.1.2 are used to model the behavior of the centercore igniter charges at all times and are also used to describe the behavior of the main propelling charge increments following the transformation of the problem to a quasi-two-dimensional representation.

Corresponding to these equations we have in sections 2.1.3 and 2.1.4 two-dimensional and quasi-one-dimensional forms of the balance equations which govern the flow of an inviscid, compressible gas. These are used to model the gas in the regions of ullage which may be situated around the charge, behind it, in front of it, within it or between successive increments of the charge. Finally, in 2.1.5 we describe the governing equations for a lumped parameter region of gas. These equations are used to model the corner regions during the fully two-dimensional part of the calculation and also the axial ullage during the quasi-two-dimensional part of the calculation.

The balance equations consist of statements of conservation of mass, momentum and energy for the gas-phase and of mass and momentum for the solid-phase which is taken to be microscopically incompressible. These are unchanged from the previous report.[2] We also note, in context, the relevant equations for the time dependence of M_w and γ.

It should be noted that the influence of composition on M_w and γ is modeled only partially. We do not, for example, consider the variation of composition with temperature. Initially, the gas-phase is presumed to consist of air at an ambient pressure and temperature. Fully reacted products of combustion of the centercore charge, the main charge or the predetermined external ignition stimulus are added locally. Each of these combustion products is characterized by fixed, predetermined values of M_w and γ. The time dependence of M_w and γ is due to the assumed mixing of the combustion products with the ambient gas without further chemical reaction.

Variations in M_w and γ are also due to the reactivity of the bag, the combustion products of which are likewise assumed to be fully reacted and characterized by unique values of M_w and γ. However, the influence of the reactive substrates is expressed through the internal boundary conditions and is therefore discussed in section 2.3.

2.1.1 Two-Dimensional Two-Phase Flow

In cylindrical coordinates such that z is the axial coordinate, r is the radial coordinate and t is the time, the balance equations take the forms:

Balance of Mass of Gas Phase

$$\frac{D\varepsilon\rho}{Dt} + \varepsilon\rho\left[\frac{\partial u}{\partial z} + \frac{\partial v}{\partial r}\right] = \dot{m} + \psi - \frac{\varepsilon\rho v}{r} \qquad 2.1.1.1$$

The notation conforms with that used previously.[2] We have ρ, the density of the gas, ε the porosity, u and v the z- and r-components of gas-phase velocity, D/Dt the convective derivative along the gas phase streamline, ψ the source term associated with a stimulus, $\dot{m}$ the rate of production of gas due to combustion of the solid-phase.

We recall:

$$\frac{D}{Dt} \equiv \frac{\partial}{\partial t} + u \frac{\partial}{\partial z} + v \frac{\partial}{\partial r} \qquad 2.1.1.2$$

$$\dot{m} = (1 - \varepsilon) \frac{S_p}{V_p} \dot{d}\rho_p = s_p \dot{d}\rho_p \qquad 2.1.1.3$$

Here S_p, V_p are the surface area and volume of an individual grain and $\dot{d}$ is the rate of surface regression. We have introduced s_p as the surface area per unit volume.

It should be noted that while the present version of the code admits a variety of propellant types, only one species is assumed to exist at a given point so that a summation over species is not required in 2.1.1.3. This assumption precludes the modeling of bimodal charges in which different species are present within a macroscopically infinitesimal control volume. The modeling of local mixtures of propellants has been considered in the one-dimensional NOVA code[13] to which reference may be made for the relevant governing equations.

Balance of Momentum of Gas Phase

$$\varepsilon\rho\frac{D\vec{u}}{Dt} + \varepsilon g_o \nabla p = -\vec{f} + \dot{m}(\vec{u}_p - \vec{u}) - \psi\vec{u} \qquad 2.1.1.4$$

Here $\vec{u}$ is the velocity with components u and v, and $\vec{f}$ represents the velocity dependent interphase drag.

Balance of Energy of Gas Phase

$$\varepsilon\rho\frac{De}{Dt} + \varepsilon p\left[\frac{\partial u}{\partial z} + \frac{\partial v}{\partial r}\right] + p\frac{D\varepsilon}{Dt} = \vec{f} \cdot (\vec{u} - \vec{u}_p) - s_p q \qquad 2.1.1.5$$

$$+ \dot{m}\left(e_p - e + \frac{p}{\rho_p} + \frac{|u - u_p|^2}{2g_o}\right)$$

$$+ \psi\left(e_{IG} - e + \frac{\vec{u} \cdot \vec{u}}{2g_o}\right) - \varepsilon p \frac{v}{r}$$

---

[13] *Gough, P. S.*
"The NOVA Code: A User's Manual "
Final Report, Task I, Contract N00174-79-C-0082. *1979*

Here $e = e(p,\rho)$ is the internal energy of the gas phase and q is the interphase heat transfer per unit surface area of the solid phase.

Balance of Mass of Solid Phase

$$\frac{D\varepsilon}{Dt_p} - (1 - \varepsilon)\left[\frac{\partial u_p}{\partial z} + \frac{\partial v_p}{\partial r}\right] = \frac{\dot{m}}{\rho_p} + (1 - \varepsilon)\frac{v_p}{r} \qquad 2.1.1.6$$

The subscript p denotes properties of the solid-phase and D/Dt_p is defined by analogy with 2.1.1.2.

Balance of Momentum of Solid-Phase

$$(1 - \varepsilon)\rho_p \frac{D\vec{u}_p}{Dt_p} + (1 - \varepsilon)g_o\nabla p + g_o\nabla\sigma = \vec{f} \qquad 2.1.1.7$$

The vector form of this equation should be noted. We have $\sigma = (1 - \varepsilon)R(\varepsilon,\dot{\varepsilon})$ where R is the average stress due to contacts between particles and is assumed to depend upon porosity according to an irreversible differential constitutive law.

Time-Dependence of Molecular Weight

$$\frac{DM_w}{Dt} = \frac{M_w}{\varepsilon\rho}\left\{(1 - \frac{M_w}{M_{IG}})\psi + (1 - \frac{M_w}{M_{PROP}})\dot{m}\right\} \qquad 2.1.1.8$$

Here M_{IG} and M_{PROP} are respectively the molecular weights of the combustion products of the external stimulus and the solid propellant.

Time-Dependence of Specific Heats

With c used to signify a specific heat at either constant volume or constant pressure, we have

$$\frac{Dc}{Dt} = \frac{1}{\varepsilon\rho}\left\{(c_{IG} - c)\psi + (c_{PROP} - c)\dot{m}\right\} \qquad 2.1.1.9$$

where c_{IG} and c_{PROP} are the corresponding specific heats of the combustion products of the external stimulus and the propellant, respectively.

2.1.2 Quasi-One-Dimensional Two-Phase Flow

In the applications of interest to us, the nontrivial spacewise coordinate is aligned with the axis of the tube so that u, u_p are the nontrivial components of gas and solid phase velocity, respectively. The cross-sectional area of the annulus through which the flow occurs is taken to be $A(z,t)$ and therefore depends upon both position and time. It is supposed that the circumferential boundaries are permeable to the gas-phase and that mass transfers must be considered. We use R_i and R_o to denote respectively the radii of circumferential surfaces on which influx ($\dot{m}_i$) or efflux ($\dot{m}_o$) occur. Attention should be paid to this convention. The subscripts i and o do not refer to the interior and exterior surfaces, only to the direction of mass transfer. We understand $\dot{m}_i$ and $\dot{m}_o$ to represent rates of transfer per unit surface area. Moreover, we will also denote the properties transported with $\dot{m}_i$ by the subscript i. Thus u_i will be the axial velocity associated with the incoming gas. The exiting properties are, of course, those of the gas in the quasi-one-dimensional region presently under consideration.

Balance of Mass of Gas Phase

$$\frac{\partial}{\partial t}\varepsilon A\rho + \frac{\partial}{\partial z}\varepsilon A\rho u = A\dot{m} + A\psi + 2\pi[\Sigma R_i\dot{m}_i - \Sigma R_o\dot{m}_o] \qquad 2.1.2.1$$

The summations are over all entering and all exiting fluxes.

Balance of Momentum of Gas Phase

$$\varepsilon\rho\frac{Du}{Dt} + \varepsilon g_o\frac{\partial p}{\partial z} = -f - \psi u + \dot{m}(u_p - u) + \frac{2\pi}{A}\Sigma R_i\dot{m}_i(u_i - u) \qquad 2.1.2.2$$

Balance of Energy of Gas Phase

$$\begin{aligned}\varepsilon\rho\frac{De}{Dt} + \frac{p}{A}\frac{D\varepsilon A}{Dt} + \varepsilon p\frac{\partial u}{\partial z} = {} & \frac{f}{g_o}(u - u_p) - s_p q \\ & + \psi\left[e_{IG} - e + \frac{u^2}{2g_o}\right] \\ & + \dot{m}\left[e_p - e + \frac{p}{\rho_p} + \frac{(u - u_p)^2}{2g_o}\right] \\ & + \frac{2\pi}{A}\Sigma\dot{m}_i R_i\left[e_i + \frac{p_i}{\rho_i} + \frac{(u - u_i)^2}{2g_o} - e\right] \\ & - \frac{2\pi}{A}\frac{p}{\rho}\Sigma\dot{m}_o R_o\end{aligned} \qquad 2.1.2.3$$

Balance of Mass of Solid Phase

$$\frac{1}{A}\frac{D}{Dt_p}(1-\varepsilon)A + (1-\varepsilon)\frac{\partial u_p}{\partial z} = -\frac{\dot{m}}{\rho_p} \qquad 2.1.2.4$$

Balance of Momentum of Solid Phase

$$\rho_p(1-\varepsilon)\frac{Du_p}{Dt_p} + (1-\varepsilon)g_o\frac{\partial p}{\partial z} + g_o\frac{\partial \sigma}{\partial z} = f \qquad 2.1.2.5$$

Time-Dependence of Molecular Weight

$$\frac{DM_w}{Dt} = \frac{M_w}{\varepsilon\rho}\left\{(1-\frac{M_w}{M_{IG}})\psi + (1-\frac{M_w}{M_{PROP}})\dot{m}\right\} + \frac{2\pi M_w}{\varepsilon\rho A}\Sigma\dot{m}_i R_i(1-\frac{M_w}{M_{w_i}}) \qquad 2.1.2.6$$

Here M_{w_i} is the molecular weight of the gas transferred into the quasi-one-dimensional region. An efflux, of course, has no effect on M_w.

Time-Dependence of Specific Heats

$$\frac{Dc}{Dt} = \frac{1}{\varepsilon\rho}\left\{(c_{IG}-c)\psi + (c_{PROP}-c)\dot{m}\right\} + \frac{2\pi}{\varepsilon\rho A}\Sigma\dot{m}_i R_i(c_i - c) \qquad 2.1.2.7$$

where c_i is a specific heat of the same type as c for the entering gas.

2.1.3 Two-Dimensional Single-Phase Flow

These familiar equations represent the limiting forms of 2.1.1.1, 2.1.1.4, 2.1.1.5, 2.1.1.8 and 2.1.1.9 as $\varepsilon \to 1$, bearing in mind that f, $\dot{m}$ and q $\to$ 0.

Balance of Mass

$$\frac{D\rho}{Dt} + \rho\left[\frac{\partial u}{\partial z} + \frac{\partial v}{\partial r}\right] = \psi - \frac{\rho v}{r} \qquad 2.1.3.1$$

Balance of Momentum

$$\rho\frac{D\vec{u}}{Dt} + g_o\nabla p = -\psi\vec{u} \qquad 2.1.3.2$$

Balance of Energy

$$\rho\frac{De}{Dt} + p\left[\frac{\partial u}{\partial z} + \frac{\partial v}{\partial r}\right] = \psi\left[e_{IG} + \frac{\vec{u}\cdot\vec{u}}{2g_o} - e\right] - p\,\frac{v}{r} \qquad 2.1.3.3$$

Time-Dependence of Molecular Weight

$$\frac{DM_w}{Dt} = \frac{M_w}{\rho}\left(1 - \frac{M_w}{M_{IG}}\right)\psi \qquad 2.1.3.4$$

Time-Dependence of Specific Heat

$$\frac{Dc}{Dt} = \frac{1}{\rho}(c_{IG} - c)\psi \qquad 2.1.3.5$$

2.1.4 Quasi-One-Dimensional Single-Phase Flow

A quasi-one-dimensional representation is made of regions of ullage which have significant extension in one direction but which are relatively thin in the perpendicular direction. In contrast to the situation in section 2.1.2, we cannot assume that the non-trivial direction is axial. The flow will be directed according to the configuration of the boundary of the propelling charge with which it is contiguous. In recognition of this fact, we designate the nontrivial coordinate by s and the corresponding component of velocity by u_T, to be interpreted as a velocity tangential to the contiguous mixture boundary.

Using the same conventions as in section 2.1.2 to describe entering and exiting mass fluxes, we have the balance equations of quasi-one-dimensional flow as follows:

Balance of Mass

$$\frac{\partial}{\partial t}A\rho + \frac{\partial}{\partial s}A\rho u_T = A\psi + 2\pi[\Sigma R_i\dot{m}_i - \Sigma R_o\dot{m}_o] \qquad 2.1.4.1$$

Balance of Momentum

$$\rho\frac{Du_T}{Dt} + g_o\frac{\partial p}{\partial s} = -\psi u + \frac{2\pi}{A}\Sigma R_i\dot{m}_i(u_i - u_T) \qquad 2.1.4.2$$

Balance of Energy

$$\rho\frac{De}{Dt} + \frac{p}{A}\frac{DA}{Dt} + p\frac{\partial u_T}{\partial s} = \psi[e_{IG} - e + \frac{u_T^2}{2g_o}] \qquad 2.1.4.3$$

$$+ \frac{2\pi}{A}\Sigma\dot{m}_i R_i[e_i + \frac{p_i}{\rho_i} + \frac{(u_T - u_i)^2}{2g_o} - e]$$

$$- \frac{2\pi}{A}\frac{p}{\rho}\Sigma\dot{m}_o R_o$$

Time-Dependence of Molecular Weight

$$\frac{DM_w}{Dt} = \frac{M_w}{\rho}(1 - \frac{M_w}{M_{IG}})\psi + \frac{2\pi M_w}{\rho A}\Sigma\dot{m}_i R_i(1 - \frac{M_w}{M_{w_i}}) \qquad 2.1.4.4$$

Time-Dependence of Specific Heats

$$\frac{Dc}{Dt} = \frac{1}{\rho}(c_{IG} - c)\psi + \frac{2\pi}{\rho A}\Sigma\dot{m}_i R_i(c_i - c) \qquad 2.1.4.5$$

The previous final report[2] may be consulted for some comments on the validity of these equations.

2.1.5 Lumped Parameter Single-Phase Flow

As in previous work,[2] we do not furnish a momentum balance. It is assumed that the state of motion of the gas in the lumped parameter region can be deduced from the boundary values of the neighboring continua and from the state of motion of those external surfaces which bound the region in question.

Using V to denote the volume of the region and S the bounding surface, we have

$$\frac{dV}{dt} = \int_S \vec{w} \cdot \vec{n}\, da \qquad 2.1.5.1$$

where $\vec{w}$ is the boundary velocity and $\vec{n}$ is the outward facing normal. The mass balance is:

$$\frac{d}{dt}\rho V = \int_V \psi dv + \Sigma \dot{m}_i - \Sigma \dot{m}_o \qquad 2.1.5.2$$

where the $\dot{m}_i$ and $\dot{m}_o$ now refer to the total fluxes rather than the fluxes per unit area used previously.

The energy balance is:

$$\frac{d}{dt}\rho EV = \int_V \psi e_{IG} dv + \Sigma \dot{m}_i \left(e_i + \frac{p_i}{\rho_i} + \frac{u_i^2}{2g_o}\right) - p \int_S \vec{w} \cdot \vec{n}\, da - \Sigma \dot{m}_o \left(E + \frac{p}{\rho}\right) \qquad 2.1.5.3$$

where E is the total energy $e + u^2/2g_o$.

The time-dependence of M_w and γ may be expressed as

$$\frac{dM_w}{dt} = \frac{M_w}{\rho}\left(1 - \frac{M_w}{M_{IG}}\right)\psi + \frac{M_w}{\rho V}\Sigma \dot{m}_i \left(1 - \frac{M_w}{M_{w_i}}\right) \qquad 2.1.5.4$$

and

$$\frac{dc}{dt} = \frac{1}{\rho}(c_{IG} - c)\psi + \frac{1}{\rho V}\Sigma \dot{m}_i (c_i - c) \qquad 2.1.5.5$$

in which $\dot{m}_i$ is understood to be a total flux and not a flux per unit area.

2.2 Constitutive Laws

We describe, in the present section, both the equations of state for the solid and gas phases as well as the relationships between the interphase transfer processes--drag, heat transfer and combustion-- and the macroscopic state variables. The relationships governing mass transfer from one region to another are, however, viewed as boundary conditions, as are the properties of the bag, and these topics are addressed in the next section.

2.2.1 Equation of State of Gas

It is assumed that the gas obeys the covolume equation of state:

$$e = c_v T = \frac{p(1 - b\rho)}{(\gamma - 1)\rho} \qquad 2.2.1.1$$

where b is the covolume, γ is the ratio of specific heats and c_v is the specific heat at constant volume.

2.2.2 Intergranular Stress Law

The intergranular stress is taken to depend on porosity and also on the direction of loading. We embed the constitutive law into the formula for the rate of propagation of intergranular disturbances:

$$a(\varepsilon) = \left[- \frac{g_o}{\rho_p} \frac{d\sigma}{d\varepsilon} \right]^{1/2} \qquad 2.2.2.1$$

We may recast 2.2.2.1 into a form more suitable for numerical integration, namely:

$$\frac{D\sigma}{Dt_p} = - \rho_p \frac{a^2}{g_o} \frac{D\varepsilon}{Dt_p} \qquad 2.2.2.2$$

In order to formulate the functional behavior of $a(\varepsilon)$, we introduce ε_o, the settling porosity of the bed, and values of $a(\varepsilon)$ equal to a_1 and a_2 which respectively correspond to loading at ε_o and to unloading/reloading. The nominal loading curve, corresponding to monotonic compaction of the bed from ε_o to a smaller value of the porosity ε is given by:

$$\sigma = \sigma_{nom}(\varepsilon) = \rho_p \frac{a_1^2}{g_o} \varepsilon_o^2 \left(\frac{1}{\varepsilon} - \frac{1}{\varepsilon_o} \right) \qquad 2.2.2.3$$

The functional dependence of $a(\varepsilon)$ may now be stated as:

$$a(\varepsilon) = \begin{cases} a_1\varepsilon_o/\varepsilon & \text{if } \dot{\varepsilon} \le 0,\ \sigma = \sigma_{nom},\ \varepsilon \le \varepsilon_o \\ a_2 & \text{if } 0 \le \sigma < \sigma_{nom},\ \varepsilon \le \varepsilon_o \\ & \text{or if } \dot{\varepsilon} > 0,\ \sigma = \sigma_{nom},\ \varepsilon \le \varepsilon_o \\ 0 & \text{if } \sigma = 0 \text{ and } \dot{\varepsilon} > 0 \text{ or if } \varepsilon > \varepsilon_o \end{cases} \qquad 2.2.2.4$$

where we understand $\dot{\varepsilon}$ to mean $D\varepsilon/Dt_p$.

The values of a_1, a_2 and ε_o are understood to depend on the type of propellant under consideration. Both the main charges and the centercore charges are assumed to be governed by 2.2.2.4.

2.2.3 Propellant Form Functions

Two types of form functions are supported in the present code version. The grains may be spheres of initial diameter D_o whose surface area and volume vary with surface regression according to the following equations.

$$S_p = \pi(D_o - 2d)^2 \qquad 2.2.3.1$$

$$V_p = \frac{\pi}{6}(D_o - 2d)^3 \qquad 2.2.3.2$$

Alternatively, the propellant grains may be multiperforated cylinders having initial length L_o, external diameter D_o and perforation diameter d_o. In this case, until such time as slivering occurs, that is to say, the time at which the regressing perforation surfaces intersect, the surface area and volume are given by:

$$S_p = \pi(L_o - 2d)[(D_o - 2d) + N(d_o + 2d)] \qquad 2.2.3.3$$
$$+ \pi/2[(D_o - 2d)^2 - N(d_o + 2d)^2]$$

$$V = \pi(L_o - 2d)[(D_o - 2d)^2 - N(d_o + 2d)^2]/4 \qquad 2.2.3.4$$

where N is the number of perforations and d is the total linear surface regression, assumed uniform over all the surfaces of a grain.

Once slivering occurs, the form functions become rather complicated for N > 1. Formulae for the form functions following the slivering of seven-perforation grains may be found in Krier et al.[14] The present version of the code supports single-, seven- and nineteen-perforation grains in the propelling charge, the form functions for the latter in the slivering phase being calculated by means of a subroutine furnished by the Naval Ordnance Station, Indian Head, MD.[15]

The surface area per unit volume is related to the individual surface area S_p and volume V_p of each particle according to:

$$s_p = (1 - \varepsilon)S_p/V_p \qquad 2.2.3.5$$

2.2.4 Interphase Drag

The interphase drag is assumed to be governed by the relationship

$$\vec{f} = \frac{1 - \varepsilon}{D_p} \rho |\vec{u} - \vec{u}_p| (\vec{u} - \vec{u}_p) \hat{f}_s \qquad 2.2.4.1$$

where D_p is the effective particle diameter given by:

$$D_p = \frac{6V_p}{S_p} \qquad 2.2.4.2$$

and $\hat{f}_s$ is governed by the high Reynolds number limit of the empirical

---

[14] *Krier, H., Shimpi, S. A. and Adams, M. J. "Interior Ballistic Predictions Using Data From Closed and Variable Volume Simulators." Univ. of Illinois at Urbana-Champaign. TR-AAE-73-6 1973*

[15] *Horst, A. Private Communication.*

correlation of Ergun,[16] for packed beds, extended into the fluidized regime by the tortuosity factor of Anderssen:[17]

$$\hat{f}_s = \begin{cases} 1.75 & \varepsilon \le \varepsilon_o \\ 1.75\left[\frac{1-\varepsilon}{\varepsilon}\frac{\varepsilon_o}{1-\varepsilon_o}\right]^{0.45} & \varepsilon_o \le \varepsilon \le \varepsilon_1 \\ 0.3 & \varepsilon_1 \le \varepsilon \le 1 \end{cases} \qquad 2.2.4.3$$

where

$$\varepsilon_1 = \left[1 + 0.02\left(\frac{1-\varepsilon_o}{\varepsilon_o}\right)\right]^{-1} \qquad 2.2.4.4$$

Equation 2.2.4.3 is assumed to apply to both the granular main charges and the granular centercore igniter charges.

2.2.5 Interphase Heat Transfer

The interphase heat transfer, in both the propelling charge and the centercore ignition charge, is assumed to be governed by the empirical correlation of Gelperin and Einstein.[18] We express the heat transfer in the form

$$Nu_p = 0.4\ Pr^{1/3} Re_p^{2/3} \qquad 2.2.5.1$$

where

$$Nu_p = hD_p/k_f$$

$$Re_p = \rho_f |\vec{u} - \vec{u}_p| D_p/\mu_f$$

$$h = q/(T - T_p)$$

---

[16] *Ergun, S.*
"Fluid Flow Through Packed Columns"
Chem. Eng. Progr. v. 48, p. 89. *1952*

[17] *Anderssen, K. E. B.*
"Pressure Drop in Ideal Fluidization"
Chem. Eng. Sci. v. 15, pp. 276-297. *1961*

[18] *Gelperin, N. I. and Einstein, V. G.*
"Heat Transfer in Fluidized Beds"
Fluidization, edited by Davidson, J. F. and Harrison, D.
Academic Press, NY. *1971*

The subscript f denotes an evaluation of properties at the film temperature $(T + T_p)/2$ where T and T_p are respectively the gas bulk average temperature and the particle surface average temperature. The viscosity is taken to have a Sutherland-type dependence on temperature:

$$\mu = 0.134064 \frac{(T/298)^{1.5}}{T + 110} \qquad 2.2.5.2$$

The thermal conductivity follows from the Prandtl number which is assumed to satisfy:

$$Pr = \frac{c_p \mu}{k} = \frac{4\gamma}{9\gamma - 5} \qquad 2.2.5.3$$

2.2.6 Solid Phase Surface Temperature

Assuming that ignition is an essentially uniform event with respect to the surface of each grain of either the propelling charge or the centercore ignition charge, and supposing that the temperature distribution within the solid phase can be captured by a cubic profile, leads to the following expression for the surface temperature

$$T_p = T_{p_o} - \frac{2}{3}\frac{hH}{k_p^2} + \left[\left(T_{p_o} - \frac{2}{3}\frac{hH}{k_p^2}\right)^2 + \frac{4}{3}\frac{hTH}{k_p^2} - T_{p_o}\right]^{1/2} \qquad 2.2.6.1$$

where T_{p_o} is the initial surface temperature and H satisfies:

$$\frac{DH}{Dt_p} = \alpha_p q \qquad 2.2.6.2$$

2.2.7 Ignition and Combustion

Ignition is assumed to occur when the surface temperature exceeds a predetermined value. The rate of surface regression is given by:

$$\frac{Dd}{Dt_p} = B_1 + B_2 p^n \qquad 2.2.7.1$$

It should be noted that only one of 2.2.6.2 and 2.2.7.1 has to be solved at each point according as the temperature is less than or equal to the ignition temperature.

2.3 Initial and Boundary Conditions

We may state the initial conditions directly. We take both phases to be at rest and at atmospheric pressure. The propellant is packed within a number of bags and is assumed to be free of intergranular stresses. The temperatures of the two phases may differ initially but are uniform throughout each of the respective media. The porosity is piecewise continuous, the discontinuities being defined by the boundaries of the beds of propellant.

Our subsequent discussion addresses the boundary conditions, external and internal. In section 2.3.1 we discuss the external boundary conditions, including the motion of the projectile. In section 2.3.2 we discuss the conditions which apply at boundaries between regions of ullage. In section 2.3.3 we discuss the boundary conditions to be used at the discontinuities in porosity. The discussion of section 2.3.3 addresses the influence of the bag, viewed as a surface phenomenon.

2.3.1 External Boundary Conditions

We do not consider the possibility of flow of either phase through any external boundary. Since both phases are assumed to be inviscid at the macroscopic level, slip boundary conditions apply not only to the gas but also to the solid phase whenever it is in contact with an external boundary. The breech, the tube and the centerline constitute stationary boundaries on which the conditions of kinematic compatibility are simply

$$\vec{u} \cdot \vec{n} = \vec{u}_p \cdot \vec{n} = 0 \qquad 2.3.1.1$$

where $\vec{n}$ is a vector normal to the external boundary. We will take the convention that $\vec{n}$ is positive when directed out of the combustion chamber.

Now let S_{PROJ} be the surface of the projectile which intrudes into the combustion chamber. Let n_z be the z-component of $\vec{n}$. Let the axial speed of the projectile be u_{PROJ}. Then the boundary conditions at the projectile surface are:

$$\vec{u} \cdot \vec{n} = \vec{u}_p \cdot \vec{n} = n_z u_{PROJ} \qquad 2.3.1.2$$

Of course, the condition on the solid phase applies only in a region of two-phase flow.

The projectile motion is assumed to be governed by:

$$\frac{M}{g_o}\frac{d}{dt}u_{PROJ} = \int_{S_{PROJ}} (p + \sigma)n_z da - F_{res} \qquad 2.3.1.3$$

where M is the projectile mass and F_{res} is the bore resistance, assumed to be available from an empirical correlation.

2.3.2 Internal Boundary Conditions Between Regions of Ullage

Regions of ullage may be represented as lumped parameter, quasi-one-dimensional or fully two-dimensional. We therefore discuss each of the following possible configurations:

(i) A boundary between two fully two-dimensional regions of ullage.

(ii) A boundary between a two-dimensional region and a quasi-one-dimensional region.

(iii) A boundary between two quasi-one-dimensional regions which are placed end-to-end.

(iv) A boundary between a quasi-one-dimensional region and a lumped parameter region.

We note that only cases (iii) and (iv) arise in the static mesh allocation mode, and case (iii) only arises when two bags are in contact.

Three physical principles are easily identified in respect to the transfer of mass between regions of ullage. Mass is conserved, the transfer may be assumed to be adiabatic and the tangential component of velocity may be assumed to be transported without change. The fourth principle to be invoked is a mechanical condition on the normal momentum flux and its specification requires a certain amount of care, particularly in cases (ii) and (iv).

We note once and for all that the present version of the code supports only subsonic and sonic transfers across internal boundaries. This assumption is analytically necessary in some cases, but is potentially an unnecessary restriction in others as we discuss below. Calculations to date have not, however, revealed the need to extend the code to the case of supersonic transfers.

(i) Boundary Between Two Two-Dimensional Regions

Let us distinguish properties on each side of the boundary by the subscripts 1 and 2 and let us use the subscripts n and t to distinguish velocity components normal and tangential to the boundary, respectively. Then the finite continuity equation may be stated as:

$$j = \rho_1 u_{n_1} = \rho_2 u_{n_2} \qquad 2.3.2.1$$

and we understand u_n to mean $(\vec{u} - \vec{u}_s) \cdot \vec{n}$ where $\vec{u}_s$ is the velocity of the boundary at the point in question.

We assume the transfer to be adiabatic so that:

$$j(e_1 + \frac{p_1}{\rho_1} + \frac{u_{n_1}^2}{2g_o}) = j(e_2 + \frac{p_2}{\rho_2} + \frac{u_{n_2}^2}{2g_o}) \qquad 2.3.2.2$$

Here we have incorporated the mass flux j as a multiplier so as to imply the possibility of a slip discontinuity or a contact discontinuity on which j may be zero and the enthalpy may be discontinuous. We express the tangential momentum jump analogously:

$$ju_{t_1} = ju_{t_2} \qquad 2.3.2.3$$

thereby admitting the possibility of a slip discontinuity. We also note that relationships completely analogous to 2.3.2.3 apply to the molecular weight and the ratio of specific heats.

The remaining physical boundary condition is easy to state in this particular case. We may assume that unless the boundary fortuitously coincides with a shock, the pressure is continuous:

$$p_1 = p_2 \qquad 2.3.2.4$$

As noted above, however, supersonic transfers are not supported by the present version of the code. Thus 2.3.2.4 is used provided that $|u_{n_1}| < c$ where

$$c = \sqrt{\frac{g_o \gamma p}{\rho(1 - b\rho)}}$$

If 2.3.2.4 leads to a value $|u_{n_1}| > c$, 2.3.2.4 is replaced by the condition $|u_{n_1}| = c$.

It is emphasized that the restriction to sonic transfers is, in this particular case, dictated neither by physical nor by analytical considerations. It represents simply a limitation on the physical scope of applicability of the code which may be relaxed, when the need arises, at the expense of somewhat more complex coding.

We also note prior to considering the subsequent cases that all the state variables referred to in equations 2.3.2.1-2.3.2.3 are explicitly modeled on both sides of the boundary between the two-dimensional regions. Such will not be the case when we consider the remaining possibilities. Care must therefore be taken, in the subsequent discussion, in respect to the interpretation of the state variables in 2.3.2.1-2.3.2.3.

(ii) Boundary Between Two-Dimensional Region and Quasi-One-Dimensional Region

Let us take the subscript 1 to refer to the two-dimensional flow and let 2 refer to the quasi-one-dimensional flow. The value of u_{n_2} is not modeled explicitly, but may be assumed equal to the normal velocity of the neighboring external boundary from which the two-dimensional region is presumably separated by the quasi-one-dimensional region. The mass flux j then refers to boundary values for the two-dimensional region and to a rate of mass addition or loss insofar as the quasi-one-dimensional region is concerned. With regard to the overall interpretation of equations 2.3.2.1, 2.3.2.2, and 2.3.2.3, it must be understood that ρ_2, p_2, e_2, u_{t_2} can only be identified with the state of the quasi-one-dimensional flow in the event that the flow corresponds to a mass transfer directed into the two-dimensional region. When the direction of the flow is such as to correspond to mass addition to the quasi-one-dimensional region, the quantities ρ_2, p_2, e_2, u_{t_2} may be thought of as describing the state of transferred gas prior to irreversible mixing. In particular, 2.3.2.2 may be understood to determine the total enthalpy of the fluid added to the quasi-one-dimensional flow.

The remaining physical condition is that pertaining to the normal momentum flux. As discussed in the previous final report,[2] we assume that the condition depends on the direction of the flow. If the gas is transferred from the two-dimensional region to the quasi-one-dimensional region, we assume

$$p_1 = p_2 \qquad 2.3.2.5$$

where p_2 is the instantaneous, explicitly modeled pressure in the quasi-one-dimensional region. On the other hand, if the gas is transferred from the quasi-one-dimensional region to the two-dimensional region, we assume

$$p_1 = p_2(T_1/T_2)^{\frac{\gamma}{\gamma-1}} \qquad 2.3.2.6$$

where both p_2 and T_2 are identified with the explicitly modeled properties of the quasi-one-dimensional region.

Equation 2.3.2.6 asserts that the transfer from the quasi-one-dimensional region is isentropic, which is reasonable if the quasi-one-dimensional flow is, in effect, expanding across the boundary. Equation 2.3.2.5, on the other hand, anticipates that the transfer into the quasi-one-dimensional region will involve an adjustment of velocity by dissipative mechanisms. In either case we require $|u_{n_1}| \leq c$.

(iii) Boundary Between Two Quasi-One-Dimensional Flows

In this instance the quasi-one-dimensional regions are to be thought of as placed end-to-end. The quantity u_t is modeled in neither region and only 2.3.2.1 and 2.3.2.2 are applicable. The quantities in these two equations correspond with explicitly represented state variables and the remaining physical condition is 2.3.2.4 unless it leads to supersonic flow.

(iv) Boundary Between Quasi-One-Dimensional Region and Lumped Parameter Region

The lumped parameter region is to be thought of as terminating the quasi-one-dimensional region. Again, u_t is modeled in neither region and only 2.3.2.1 and 2.3.2.2 are applicable. If we now identify the subscript 1 with the state of the quasi-one-dimensional flow and 2 with the lumped parameter side of the interface, the discussion of the remaining physical condition and the interpretation of the terms in 2.3.2.1 and 2.3.2.2 parallels that for the interface between the two-dimensional and the quasi-one-dimensional regions. The mechanical condition is therefore 2.3.2.6 for transfer from the lumped parameter region and 2.3.2.5 for transfer to the lumped parameter region, both being replaced by $|u_{n_1}| = c$ if they yield supersonic flow.

When the lumped parameter region connects two or more quasi-one-dimensional regions, the use of 2.3.2.5 and 2.3.2.6 results in an overall pressure loss as gas flows from one quasi-one-dimensional region,

through the lumped parameter region, and into another quasi-one-dimensional region. It is easy to see that the magnitude of the loss is influenced directly by the value of u_n used to characterize the lumped parameter region.

Consider the situations illustrated in the sketch below. In (a)

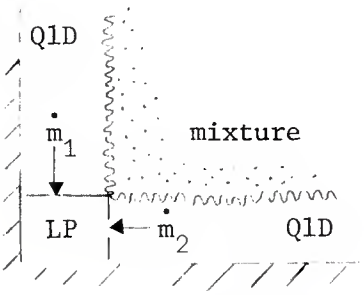

(a) Lumped parameter region interfacing radial ullage with axial ullage at end of charge

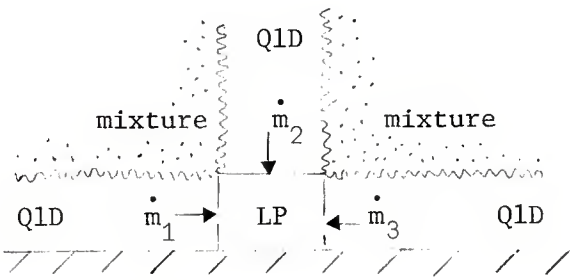

(b) Lumped parameter region interfacing radial ullage with axial ullage between bags.

we show the computational configuration which may arise at a corner of a bag near a corner of the combustion chamber. Each side of the mixture region is shown as bounded by a region of quasi-one-dimensional flow which is to be thought of as single-phase in the present discussion. The two quasi-one-dimensional regions are linked by a lumped parameter region. The normal fluxes $\dot{m}_1$ and $\dot{m}_2$ have been represented in the sketch by arrows which correspond to positive values, that is to say, transfers into the lumped parameter region. In case (a), the value of u_n in the lumped parameter region is assumed to be determined entirely by the velocities of the external boundaries. For $\dot{m}_1$, therefore, we characterize the lumped parameter region by a normal velocity equal to zero since there are no moving radial boundaries. For $\dot{m}_2$, however, the lumped parameter region may be characterized by a nonzero normal velocity, provided that the terminating axial boundary is the base of the projectile.

By considering a steady flow around the corner, in which case one of $\dot{m}_1$ or $\dot{m}_2$ must be negative, it is easy to see that the use of 2.3.2.5 and 2.3.2.6 introduces a pressure loss. Our present choice of the mechanical boundary conditions has been motivated strongly by this fact which stems from the dependence of the mechanical condition on the direction of the flux. The present choice should be viewed as interim, however, since an experimental determination of the flow losses is expected to be made at BRL. When such data become available, the present theoretical estimate of the flow loss will be superseded.

In (b) we consider a lumped parameter region associated with the axial ullage which may separate two bags of propellant. Again, the arrows associated with the fluxes $\dot{m}_1$, $\dot{m}_2$ and $\dot{m}_3$ indicate positive values. With regard to $\dot{m}_2$ we characterize the lumped parameter region with the value $u_n = 0$. But for $\dot{m}_1$ and $\dot{m}_3$ we use

$$u_{n,LP} = \frac{\dot{m}_1 - \dot{m}_3}{\frac{\partial \dot{m}_1}{\partial u_{n_1}} - \frac{\partial \dot{m}_3}{\partial u_{n_3}}} \qquad 2.3.2.7$$

It is easy to see that this choice induces a pressure loss for the part of the net flux which is turning either of the bag corners. However, gas transferred from left to right without turning the corner does not contribute to a pressure loss. In the limit, if the bags are in contact and the flow area is continuous from the left-hand radial ullage region to the right-hand region, 2.3.2.7 yields a continuous pressure field. The lumped parameter region is collapsed in this case.

An even more complex situation exists when the quasi-two-dimensional analysis is in effect. The axial ullage between two bags may be intercepted by as many as six gas streamlines. On each side one has the external ullage, the main charge and the internal ullage or the centercore. While we defer, to the next section, the discussion of the mechanical boundary condition associated with a two-phase region, we may note that we use the obvious generalization of 2.3.2.7 to characterize u_n in the lumped parameter region in such a case.

2.3.3 Internal Boundary Conditions Involving the Mixture

In the present model the boundary of each region occupied by a bag of propellant is represented explicitly and, from a macroscopic perspective, these boundaries are seen to be accompanied by discontinuities of porosity. The discontinuities in porosity, in turn, induce discontinuities in the properties of the gas-phase whenever there is a normal flux. In addition, we view the influence of the bag itself as a surface phenomenon within the macroscopic framework of the model. The bag has properties of reactivity, impermeability and mechanical strength which we embed within the boundary conditions which couple the two-phase flow in each mixture region to the flow in neighboring regions. These neighboring regions may be single-phase and either two-dimensional or quasi-one-dimensional as when the bag is bounded by ullage, or they may be two-phase and quasi-one-dimensional, as when the neighboring region is a centercore charge or they may be two-phase and two-dimensional, as when the neighboring region is another bag of propellant.

The boundary conditions involving the mixture differ from those described in the previous final report in certain minor ways. First, we consider herein that the molecular weight and the ratio of specific heats are functions of composition. The transport across internal boundaries may be assumed to occur without chemical change so that these properties of the gas are simply transferred from one side to the other. However, we also must make an allowance for the change in composition, during transfer, when reactive substrates of the bag yield gas which is assumed to be mixed, without chemical reaction, to the gas being transported through the boundary. Second, we consider, in the present work, that the bag has a finite thickness. This does not affect the internal boundary conditions which may be viewed as quasi-steady balances of mass, momentum and energy, but we are required to discuss the implications of finite bag thickness insofar as it is recognized by the model. Third, in contrast to the previous code version,[2] we do not assume that a reactive section of the bag is fully permeable. This point requires some discussion in order to clarify the code conventions which apply in such a case. Finally, we must comment on the case when one bag is in contact with another so that two layers of bag material separate the two mixture regions.

Our discussion of the boundary conditions involving the mixture is provided in three subsections. First, we discuss in purely physical terms the manner in which each of the bag attributes is embedded into the model and explain the conventions which have been adopted in the code. Second, we discuss some of the implications of our basic assumption that the bag can be viewed as an attribute of the boundary of the mixture. Finally, we tabulate the equations which apply to each of the phases at a mixture boundary. These equations constitute all the relevant physical principles. It will be obvious that they are fewer in number than the state variables which characterize each side of the internal boundary. Mathematical closure follows from the structure of the governing equations themselves as is discussed briefly in chapter 3.0.

2.3.3.1 Properties of the Bag

The properties of the bag which we discuss in the present section are reflected in the model as attributes of the boundary of each mixture region defined by an increment of the main charge. Motion of the bag independently of that of the solid propellant on the mixture boundary is not considered. We defer the discussion of some of the implications of this assumption to the next section.

Here we simply review the physical role played by each of the bag properties as attributes of the boundary and explain certain conventions which have been adopted within the code.

Reactivity

Some of the components of the bag are reactive. For example, the basepad which may be sewn to the rear face of a bag may contain either black powder or a clean burning igniter material. The thickness of the basepad, measured in a direction normal to the surface of the bag, is comparable to the dimensions of a typical propellant grain. Hence, the generation of products of combustion by the basepad is strongly localized and may be viewed as occurring on the exterior surface of the bag.

At present we do not provide a detailed combustion model of the basepad. The rate of generation of combustion products is assumed to be predetermined and specified in tabular form. We treat similarly the exothermic reaction associated with a centercore igniter tube, if one is present. The tube is viewed as a substrate of the bag, the rate of mass generation is assumed to be predetermined and is assumed, by convention, to occur on the outer face of the bag, which is the inner face of the centercore tube. This convention expresses the assumption that reactivity of the centercore tube is to be stimulated by the combustion of the centercore igniter charge. In the event that reactivity of the tube is stimulated by the combustion of the main charge, it would be appropriate to assume that the mass generation occurred on the inner face of the bag, which is the outer face of the centercore tube. A model extension to permit reactivity attributed to either side of the bag is not difficult to incorporate, but has been deferred for future work. For the present, it should be noted that the reactivity of the igniter tube is expected to play a significant role in respect to the path of flamespreading only when it is stimulated by the centercore charge. If the main charge is already burning, the location of the mass generation associated with the centercore tube is expected to be of relatively minor interest.

Of course, the question of which side of the bag the mass generation is to be attributed to is only of physical interest when the bag resists penetration by the gas phase. This will become clearer below when we discuss the flow resistance of the bag. First, however, we discuss the attribute of bag thickness.

Thickness

In contrast to our previous work,[2] we incorporate a representation of the thickness of the bag. The significance of this attribute is simply that it allows a more precise representation of the initial porosity of the main charge within the bag and, through coupling to the reactivity, it permits a representation of a potentially important contribution to the ullage on a time-dependent basis.

If θ is the thickness of the bag at any point, $\dot{m}_s$ is the rate of mass generation due to surface reactivity, and ρ_s is the density of the solid-phase responsible for the reactivity, then

$$\dot{\theta} = \frac{\dot{m}_s}{\rho_s} \qquad 2.3.3.1$$

Impediment to Gas-Phase

The composition of the bag may vary from point to point along the surface. Some parts of the bag may consist only of cloth which may be relatively permeable to the gas-phase, even prior to decomposition and rupture. Other parts of the bag may be completely impermeable as long as they retain their structural integrity. For example, the bag may have a lead foil liner wrapped around the outer circumference. If a centercore tube of nitrocellulose is present, it, too, represents an initially impermeable boundary. Of course, with progressive decomposition due to combustion or thermal attack, or as a result of purely mechanical forces, an initially impermeable section will be expected to weaken and become fully permeable.

At present we characterize the flow resistance of each section of the bag by a dimensionless friction factor K with the convention that a normal flux induces a pressure drop in the form $\Delta p = (K\rho/g_o)u_n|u_n|$ where ρ is the density of the gas inside the bag and u_n is the normal velocity of the gas, relative to the boundary, taken to be positive when the flow is directed outward. Hence Δp is understood to be positive for an efflux and negative for an influx. The friction factor K may be time-dependent as a consequence of rupture of the bag as we discuss subsequently.

When the flow resistance of the bag is taken into consideration, the convention that the reactivity of the bag is associated with an exterior surface flux becomes significant. If a section of the bag is both reactive and impermeable, so that $K \to \infty$, then evidently the finiteness of Δp requires $u_n \to 0$, whereupon the products of decomposition of the bag are vented completely to the exterior of the bag. As $K \to 0$, the surface flux may be vented to both sides of the bag, the ratio of the inward to the outward contributions being influenced by the pressure field on each side of the bag as well as the value of K.

Impediment to Solid-Phase

Until rupture occurs, the outer circumferential boundary of the bag impedes radial expansion of the solid-phase. We do not attempt

to model the elasticity of the outer circumference of the bag. We assume that it offers no resistance to compression. However, we also assume that it cannot be dilated beyond its initial diameter without being ruptured. Similarly, if a centercore tube is present it, too, provides an impediment to radial motion of the main charge. In contrast to the outer circumference, however, the centercore tube is assumed to resist both compression and expansion until it is ruptured.

With regard to the endwalls of the bag, however, we simply neglect the possible confinement of the charge due to the inextensibility of the bag. In contrast to the sidewalls, the endwalls are initially planar. Since the material behaves like a membrane, when loaded, its resistance to normal motion is negligible in its initial condition. Only when local curvature has been established in the endwalls can the tensile stresses in the constituent fibers develop components of force in the axial direction. Whereas the confinement imposed by the sidewall can be evaluated from a simple consideration of the local diameter of the bag, that due to the endwall requires a consideration of the state of deformation of the entire bag. For, if we suppose the existence of stresses within the surface of the endwall, these must be transferred to the sidewall and then communicated over the length of the bag to the opposing endwall.

In considering the impediment of the bag to motion of the solid phase, it should perhaps be noted that its impermeability is an important factor. The solid phase is expected to be dispersed not only by the action of forces transmitted from grain to grain, but also by the gas dynamic processes of pressure gradient and drag. Taking the bag to be impermeable eliminates the possible contribution of drag to the local expansion of the bed.

Structural Integrity

At present only mechanical failure of the bag is modeled. Undoubtedly, thermal attack and chemical decomposition play important physical roles in respect to the destruction of the bag. However, the modeling of these latter processes is deferred for future work.

As discussed previously, if a centercore tube is present, it is assumed to resist radial deformation until it ruptures. Rupture of the centercore tube is assumed to occur when a predetermined value of the absolute value of the difference between the stress on the outside and the stress on the inside is exceeded. Thus the rupture strength of the centercore is taken to be the same in expansion and in compression. By stress we mean here the sum of the contributions of gas pressure and intergranular stress.

As far as the outer circumferential boundary and the endwalls are concerned, however, we assume that rupture can occur only as a consequence of an excess of the internal stress over the external stress, stress being understood to have the same meaning as in the previous paragraph. This assumption follows from the observation that the bag material offers no resistance to inward compression. Thus, excessive external pressure is assumed to result in a collapse of the bag material onto the solid-phase inside the bag with the result that the load is supported by intergranular stresses rather than by stresses within the bag fibers.

2.3.3.2 Implications of Representation of Bag as an Attribute of the Boundary of the Charge

Our treatment of the bag as an attribute of the boundary of the propelling charge involves certain assumptions which we must keep in mind. First, it is clear that slip of the solid-phase relative to the bag is not considered. Second, if the bag is locally compressed and then, due to changes in the local pressure, begins to dilate, we do not consider the possible separation of the cloth from the propelling charge; the diameter of the bag remains equal to the local diameter of the bed. To be useful, the present model should only be applied to cases in which the bag properties vary relatively weakly by comparison with typical relative displacements of the propellant bed prior to rupture. Moreover, the potential flow channel induced by bag separation prior to rupture must not be extensive.

As with the analysis of direct confinement of the solid phase by the endwalls, the effects of relative slip and of normal separation require a detailed representation of the displacement field of the entire bag.

It should be kept in mind that if the bag is specified as having finite thickness, the volume occupied by the bag will increase as the charge extends axially since there is not, at present, any coupling between bag thickness and axial strain. This may possibly result in an overestimate of maximum chamber pressure.

A similar consideration applies to sidewall reactivity which is specified as rate of mass generation per unit area. Coupling of the flux to the deformation of the charge is not at present modeled, although such extensions are planned for future efforts.

2.3.3.3 Analytical Statement of Boundary Conditions

Mathematically, we express the influence of the bag within the physical boundary conditions which link the flow within each two-phase mixture region to that in the region outside the bag. We adopt the following convention. We label state variables on the mixture boundary inside the bag by a subscript 1. The state variables in the region outside the bag are labeled by a subscript 2. We assume that the exterior region may also be two-phase so that we must consider the possibility of intergranular stresses in the exterior region and, moreover, we cannot assume $\varepsilon_2 = 1$.

However, only one layer of bag material--which may consist of several substrates, in principle--is assumed to separate the two regions. Thus, if the exterior region is two-phase, it corresponds physically to the centercore igniter charge and not to another increment of the main charge. The boundary conditions which apply when one increment is in contact with its neighbor so that the two mixture regions are separated by two layers of bag material--one for each increment--may be thought of as following from the subsequent equations in the limit as each of the mixture regions is made compatible with an intervening layer of ullage whose transverse dimension becomes vanishingly small. This, in fact, is the basis for the method of numerical solution discussed in the next chapter, and an explicit statement of the limiting conditions is therefore not required.

When the boundary element pertains to the main charge, we always assume that the normal velocity of the boundary is equal to that of the solid-phase. The same physical principles which govern the boundary values of the main charge apply also to the ends of the centercore charge. In respect to the latter, however, we do not assume, as in previous work,[2] that the normal component of the solid-phase is equal to that of the boundary. In the present version of the code, we have allowed for the possibility of an efflux of the centercore solid-phase from the ends of the tube under certain conditions. We will return to this point at the conclusion of the present section, following the statement of the boundary conditions which apply to the main charge.

We denote the normal component of the gas-phase velocity by u_n which is understood to be positive in the outward direction. In other words a value $u_{n_1} > 0$ implies an efflux of gas from the mixture region.

The reactivity of the bag is characterized by a rate of mass generation per unit area, $\dot{m}_s$, a chemical energy, e_s, which is positive if the reaction is exothermic and negative if the reaction is endothermic, and by a molecular weight, M_{w_s}, and specific heats c_{p_s}, c_{v_s}, at constant pressure and volume, respectively. The resistance to penetration by the gas-phase is characterized by a dimensionless friction factor K, as was previously noted.

We may now tabulate the physical boundary conditions.

Gas-Phase Mass Balance

$$\varepsilon_1 \rho_1 u_{n_1} + \dot{m}_s = \varepsilon_2 \rho_2 u_{n_2} \qquad 2.3.3.2$$

Gas-Phase Energy Balance

$$\varepsilon_1 \rho_1 u_{n_1} \left(e_1 + \frac{p_1}{\rho_1} + \frac{u_{n_1}^2}{2g_o}\right) + e_s \dot{m}_s = \varepsilon_2 \rho_2 u_{n_2} \left(e_2 + \frac{p_2}{\rho_2} + \frac{u_{n_2}^2}{2g_o}\right) \qquad 2.3.3.3$$

Gas-Phase Tangential Momentum Balance

$$\varepsilon_1 \rho_1 u_{n_1} u_{t_1} = \varepsilon_2 \rho_2 u_{n_2} u_{t_2} \qquad 2.3.3.4$$

Gas-Phase Molecular Weight

$$\frac{\varepsilon_1 \rho_1 u_{n_1}}{M_{w_1}} + \frac{\dot{m}_s}{M_{w_s}} = \frac{\varepsilon_2 \rho_2 u_{n_2}}{M_{w_2}} \qquad 2.3.3.5$$

Gas-Phase Specific Heat

$$\varepsilon_1 \rho_1 u_{n_1} c_1 + \dot{m}_s c_s = \varepsilon_2 \rho_2 u_{n_2} c_2 \qquad 2.3.3.6$$

where $c = c_p$ or c_v.

Gas-Phase Normal Momentum Balance

$$p_1 + \frac{\varepsilon_1 \rho_1}{g_o} u_{n_1}^2 - \frac{K\rho_1}{g_o} u_{n_1} |u_{n_1}| = p_2 + \frac{\varepsilon_2 \rho_2}{g_o} u_{n_2}^2 \qquad 2.3.3.7$$

Solid-Phase Normal Momentum Balance

The following equation applies only on flexible sections of the bag:

$$\sigma_1 - \sigma_2 = \begin{cases} -\frac{K\rho_1}{g_o} u_{n_1} |u_{n_1}| & \text{if } u_{n_1} < 0 \\ 0 & \text{if } u_{n_1} \geq 0 \end{cases} \qquad 2.3.3.8$$

On a section of the external circumferential boundary at which the bag is locally dilated to its initial radius, or on a section of the rigid centercore tube, 2.3.3.8 is replaced by

$$\vec{u}_p \cdot \vec{n} = 0 \qquad 2.3.3.9$$

Finally, we have the following expression for the stress supported by the bag:

$$F_{bag} = \begin{cases} \sigma_1 - \sigma_2 + \frac{K\rho_1}{g_o} u_{n_1} |u_{n_1}| & \text{if section rigid or if flexible and } u_{n_1} > 0 \\ 0 & \text{if flexible and } u_{n_1} < 0 \end{cases} \qquad 2.3.3.10$$

Equation 2.3.3.10 permits the determination of bag failure as a consequence of overpressure. Each point on the bag is characterized initially by a value K_o of the friction factor and a value σ_{bag} of the stress differential that the bag can support. When $F_{bag} \geq \sigma_{bag}$, locally, on the outer circumferential boundaries or the endwalls, or when $|F_{bag}| \geq \sigma_{bag}$ on the rigid centercore tube, we assume that failure occurs at the point in question. The flow resistance friction factor K is taken to be equal to the local value of K_o until

rupture occurs and is then taken to decrease to zero linearly with time over an interval t_{rupt} which may vary from point to point.

Equation 2.3.3.4 expresses the assumption that there is no surface source of momentum of the gas phase. In fact, this assumption may be difficult to support when it is considered that the jump conditions are only meaningfully applied to points separated by a distance which is large by comparison with the scale of heterogeneity of the mixture. As we have discussed previously,[2] a significant loss of tangential momentum can be experienced by gas entering the mixture as it penetrates a depth equal to a typical particle diameter. However, a priori criteria are not presently available for the determination of such losses and their representation as surface effects within the macroscopic formulation. Accordingly, we retain the previously developed estimate of the tangential momentum loss in the present version of the code. As described previously,[2] our motivation in including the tangential momentum loss for flow entering the mixture has been one of providing a better-posed computational problem.

As in the case of the conditions linking regions of ullage, it should be kept in mind that the state variables labelled with subscript 2 are not necessarily explicitly modeled quantities and that they must therefore be interpreted with some care.

Computational experience shows the pressure jumps to be almost always negligible during the quasi-two-dimensional phase of the calculation. Accordingly, as in the previous version of the code,[2] we assume continuity of pressure across all the interfaces during the quasi-two-dimensional phase.

It remains to comment on the boundary conditions pertinent to the igniter solid-phase at the ends of the centercore tube. Consistently with the overall treatment of the bag, the ends of the centercore tube are assumed to move with the corners of the contiguous main charge mixture region. In the previous version of the code, we imposed the boundary condition that the centercore solid-phase move with the ends of the tube.

This assumption, which was made for the sake of simplicity of coding, has been relaxed to a certain extent in the present version of the code. At the extreme ends of the charge we allow, as an option, efflux of the solid-phase from the centercore. Once ejected from the extreme ends of the centercore tube, the solid-phase igniter charge is assumed to play no further role of significance in respect

to either flamespreading or the overall ballistics of the charge. At adjacent ends of the centercore tubes associated with successive increments, we allow the possibility, as an option, of efflux of the solid-phase from one centercore tube and influx into the neighboring tube. The transfer is assumed to occur without losses, independently of the spacing between the increments, provided that both tubes have been described to the code as permeable to the solid-phase. If only one tube has been described as permeable to the solid-phase at the bag-to-bag interface, efflux may occur, but the solid-phase so ejected will be lost from the subsequent calculation.

3.0 METHOD OF SOLUTION

Although there are significant differences between the present version of TDNOVA and that described in the previous report,[2] the method of solution is fundamentally the same. The mathematical problem to be solved consists of a system of partial differential equations subject to initial and boundary conditions. The boundary conditions are both external, namely those which pertain to points on the container--the spindle, the tube wall and the projectile base--and internal, namely those which pertain to points on the boundaries between contiguous regions.

As in the previous version of the code, we always transform each region onto a regular figure. A quasi-one-dimensional region is transformed onto a unit line. A two-dimensional region is transformed onto a unit square. Because the regions move, the transformation to a regular figure is necessarily time-dependent. In section 3.1 we discuss the manner in which the transformation is effected and we also describe the manner in which the finite difference mesh is established for the various regions.

In section 3.2 we discuss the procedures according to which the partial differential equations are discretized so as to yield an integration scheme based on the method of finite differences. The discussion of section 3.2 distinguishes among mesh points located in the interior, on the boundaries, and at the corners of the computational regions. We conclude, in section 3.3, with some comments on special topics and numerical devices which have been incorporated into the present version of the code.

In the previous report we tabulated explicitly the forms taken by the differential governing equations following the transformation of coordinates.[2] These are not repeated here. Neither do we state explicitly the forms taken by the governing equations for the molecular weight and the specific heats. Although these are not available from Reference 2, they are easily derived.

A second level of transformation of coordinates is used in connection with the method of solution at points lying on the boundaries, both internal and external. The transformation to characteristic forms is discussed in detail in Reference 1, the algebraic results are summarized in Reference 2, and here we simply comment on the relevance of these results in the context of the determination of the boundary values. We also direct the reader to Reference 2 for a full discussion of those special devices which are unchanged in the present version of the code.

3.1 Mesh Allocation and Computational Coordinate Scheme

Two separate mesh allocation schemes are encoded into TDNOVA. The first of these, referred to as the static mesh allocation mode, assigns a fixed number of mesh points to all regions. Only the propelling charge increments are treated as two-dimensional. Regions of ullage are represented as quasi-one-dimensional or as lumped parameter. Once flamespreading and bag rupture are complete and the radial pressure gradients have subsided to within a user-selectable tolerance, the problem will be transformed to a quasi-two-dimensional representation. The second scheme, referred to as the dynamic mesh allocation mode, assigns varying numbers of mesh points to the regions of ullage as the problem evolves. The number of points allocated to a given region of ullage depends on its size relative to the overall chamber dimensions. Moreover, regions of ullage may be treated as fully two-dimensional as well as quasi-one-dimensional and lumped parameter. In contrast to the previous code version, we do not admit a transformation to a quasi-two-dimensional representation within the dynamic mesh allocation mode.

The overall approach to both the static and the dynamic mesh allocation modes may be summarized as follows. A fixed complement of mesh points is assigned to each propelling charge increment. These are initially distributed uniformly over each of the segments which define each boundary element. Subsequently, they move in a fashion determined by the overall motion of each increment as we describe in section 3.1.4. By projecting points on the boundaries of the propelling charge regions along lines of fixed radial or axial location, according as we are dealing with the endwalls or the circumferential boundaries respectively, we may define mesh point locations for the various regions of ullage. Thus, in all cases in which an internal boundary is involved, the mesh points on either side of the boundary coincide in pairs, thereby facilitating the determination of boundary values.

The scheme described in the preceding paragraph defines the boundary locations of the mesh for two-dimensional regions. The algorithm of Thompson et al[19] is used to construct the interior distribution. As a consequence of the transformation of coordinates, the independent variables become ζ and η rather than z and r. In general ζ tends to be a z-wise coordinate and η tends to be an r-wise coordinate.

---

[19] *Thompson, J. F., Thames, F. C. and Mastin, C. W.*
"Automatic Numerical Generation of Body-Fitted Curvilinear Coordinate System for Field Containing Any Number of Arbitrary Two-Dimensional Bodies"
J. Comp. Phys. 15, *pp. 299-319.* *1974*

Each propelling charge increment is assumed to be described, at all times, by four boundary elements each of which has a continuously turning tangent. In most cases of practical interest, the boundary elements are initially straight and consist of the rear and forward endwalls and the inner and outer circumferential boundaries. The rear endwall is taken to be a computational boundary defined by $\zeta = 0$ while the forward endwall is characterized by $\zeta = 1$. Similarly, the inner and outer circumferential boundaries correspond to $\eta = 0$ and $\eta = 1$, respectively.

The two-dimensional mesh in the propelling charge always involves a total of INDIMZ ζ-points and INDIMR η-points. The distribution of these points along each of the boundary elements is at the discretion of the user subject to certain constraints at the bag-to-bag interfaces. If freedom of allocation is given to the code, the minimum mesh spacing will be maximized on each boundary element subject to the constraints imposed by the user.

The allocation of the INDIMZ ζ-points to the various increments of the charge is made, once and for all, on the basis of their relative initial lengths and is not subject to the discretion of the user.

The external boundaries are defined similarly to the boundaries of the propelling charge and are assumed to consist of four elements, each of which has a continuously turning tangent. The elements are, in order of correspondence to their counterparts on the propelling charge boundary, the breechface, the projectile base, the tube centerline and the tube wall.

It is important to note that, in its present configuration, TDNOVA requires that the values of r increase monotonically on the breechface and projectile base and that the values of z increase monotonically on the tube centerline and the tube wall.

In section 3.1.1, we provide further details of the static mesh allocation mode, and in 3.1.2, we describe the manner in which a transformation to a quasi-two-dimensional representation is effected. In section 3.1.3 we describe the dynamic mesh allocation mode. In section 3.1.4 we describe the two-dimensional mapping algorithm and provide additional details concerning the time dependence of the distributions on the boundaries.

3.1.1 Static Mesh Allocation Mode

Figure 3.1 illustrates the region representations corresponding to the static mode in both the two-dimensional and quasi-two-dimensional phases of the calculation. Initially, the representation is always as in Figure 3.1(a). The transformation to the quasi-two-dimensional representation, Figure 3.1(b), occurs at most once during the calculation and is irrevocable.

2D2P - Two-Dimensional, Two-Phase
Q1DA - Quasi-One-Dimensional, Axial (Single- or Two-Phase)
Q1DR - Quasi-One-Dimensional, Radial
LP - Lumped Parameter

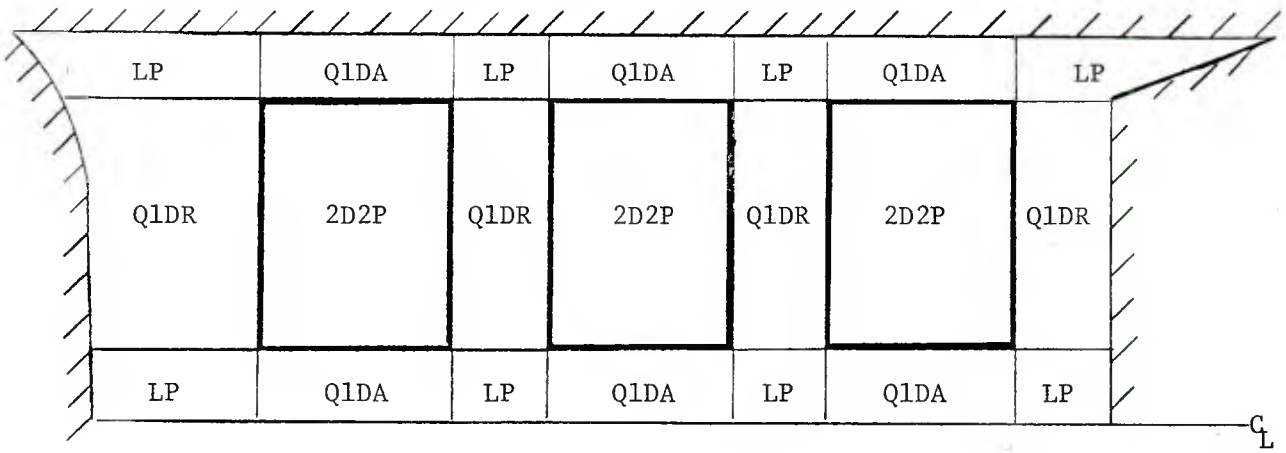

(a) Two-Dimensional Representation

Q1DA - Quasi-One-Dimensional, Axial (Single- or Two-Phase)
LP - Lumped Parameter

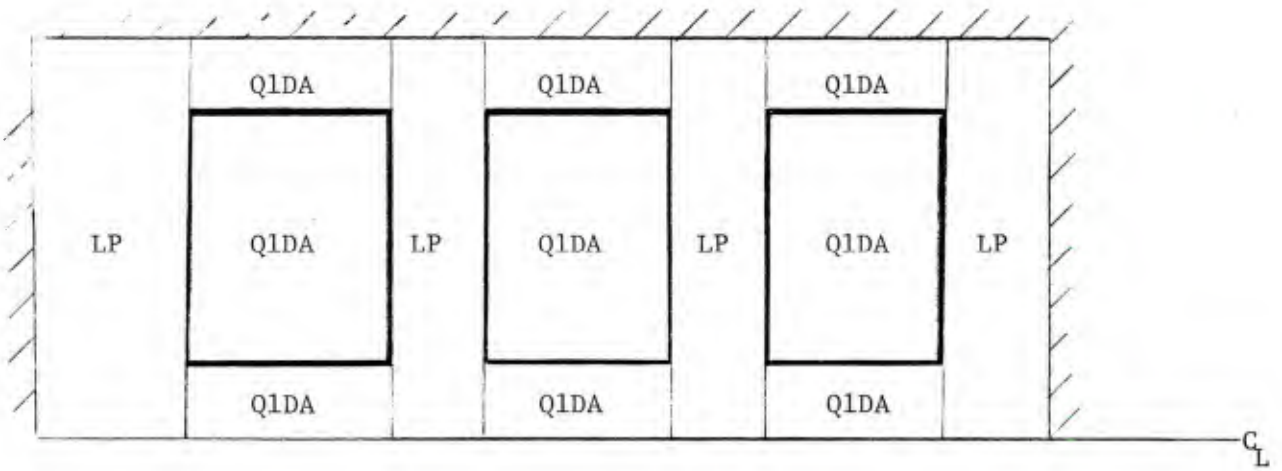

(b) Quasi-Two-Dimensional Representation

Figure 3.1 Two-Dimensional and Quasi-Two-Dimensional Representations Associated with Static Mesh Allocation Mode

As we see in Figure 3.1(a), during the two-dimensional part of the calculation, each region of ullage contiguous with a mixture boundary element is represented as quasi-one-dimensional, and each corner region of ullage is represented as lumped parameter. The distribution of mesh points in each quasi-one-dimensional region is controlled by the distribution of points on the boundary element of the propelling charge increment with which it is contiguous. For example, all mesh points in the region of ullage bounded by the breechface and rear endwall of the first bag are defined by r-coordinates identical with their counterparts on the rear endwall of the bag. But, for convenience in the tabulation of the solutions, the preparation of plots, and the determination of flow cross-sections, the z-coordinates are selected so as to place the mesh points on the breechface. Similarly, the mesh points corresponding to the ullage in front of the propelling charge are formally located on the projectile base, those corresponding either to radial ullage interior to the propelling charge or to a centercore igniter, are placed on the tube centerline, and those corresponding to radial ullage exterior to the propelling charge are placed on the tube wall.

The single point corresponding to each of the lumped parameter corner regions at the ends of the charge is located formally on the appropriate corner of the external boundary in the static mesh allocation mode. The point corresponding to a corner region associated with a bag-to-bag interface is co-located with the point which terminates the left-hand region of radial ullage contiguous with the corner region.

Figure 3.2(a) indicates the manner in which the mesh points are allocated in the regions of axial ullage between bags. First, we observe that the radial coordinates of each corresponding pair of mesh points on the mixture boundaries, except for those at corners, are made to coincide. Only the axial coordinates differ. Second, the mesh points in the ullage coincide with those on the forward face of the left-hand increment, except possibly at the corners. Let r_{i_1} and r_{i_2} be the radial coordinates of the inner corners of the two mixture boundaries. Then the inner endpoint of the radial ullage is located at max (r_{i_1}, r_{i_2}). Similarly, if r_{o_1}, r_{o_2} are the radial coordinates of the outer corners of the mixture boundaries, the outer endpoint of the ullage is located at min (r_{o_1}, r_{o_2}).

The advantage of this approach is that radial interpolation is not required in order to determine updated boundary values at the bag-to-bag interfaces. The solution may be determined locally for each radial location. Two restrictions are evidently associated with the approach. First, since there is no radial flow resolution in the region between each pair of outer and inner mixture corners, the

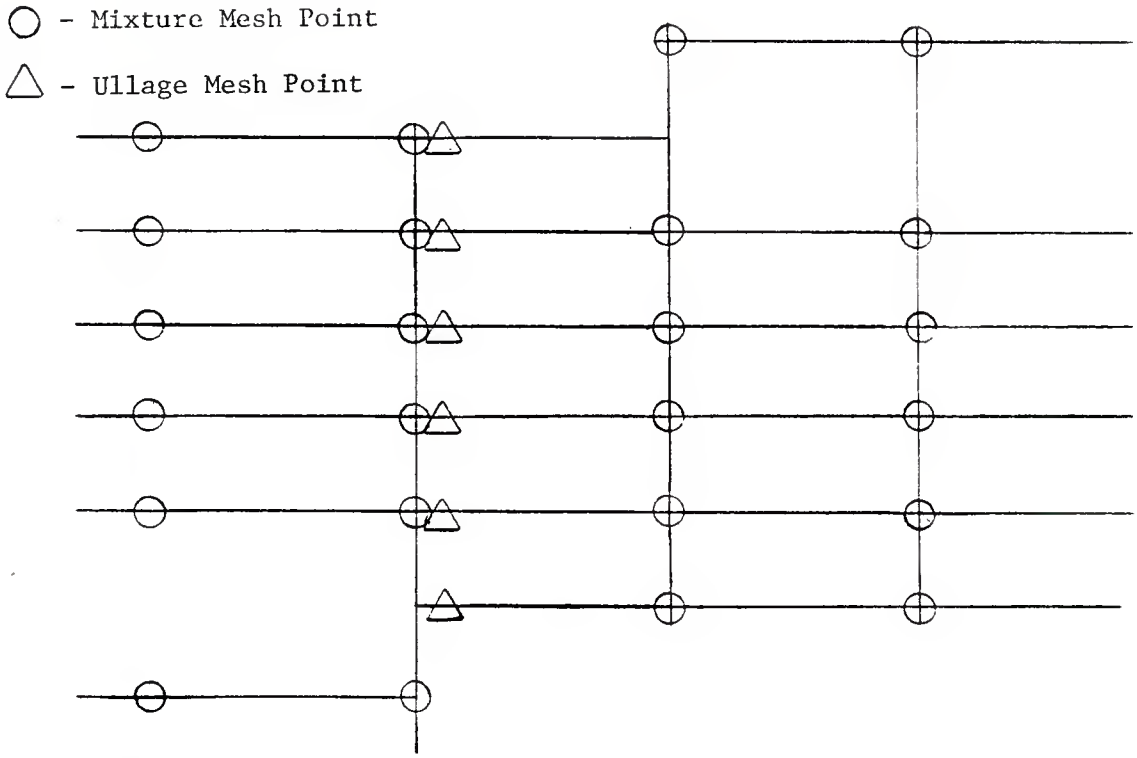

(a) Mesh at Bag-to-Bag Interface in Static Allocation Mode

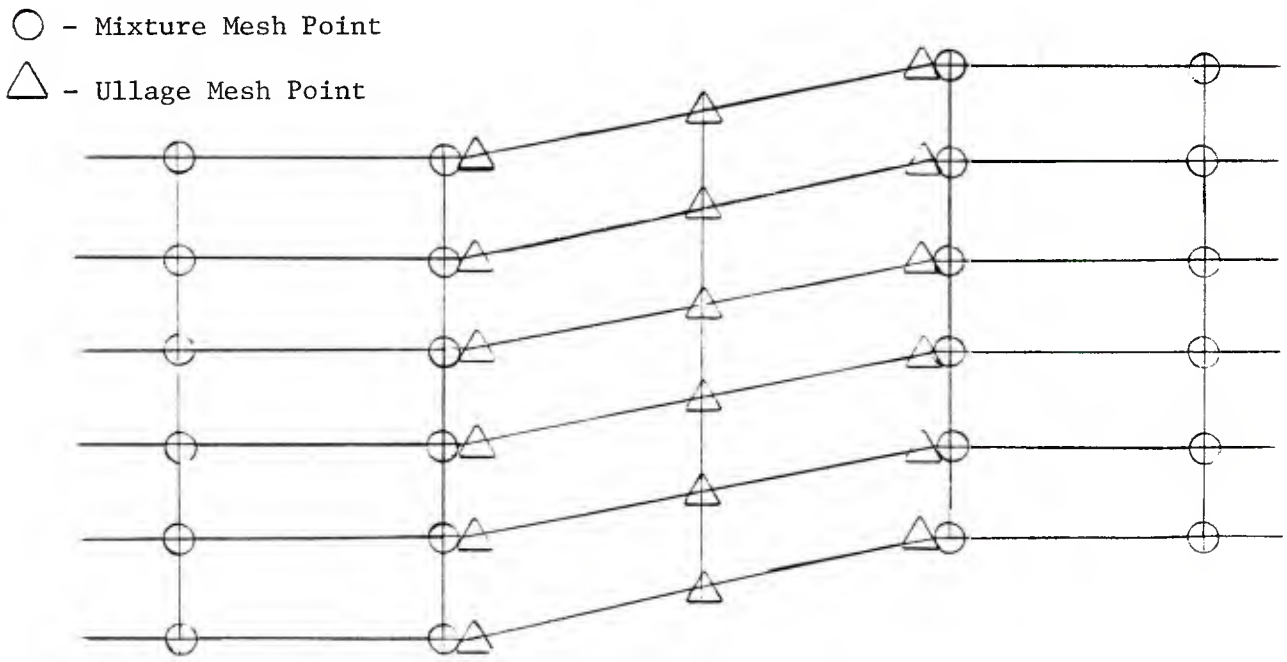

(b) Mesh at Bag-to-Bag Interface in Dynamic Allocation Mode

Figure 3.2 Mesh Configurations at Bag-to-Bag Interfaces

increments must be of nearly the same diameter throughout the calculation or accuracy will be compromised. This is not thought to be a severe constraint when the macroscopic basis of the present model is considered. However, the user should keep it in mind. Second, whereas the user has essentially arbitrary control over the initial distribution of mesh points along the increment boundaries, the distributions are obviously constrained to coincide radially at the bag-to-bag interfaces.

An additional point to note is the following. The flow through the regions of axial ullage--both at the ends of the charge and between increments--is assumed always to be essentially radial so that the normal section of the flow is always captured adequately by a surface on which r = constant. Similarly, the flow through the inner and outer radial ullage regions is assumed to be sufficiently close to axial that the flow sections can be described as surfaces of constant z.

We also note that in the static mesh allocation mode, a total of (INDIMZ + NBAGS + 1)(INDIMR + 2) mesh points is used to describe the flow, where NBAGS is the number of increments. At present TDNOVA supports a maximum of 333 mesh points.

3.1.2 Transformation to Quasi-Two-Dimensional Representation

When the propelling charge has been ignited at all points and all the bags have ruptured completely, the input datum PTOL is used to determine the suitability of a quasi-two-dimensional analysis. At each axial location in the chamber, the difference between the values of pressure at the tube wall and the centerline is divided by the value at the tube wall. If this quantity is less than PTOL at all axial stations, an irrevocable transformation to a quasi-two-dimensional representation is made.

The axial distribution of the propellant is assumed to be defined by the current storage for the line $\eta = 0$ of each increment. Values of the porosity are defined by integrating with respect to η at each ζ-mesh point and normalizing by the local cross-sectional area of the propelling charge. This approach provides values of porosity which satisfy a global mass balance as estimated by a trapezoidal rule. The solid-phase axial velocity field is also defined as an average with respect to η. At each ζ-location, the radial coordinates and velocities of the inner and outer boundaries of the propelling charge are taken to be the values in current storage at $\eta = 0$ and $\eta = 1$ respectively. The intergranular stress and surface regression are taken to be the values corresponding to $\eta = 0$ of each increment.

The rear and forward external boundaries are defined respectively by the intersections of the breechface and projectile base with the centerline of the tube. The gas-phase properties are not averaged with respect to η in the present version of the code. The values used to initialize the quasi-two-dimensional region are taken to be those in current storage for the line $\eta = 0$. Values of the radial component of the gas velocity are, however, saved at both the internal and external circumferential boundaries since these are used in the quasi-two-dimensional representation to define the transverse mass fluxes between the coaxial quasi-one-dimensional flows.

In view of the loss of detail in respect to the ends of the charge increments concomitant to the transformation, the thickness of the bags is subsequently modeled only along the sidewalls of the charge.

Consistently with the previous treatment of the axial ullage at the ends of the charge,[2] we treat the axial ullage between bags as lumped parameter, as may be seen in Figure 3.1(b). It may be desirable at some future time to decompose the axial ullage between the bags so as to distinguish thermal properties in that part which terminates the radial ullage from that part which terminates the propelling charge increments. In regions occupied by the increments of the charge, it should be noted that only the pressure and the intergranular stress are assumed uniform over the cross-section of the tube. The phase velocities, the density, temperature, molecular weight, specific heats and porosity are all allowed to take different values in each of the three coaxial regions of quasi-one-dimensional flow. In the regions of axial ullage, however, the lumped parameter treatment necessarily incorporates the assumption that all the gas-phase attributes are uniform over the cross-section. In the limit as the thickness of the ullage vanishes, it might be desirable to admit some radial structure in respect to temperature, molecular weight and specific heat. Of course, the velocity is not modeled explicitly for the lumped parameter regions. If it were, it would be essential to provide resolution of the radial structure of the velocity within the axial ullage to a degree consistent with the other regions.

3.1.3 Dynamic Mesh Allocation Mode

When the dynamic mesh allocation mode is selected by the user, the allocation of points to the propelling charge increments is identical to that described in connection with the static mode, except possibly at the bag-to-bag interfaces as we discuss subsequently.

The representation of the ullage depends on the input quantities NMPT, ZFRAC and RFRAC as we now describe.

NMPT represents a maximum value for the number of mesh points which may be utilized at any time and is taken to include a minimum contribution of INDIMZ*INDIMR points which are necessarily allocated to the propelling charge.

Consider now the region of ullage contiguous with the rear endwall of the bag. As in the static mesh allocation mode, INDIMR points are allocated to this region for the purpose of resolving the radial structure of the flow. The input quantity ZFRAC is used to establish the necessity of treating this region as two-dimensional rather than quasi-one-dimensional. The region will be treated as two-dimensional if each point on the rear endwall of the bag is located a distance from the breechface which is at least equal to two times ZFRAC times the length of the combustion chamber as a whole, as measured along a line of constant radius. The length of the combustion chamber as a whole is taken to be a measurement along the tube centerline.

Not only the region of ullage contiguous with the rear endwall, but also the corner regions of ullage which terminate it are tested in respect to minimum axial extent since the representation of the corner regions must be consistent with those of the regions with which they are contiguous.

A similar procedure is conducted with respect to the ullage contiguous with the forward endwall of the propelling charge and also with the inner and outer regions of ullage, except that in the latter case, the quantity RFRAC is used and the length of the chamber is replaced by the radius of the tube.

However, a centercore igniter, if present, is always treated as a quasi-one-dimensional flow, independently of NMSH and independently of its lateral dimensions.

The eligibility for two-dimensional representation of the regions of ullage between the increments is, of course, based on the same length criterion as that which we have described in connection with the ullage at the ends of the charge.

When the eligibility of the regions of ullage for treatment in a fully-two-dimensional fashion has been established, mesh points are allocated in such a fashion that the total does not exceed NMPT, that no two-dimensional region of ullage has a mesh spacing normal to the mixture which violates the ZFRAC or RFRAC criterion as the case may be, and so that the minimum mesh spacing is maximized. With regard to the ZFRAC and RFRAC criteria, it should be noted that each two-dimensional region always has a minimum of three mesh points in each direction. It is for this reason that the factor of two is incorporated into the test for minimum extension normal to the propelling charge.

If a region of ullage contiguous with the mixture is determined to be quasi-one-dimensional, its mesh points are distributed in exactly the same fashion as in the static mesh allocation mode. If the region is determined to be two-dimensional and is contiguous, let us say, with the rear endwall, the mesh is allocated as follows.

The boundary of the region of ullage contiguous with the rear endwall of the bag, for which $\zeta = 0$ in the mixture, is taken to be a line of $\zeta = 1$ for the ullage, and mesh points are located with the same z- and r-coordinates as their counterparts on the bag endwall. The points on the breechface become points of $\zeta = 0$ for the mesh in the ullage and are given r-coordinates identical with their counterparts on the ullage boundary $\zeta = 1$. Thus, the lines on which η = constant in the ullage are lines of constant radius. On $\eta = 0$ and on $\eta = 1$, the mesh is specified so as to yield a uniform spacing. The distribution in the interior is determined according to the algorithm described in section 3.1.4.

If the corner region contiguous with the $\eta = 0$ boundary of the ullage region in question is quasi-one-dimensional, its axial distribution of mesh points is governed by those on the $\eta = 0$ coordinate line, but the radial coordinates are chosen so as to place the points formally on the centerline.

If the corner region is two-dimensional, the mesh on its boundary is defined as follows. The distribution on the line $\eta = 1$ of the corner region is identical with that of the line $\eta = 0$ in the region of ullage contiguous with the rear endwall of the bag. The distribution on the line $\zeta = 1$ of the corner region is identical with that on the line $\zeta = 0$ of the region of ullage contiguous with the inner boundary of the bag. To define the distribution on the line $\zeta = 0$ in the corner region, a chord is drawn from the point ($\zeta = 0$, $\eta = 1$) to the corner of the external boundary. A series of equispaced points is defined on this line, and these in turn are projected along lines of constant radius so as to be located on the curved breechface. A similar procedure is conducted at the centerline.

With regard to the manner in which mesh points are distributed at the bag-to-bag interfaces, we note that the procedure is identical to that described for the static mesh if the ullage is quasi-one-dimensional. If, however, the increments separate sufficiently as to justify a two-dimensional representation of the ullage between them, then, as shown in Figure 3.2(b), the mesh points on corresponding sides of bag boundaries are no longer required to have the same radial location.

The procedure we have outlined is conducted in a similar fashion for all the two-dimensional regions of ullage until the mesh has been defined on the boundaries of all two-dimensional regions and completely for all quasi-one-dimensional and lumped parameter regions.

When the number of mesh points assigned to a given region changes, the state variables at the new complement of mesh points are defined by a linear interpolation of the old values. If the old mesh was one-dimensional, the old values are applied uniformly along the freshly introduced coordinate line. Conversely, if the new mesh is one-dimensional, the values are taken to be those corresponding to the coordinate lines adjacent to the mixture or adjacent to the regions of ullage contiguous with the mixture if we are dealing with a corner region.

3.1.4 Two-Dimensional Mapping Algorithm

We first make some general comments concerning the transformation to computational coordinates so as to clarify the nomenclature. Next, we discuss the method of determining the distribution of mesh points in the interior of each two-dimensional region. Finally, we clarify the time-dependence of the distributions on the boundaries of the charge increments and note the finite difference formula used to determine the components of velocity of the mesh in the interior.

In general, we are concerned with a transformation which we may represent by:

$$\tau = t \qquad 3.1.4.1$$

$$\zeta = \zeta(z,r,t) \qquad 3.1.4.2$$

$$\eta = \eta(z,r,t) \qquad 3.1.4.3$$

where t is the time and z and r are the usual axial and radial cylindrical coordinates. By introducing τ we facilitate the representation of partial derivatives, for ϕ_t will be understood to mean a derivative of ϕ with respect to time with z and r held constant while ϕ_τ will represent a derivative with respect to time in which ζ and η are held constant.

We assume that the transformation 3.1.4.1-3.1.4.3 is one-to-one, has continuous partial derivatives, and that the Jacobian determinant

$$\frac{\partial(\zeta,\eta)}{\partial(z,r)} = \zeta_z\eta_r - \eta_z\zeta_r \qquad 3.1.4.4$$

never vanishes. Then the inverse transformation may be assumed to exist such that

$$t = \tau \qquad 3.1.4.5$$

$$z = z(\zeta,\eta,\tau) \qquad 3.1.4.6$$

$$r = r(\zeta,\eta,\tau) \qquad 3.1.4.7$$

Let J be the Jacobian determinant corresponding to the inverse transformation

$$J = \frac{\partial(z,r)}{\partial(\zeta,\eta)} = 1/(\frac{\partial(\zeta,\eta)}{\partial(z,r)}) \qquad 3.1.4.8$$

Then we note the following useful relationships between the forward and inverse transformation derivatives:

$$\zeta_r = - z_\eta/J \qquad 3.1.4.9$$

$$\zeta_z = \quad r_\eta/J \qquad 3.1.4.10$$

$$\eta_z = - r_\zeta/J \qquad 3.1.4.11$$

$$\eta_r = \quad z_\zeta/J \qquad 3.1.4.12$$

We may also introduce the velocity components of a point which is fixed in the computational plane by writing

$$u_m = z_\tau \qquad 3.1.4.13$$

$$v_m = r_\tau \qquad 3.1.4.14$$

where z and r are understood to be defined functionally by 3.1.4.6 and 3.1.4.7.

The distribution of mesh points in the interior of the two-dimensional regions is presently established by means of an algorithm due to Thompson et al.[19] The computational coordinates ζ and η may be embedded into a pair of elliptic equations as follows.

$$\zeta_{zz} + \zeta_{rr} = 0 \qquad 3.1.4.15$$

$$\eta_{zz} + \eta_{rr} = 0 \qquad 3.1.4.16$$

We do not solve 3.1.4.15 and 3.1.4.16 directly. Rather, we solve the inverted system.

$$\alpha z_{\zeta\zeta} - 2\beta z_{\zeta\eta} + \gamma z_{\eta\eta} = 0 \qquad 3.1.4.17$$

$$\alpha r_{\zeta\zeta} - 2\beta r_{\zeta\eta} + \gamma r_{\eta\eta} = 0 \qquad 3.1.4.18$$

where

$$\alpha = z_{\eta}^{2} + r_{\eta}^{2}$$

$$\beta = z_{\zeta} z_{\eta} + r_{\zeta} r_{\eta}$$

$$\gamma = z_{\zeta}^{2} + r_{\zeta}^{2}$$

As we have described in the preceding sections, Dirichlet data are prescribed for these equations on the boundaries of all two-dimensional regions. Then equations 3.1.4.17 and 3.1.4.18 are discretized by replacing all derivatives by second order accurate finite differences and the resulting system is solved by the method of successive over-relaxation.[20]

In the previous version of the code, the algorithm of Thompson et al[19] was used only to establish the initial mesh distribution. Subsequently,

---

[20] *Roache, P. J.*
"Computational Fluid Dynamics"
Hermosa Publishers. *1972*

the mesh was required to follow the motion of the solid-phase so that $u_m = u_p$ and $v_m = v_p$ at all points within the mixture. A consequence of this approach was a tendency of the mesh to become somewhat distorted and nonuniform as the solution developed. This was particularly true in the event that energetic and localized basepads were considered since these tend to induce significant boundary deformation.

Currently the distribution of mesh points on the mixture boundaries is established as follows. On the ends of each region we require v_m to be linearly interpolated, with respect to r, between the values of v_p at the inner and outer corners. Given v_m, the condition that the motion of the mesh point be tangential to the boundary yields the value of u_m. An analogous procedure is applied to the sidewalls.

The mesh point velocities are related to the positions at successive integration times according to the following formula which will be seen to be consistent with the overall method of integration discussed in the next section. We have

$$u_m = \begin{cases} (\tilde{z}_m - z_m^n)/\Delta t & \text{, predictor step} \\ (z_m^{n+1} - \frac{1}{2}(\tilde{z}_m + z_m^n))/(\Delta t/2) & \text{,corrector step} \end{cases} \qquad 3.1.4.19$$

where Δt is the time increment, z_m^n is the value of z at the n-th step, $\tilde{z}_m$ is a trial or predictor value at the (n + 1)st step and z_m^{n+1} is a corrected value at the (n + 1)st step.

Prior to the integration of the equations of motion, 3.1.4.19 and its analogue for v_m are used to establish Dirichlet data for the mesh on the boundaries of the mixture at the next level of integration. Equations 3.1.4.17 and 3.1.4.18 then establish the interior mesh and 3.1.4.19 may be used to compute u_m at the interior points as is required in the evaluation of convective terms in the equations of motion of the two-phase flow.

3.2 Discretization and Integration Algorithms

Our intention in the present section is to summarize the principles on which the method of solution is based. As in previous work we distinguish three classes of mesh points, namely interior points which have neighbors on all sides for the purpose of forming finite difference representations of spacewise derivatives, boundary points which do not have neighbors on one side and finally, in fully two-dimensional regions, corner points which are further constrained in respect to the representation of derivatives by finite differences.

No fundamental changes have been made in respect to the method of updating the solution at interior, boundary or corner points. Accordingly, in the subsequent discussion we abstract the methodology provided in the previous report and then address such differences from the previous methodology as have been found necessary in respect to the present extension to a multi-bag capability. The discussion is provided in four subsections. In sections 3.2.1, 3.2.2 and 3.2.3, we discuss the interior, boundary and corner mesh points, respectively. In section 3.2.4, we comment on the methodology associated with the solution during the quasi-two-dimensional part of the simulation.

3.2.1 Integration at Interior Mesh Points

The algorithm is basically that of MacCormack[21] with certain modifications to the convective derivatives which have been suggested by Moretti.[22] We express the algorithm for the general system of partial differential equations

$$\frac{\partial \psi}{\partial \tau} + B \frac{\partial \psi}{\partial \zeta} + C \frac{\partial \psi}{\partial \eta} = D \qquad 3.2.1.1$$

where ψ is a vector of state variables and (τ,ζ,η) are the computational coordinates. With B or C equal to zero, 3.2.1.1 reduces to a one-dimensional system and with B and C equal to zero, 3.2.1.1 reduces to the form of the lumped parameter systems of governing equations.

---

[21] *MacCormack, R. W.*
"The Effect of Viscosity in Hypervelocity Impact Cratering"
AIAA Paper No. 69-354. *1969*

[22] *Moretti, G.*
"Calculation of the Three-Dimensional, Supersonic, Inviscid, Steady Flow Past an Arrow-Winged Airframe"
POLY-AE/AM Report No. 76-8. *1976*

Let $\psi_{i,j}^{n}$ be understood to mean a value of ψ at a mesh point enumerated by the finite ζ-coordinate i, the finite η-coordinate j and the finite τ-coordinate n. Similarly let $B_{i,j}^{n}$ mean $B(\psi_{i,j}^{n})$ and likewise for C and D. Then the basic MacCormack scheme, with a consistent allowance for the non-homogeneous terms, may be expressed as follows.

$$\tilde{\psi}_{i,j} = \psi_{i,j}^{n} + [D_{i,j}^{n} - \frac{B_{i,j}^{n}}{\Delta\zeta}(\psi_{i+1,j}^{n} - \psi_{i,j}^{n}) \qquad 3.2.1.2$$

$$- \frac{C_{i,j}^{n}}{\Delta\eta}(\psi_{i,j+1}^{n} - \psi_{i,j}^{n})]\Delta\tau$$

$$\psi_{i,j}^{n+1} = 1/2\ (\psi_{i,j}^{n} + \tilde{\psi}_{i,j}) + [\tilde{D}_{i,j} - \frac{\tilde{B}_{i,j}}{\Delta\zeta}(\tilde{\psi}_{i,j} - \tilde{\psi}_{i-1,j}) \qquad 3.2.1.3$$

$$- \frac{\tilde{C}_{i,j}}{\Delta\eta}(\tilde{\psi}_{i,j} - \tilde{\psi}_{i,j-1})]\ \frac{\Delta\tau}{2}$$

The scheme is seen to involve a predictor level, yielding the trial update $\tilde{\psi}_{i,j}$, followed by a corrector level yielding the final update $\psi_{i,j}^{n+1}$. We also note that alternating forward and backward differences are used for the representation of the spacewise derivatives.

The modification suggested by Moretti relates to the discretization of the convective derivatives. These are always represented by upstream differences as follows, except where forbidden by proximity to a boundary:

Predictor

$$\frac{\partial\phi}{\partial\zeta} = \pm\frac{1}{\Delta\zeta}[\phi_{i\pm1,j} - \phi_{i,j}] \qquad 3.2.1.4$$

Corrector

$$\frac{\partial\phi}{\partial\zeta} = \pm\frac{1}{\Delta\zeta}[3\phi_{i\pm1,j} - \phi_{i\pm2,j} - 2\phi_{i,j}] \qquad 3.2.1.5$$

The upper or lower sign is used according as the pre-multiplying velocity component is negative or positive, respectively. It should be noted that 3.2.1.5 is not a second order accurate form. It only

yields formal second order accuracy in combination with 3.2.1.4. When the mesh point is adjacent to a boundary and the rule expressed by 3.2.1.4, 3.2.1.5 would require data outside the computational domain, we revert to the regular MacCormack prescription.

At present we make use of 3.2.1.5 only in regions of two-dimensional, two-phase flow. In regions of quasi-one-dimensional flow or in regions of two-dimensional single-phase flow, we use the first order form 3.2.1.4 at both the predictor and the corrector levels.

We also note that the matrices B and C involve terms like ζ_z. These are deduced by first expressing z_ζ, z_η, r_ζ, r_η by means of centered differences. Then ζ_z, ζ_r, η_z, η_r follow from equations 3.1.4.9-3.1.4.12.

The integration scheme is assumed to be stable when subjected to a usual Courant-Friedrichs-Lewy domain of dependence limitation.[23] If C is the fastest local wavespeed, we require

$$C\,\frac{\Delta\tau}{\Delta\zeta} \le \frac{r_\eta z_\zeta - z_\eta r_\zeta}{\sqrt{(r_\eta - k r_\zeta)^2 + (z_\eta - k z_\zeta)^2}} \qquad 3.2.1.6$$

where $k = \pm\Delta\zeta/\Delta\eta$ according as $z_\eta z_\zeta + r_\eta r_\zeta \lesseqgtr 0$. In practice, we further constrain this heuristic limit by dividing it by a safety factor which we have taken to be 1.1.

The scheme described above is referred to as explicit in the sense that all spacewise derivatives and all coefficients are based on data in current storage rather than on future level data. However, as discussed in the previous report, we have found it useful to introduce some implicitness in respect to the interphase drag by resolving the slip velocity as a future datum. The implicitness is purely local and does not introduce the necessity of inverting a matrix as would be the case if the spacewise derivatives were expressed implicitly.

---

[23] *Richtmyer, R. D. and Morton, K. W. "Difference Methods for Initial Value Problems" Interscience. 1967*

3.2.2 Integration at Boundary Points

The emphasis in the present section is on points which lie on the boundaries of fully two-dimensional regions. Boundary points of quasi-one-dimensional regions arise only in connection with corners of fully two-dimensional regions or in the quasi-two-dimensional representation. These latter cases are the subjects of the next two subsections.

It is always the case that the number of physical boundary conditions, as set forth in chapter 2.0, is less than the number of state variables to be determined on the boundary. Mathematical closure is effected by assuming that the differential equations themselves provide the additional relationships required to determine completely and uniquely the boundary values.

The particular relationships that we use to effect the closure are referred to herein as characteristic forms. A complete discussion of these forms is given in the previous reports.[1,2] We have noted in our earlier work that the forms should really be referred to as pseudo-characteristic since they are based on an analysis of the equations of two-phase flow in which the pressure gradient in the solid-phase momentum equation is treated as an inhomogeneous rather than differential term. Here we do not concern ourselves with the distinction. The pseudo-characteristic forms may be viewed simply as a restatement of the balance equations, together with the differential constitutive laws, in a manner guided by the theory of characteristic surfaces of a system of hyperbolic equations. The forms are not used to investigate the mathematical structure of the governing equations or to study problems of uniqueness of solutions or of sufficiency of initial and boundary data.

From the characteristic forms as documented in the previous reports,[1,2] there emerge the following linearized relationships among the state variables. For the gas-phase the pressure and normal velocity component satisfy

$$\Delta p = \xi \Delta u_n \qquad 3.2.2.1$$

Here Δp and Δu_n are understood to represent sufficiently small changes in the boundary values as to validate the linearization of the governing equations and ξ is a coefficient which emerges from the characteristic analysis.[1,2] Equation 3.2.2.1 may be viewed as expressing the elastic compliance of the gas-phase and is referred to as the acoustic characteristic condition.

Similarly, for the solid-phase one finds a relationship in the form

$$\Delta\sigma = \xi_p \Delta u_{p_n} \qquad 3.2.2.2$$

which is also an acoustic condition. In view of the interpretation of ξ_p as a stiffness, it follows that $\xi_p = 0$ when the solid-phase is dispersed or, more generally, when $a(\varepsilon) = 0$ according to Equation 2.2.2.4.

In addition to these acoustic characteristic forms, one finds material characteristic forms which relate the variations in density and pressure for the gas-phase and the variations in porosity and intergranular stress for the solid-phase. The material characteristic form for the solid-phase is degenerate whenever $a(\varepsilon) = 0$ since it is, in fact, nothing more than the relation expressed by Equation 2.2.2.2.

The method of solution at the boundary points may be summarized as follows. The governing equations are manipulated into characteristic forms by treating the pressure gradient in the solid-phase momentum equation as though it were formally algebraic or inhomogeneous in nature. The resulting acoustic forms involve only derivatives tangential to the boundary and along a bicharacteristic ray which lies in a plane defined by the τ axis and the normal to the boundary. Let the boundary be a line on which ζ = constant; then the tangential derivative involves only η. The derivative along the bicharacteristic ray may be expressed as a linear combination of derivatives with respect to τ and ζ. The forms so derived are discretized using exactly the same procedure as that described in connection with the interior mesh points except that one-sided differences are necessarily used for the representation of derivatives with respect to ζ. At present only a first order representation is used for the ζ derivatives. The use of a corrector term in the form 3.2.1.5 has been found to destabilize the solution in many cases.

The transformation derivatives ζ_z, ζ_r, η_z, η_r are deduced in the same manner as in the interior. However, a first order one-sided difference is used to evaluate the normal derivatives z_ζ and r_ζ.

A trial update of all state variables is made, using the characteristic forms of the equations, without reference to the physical boundary conditions. At the same time, we compute and save the

coefficients ξ and ξ_p as indicated in Equations 3.2.2.1 and 3.2.2.2 as well as their counterparts for the material characteristic forms. Then the physical boundary conditions are enforced to establish the necessary differential variations in p, ρ and u_n for the gas-phase and in σ, ε and u_{p_n} for the solid-phase, these variations being understood to be constrained by the characteristic relationships. Following the final determination of the normal and tangential velocity components of each phase, the cylindrical components are resolved.

In performing the present extension, absolutely no changes were made in respect to the determination of boundary values at points other than the bag-to-bag interfaces in either the fully- or the quasi-two-dimensional representations. Thus, the discussion of the previous report[2] applies in entirety for configurations involving a single increment and requires amplification here only in respect to the bag-to-bag interfaces.

3.2.2.1 The Solid-Phase

We consider a boundary on which ζ = constant. Results for a boundary on which η = constant follow from considerations of symmetry. A vector normal to the boundary is given by (ζ_z,ζ_r), while a tangent vector is $(-\zeta_r,\zeta_z)$, neither vector necessarily having unit magnitude.

By taking the inner product of each of these vectors with the solid-phase momentum equation, we may deduce normal and tangential equations of motion.[2] As previously, we ignore the tangential equation for the solid-phase and prescribe the tangential component of solid-phase velocity at the boundary by continuation of the tangential component at the neighboring interior mesh point. The previous report may be consulted for the factors which have motivated this approach.

The normal equation of motion is integrated using the rules of discretization outlined above. Next, estimates of intergranular stress and porosity are determined from the acoustic and material solid-phase characteristic forms, respectively.

At a boundary point which does not lie on a bag-to-bag interface, the physical boundary condition for the solid-phase is then imposed as described previously.[2] If the flow is adjacent to an external boundary, the solid-phase is required to satisfy a constraint on the component of velocity normal to the external boundary.

If the value of u_{p_n} obtained by integration of the momentum equation does not indicate penetration of the boundary, it is accepted. Otherwise it is replaced by the normal velocity of the boundary, and the values of ε and σ are adjusted in accordance with the characteristic conditions.

If the boundary point is adjacent to a quasi-one-dimensional two-phase flow or to a region of single-phase flow, then the relevant condition is expressed in terms of the intergranular stress. Again the necessary variations are determined and imposed consistently with the characteristic forms for the solid-phase. If the contiguous region is two-phase and quasi-one-dimensional, an implicit dependence of the intergranular stress on the normal velocity of the boundary is considered by reference to the term A_t which appears in the continuity Equation 2.1.2.4.

At a bag-to-bag interface we have, in effect, a solid-phase contact discontinuity. The normal velocity components and the intergranular stresses are required to be continuous unless the trial values indicate separation. The final values are established using the characteristic forms pertinent to each side of the interface.

3.2.2.2 The Gas-Phase

A trial value of the tangential component of velocity is deduced by integration of the tangential equation of motion, independently of whether the gas is flowing out of or into the region in question. The normal component of velocity is assigned a trial value by simply taking an inner product of the normal vector and the values in current storage. Values of pressure and density follow from the characteristic forms for the gas-phase. Updated values of the molecular weight and the specific heats are also deduced from the relevant governing equations which are automatically in characteristic form. Of course, the values of the tangential velocity, the density, the molecular weight and the specific heats obtained from these integrations are only valid provided that the state at the boundary does not correspond to an influx.

The question of the direction of the flow is resolved by imposing the mechanical boundary condition which is expressed either in terms of the normal velocity component--at an impermeable boundary--or by reference to the pressure--at a permeable boundary. When, in the latter case, the boundary is contiguous with a region of quasi-one-dimensional flow, the mechanical boundary condition is based on an implicit formulation of the response of the external region to the mass flux as indicated by the balance Equations 2.1.2.1 and 2.1.2.3 or by 2.1.4.1 and 2.1.4.3.

Following the adjustment of the values of pressure and normal velocity, the direction of the flux is established. If it corresponds to an efflux, then we accept the values of the tangential velocity component, the molecular weight and the specific heats as computed from the characteristic forms. The density is adjusted to be compatible with the pressure. If, on the other hand, the direction of flow corresponds to an influx, the tangential velocity component, the molecular weight and the specific heats are determined by the transfer conditions with allowance for a reactive substrate. The density follows from the energy balance.

At a bag-to-bag interface in which an intervening region of ullage is present and is represented as quasi-one-dimensional, trial updates as described above are established for the mixture boundaries on both sides of the ullage and for the ullage itself. The mechanical boundary conditions which relate the two sets of boundary values to the state of the intervening ullage are solved simultaneously. Then, with the pressures and the normal velocity components established for both boundaries, the remaining state variables are deduced, on each side, in the same manner as that described previously in the case of a single boundary. This procedure is also followed when the two bags contact one another and the intervening ullage disappears. In this case, of course, the mechanical boundary conditions simply reduce to statements of consistency of the states on either side of the two-phase contact discontinuity.[24]

As in the previous version of the code, we take a friction factor $K > 100$ to mean that the bag is completely impermeable.

3.2.3 Integration at Corner Points

The discussion of this topic is given in terms of a point located on a corner of the mixture. The corners of two-dimensional regions of ullage may be regarded as subcases of the present discussion for which the appropriate simplifications are readily perceived.

With regard to the corners of the mixture we will distinguish three cases. The first case may be described as a fully attached corner in which both sides of the mixture are bounded by an impermeable wall. The second case may be described as a partially separated corner in which only one side of the mixture is bounded by an impermeable wall. The third case may be described as a fully separated corner in which neither side is bounded by an impermeable wall.

---

[24] *Gough, P. S.*
"Extensions to NOVA Flamespread Modeling Capacity"
Final Report for Task I, Contract N00174-80-C-0316
PGA-TR-81-2. *April 1981*

While, in principle, a corner at a bag-to-bag interface could correspond either to a fully or a partially separated condition, we have adopted the procedure for a fully separated corner in such cases even when there is contact with an external boundary.

Fully Attached Corner

In this case, the relevant boundary conditions are given in terms of the normal velocity components of both phases with respect to each of the sides which define the corner. The intergranular stress and the pressure may be deduced from the characteristic forms. As in an earlier study,[1] we select the characteristic direction in accordance with the structure of the flow near the corner.

Partially Separated Corner

In this case we have a boundary condition for each phase in the form of the normal velocity component for the side which is attached to the external boundary. This condition replaces the determination of the tangential components of velocity of each of the phases as described in the previous sections.

It is also necessary in this case to impose boundary conditions on the external flow contiguous with the separated side. These are furnished in the form of a condition on the normal velocity component with respect to the attached side. If the exterior flow is two-phase, as in the case of the centercore igniter, it should be noted that the influence of a basepad, represented as a source term, may require the consideration of a flux condition on the gas-phase in a fashion directly analogous to the case which occurs when the mixture, bounded by a reactive bag, is adjacent to an impermeable wall.

The characteristic forms of the quasi-one-dimensional equations are used to deduce thermodynamic state variables which are consistent with the kinematic boundary conditions.

Fully Separated Corner

The normal component of velocity of each of the phases is assumed to be equal to that of its neighbor on each side of the mixture. The pressure is taken to be the average of the neighboring values. The density is taken to be an average also unless the flow corresponds to an efflux at one neighboring point. In the latter case the corner value is taken to be the same as that at the neighbor where influx occurs. Exactly the same procedure is used for two-dimensional regions of ullage exterior to the mixture.

When the exterior flow is quasi-one-dimensional on both sides of the corner, trial values are deduced for the exterior boundary values and for the state of the lumped parameter corner region, all based on normal mass fluxes across the mixture boundaries as deduced from the neighboring values. Then the physical conditions of compatibility of the exterior one-dimensional flows with the lumped parameter corner region are imposed simultaneously with the acoustic characteristic forms.

If we are dealing with a corner at a bag-to-bag interface which involves an intervening quasi-one-dimensional region of ullage, the mixture properties at each of the two bag corners are updated. Then all the exterior flows are made compatible with one another.

If the quasi-one-dimensional region is two-phase, allowance must be made in the continuity and energy balances with the inner region, for the presence of a reactive layer corresponding to the part of the basepad which overlaps the centercore tube.

A further possibility arises when one external region is two-dimensional while the other is quasi-one-dimensional. In this case, the corner region is quasi-one-dimensional, and the boundary conditions at the interface between the two quasi-one-dimensional regions contiguous with the corner are determined using the characteristic forms and the finite mass, momentum and energy balances with due allowance for a surface source term.

At a bag-to-bag interface, it may be the case that the radial ullage is two-dimensional while the axial ullage is quasi-one-dimensional. The corner values of all the two-dimensional regions are deduced by interpolation as described above and compatibility is enforced only with respect to the boundary values of the region of axial ullage which separates the two mixture regions and that which separates the two two-dimensional regions of radial ullage.

3.2.4 Integration of the Quasi-Two-Dimensional Flow

When the flow is represented as quasi-two-dimensional, we have a series of coaxial flows separated by lumped parameter regions. Each of the series of coaxial flows involves three regions, two of which may be two-phase. The lumped parameter regions are single-phase.

At each step, trial values at the interior points are deduced for each region using values of the transverse fluxes which were established at the preceding level. A suitable allowance is made for the presence of reactive substrates of the bag, even though rupture is complete, for the sake of maintaining the global balances as closely as possible.

The gas-phase pressure is assumed to equilibrate across each cross-section of the tube. The values of the transverse fluxes are therefore adjusted so as to yield identical values of pressure in each of the three regions which occupy a given cross-section. The transverse fluxes deduced in this way are used, in combination with the law governing the interphase drag and the radial component of the equation of motion of the solid-phase, neglecting pressure gradient and intergranular stress, to yield the influence of radial gas flow on radial motion of the propelling charge boundaries. The radial motion of the boundaries is also influenced by considerations of the requirement of transverse equilibrium of the intergranular stress which is hypothesized to have an isotropic character.

Intergranular stresses can exist only at a cross-section in which no radial ullage is present. In such a cross-section, the intergranular stresses in the propelling charge and the centercore, if present, must be equal. These considerations lead to the determination of an equilibrium value for the intergranular stress in much the same fashion as that used to determine the pressure.

By analogy with the fully separated corner in the two-dimensional case, an independent analysis of the radial motion of the ends of the propelling charge increments is not conducted. The radial motion of the end points is assumed to be the same as that of the neighbors in the interior.

The boundary values for the solid-phase are deduced analogously with those for the boundaries of the fully two-dimensional regions, whether at the ends of the charge or at bag-to-bag interfaces. The same is true of the gas-phase boundary values. At the bag-to-bag interfaces, we have to consider six fluxes rather than two, but the methodology is the same as in the fully two-dimensional case. All the fluxes are made mechanically compatible, and the remaining state variables follow either from the material characteristics or from the transfer conditions at a discontinuity. As discussed in section 3.1, this approach does involve the assumption of complete mixing in the intervening lumped parameter region, even as it becomes vanishingly thin.

3.3 Special Topics

The purpose of this concluding section is to summarize those aspects of the code which we regard as having an essentially ad hoc character. These special topics include: the treatment of the tangential velocity component of the gas phase; the treatment of the flow as burnout occurs; the treatment when a region of ullage, or the centercore igniter, collapses locally; the ignition of propellant

located on the boundaries; and, finally, the treatment of the boundary values of the solid-phase in the igniter charge in the quasi-two-dimensional representation.

No changes have been introduced with respect to any of these topics except the last. The previous final report[2] may be consulted for a fuller discussion than that which we provide herein.

Treatment of Tangential Velocity of Gas Entering Mixture

In order to render the numerical analysis more tractable, we introduce a loss of tangential momentum for gas entering the mixture. The loss is estimated from an approximate integral of the equation of motion of the gas-phase over a characteristic time defined by dividing the initial diameter of a propellant grain by the normal velocity of the gas entering the mixture. The procedure may be viewed as a determination of the boundary value as an average of the values external and internal to the interface using weighting coefficients which are sensitive to the mechanical relaxation time in the mixture.

Treatment at Burnout

Burnout is assumed to occur in either the propelling charge or the centercore igniter when the porosity exceeds the value 0.999. At this point the value of porosity is replaced by the value 1.0 and the velocity of the solid-phase is set equal to that of the gas-phase.

When the solution is being determined according to a quasi-two-dimensional representation, the local cross-section of the mixture is taken to fill completely the tube so that the outer and inner regions of radial ullage are formally represented as collapsed at a section where burnout occurs.

Treatment When Region Collapses

Physically reasonable values of the state variables are retained in all computational regions at all times when they are locally collapsed due to proximity of the propelling charge to an external boundary or due to the proximity of one increment to another. When a region is collapsed, the values of the state variables are taken to be equal to those in the mixture at the appropriate boundary point. At present, a region is taken to be collapsed whenever its transverse dimension is less than 1 mm.

Ignition of Boundary Points

The surface temperature of grains on the boundary of the propelling charge is replaced by the value at its neighbor in the interior whenever the neighbor has a higher value. This device is introduced to ensure ignition at the boundaries in cases when the local gas convection is very weak due to the presence of an impermeable boundary.

Boundary Values of Solid-Phase in Centercore Igniter

When the end of the centercore tube is represented as impermeable to the solid-phase, we use a continuative boundary condition to determine the porosity and the intergranular stress in the centercore during the quasi-two-dimensional part of the solution.

4.0 A COMPUTATIONAL EXAMPLE

We now illustrate the operability of the revised code by reference to a problem involving two separately bagged increments of propellant. In the previous report,[2] we selected a problem based on an existing single-bag charge, namely the M203 charge for the 155mm howitzer. The present computational example is not based on any existing charge. For the sake of exercising the code, we have simply taken the previous example and divided the propellant into two equal increments, each separately bagged, and each bag having all the attributes of the bag considered previously. Thus, each increment has its own basepad and its own centercore igniter, and each bag is represented as partially impermeable in its initial configuration.

The data base for the computational example is discussed in section 4.1. Details of the solution are presented in section 4.2.

4.1 Discussion of Input Data

In the previous report,[2] we provided an extensive discussion of the input data with a view to clarifying the input file structure for TDNOVA. This aspect of the discussion is not repeated here; however, we will comment on certain minor differences in the data formats which arise in the new code. We also provided previously[2] a detailed discussion of those data which were deliberately compromised in the specification of the problem. Here we will simply note those data which are compromised and refer the reader to the previous report for further discussion.

The computational example is illustrated in Figure 4.1, which also displays the initial configuration of the mesh. The input data used to describe the problem are contained in Table 4.1, whose format is identical with that of the code.

From Figure 4.1, we see that the simulation incorporates such geometric details as the curvature of the spindle, the taper of the gun tube and the intrusion into the chamber of the boattail of the projectile. These geometric data are based on the configuration of the M199 cannon and the M438A1 projectile. The propelling charge consists of two increments, each packed into a bag of external diameter equal to 15.24 cm and of length equal to 38.1 cm. The thickness of the bag material is not considered in the present calculation. Each bag contains a centercore igniter whose initial diameter is 2.54 cm. Within each centercore igniter tube is located a uniformly distributed charge consisting of 0.0567 kg of black powder. Each increment contains a main charge consisting of 5.931 kg of M30A1 propellant which is initially distributed uniformly within the envelope of the bag.

The initial porosities of the main charge and centercore igniter charge are 0.4455 and 0.8367, respectively. As in the previous report we have used identical gas-phase thermochemical data to describe the products of combustion of the main and centercore charges. To exercise the variable thermochemistry of the code, however, the initial values of the molecular weight and the specific heats are set equal to those for air.

Approximately one-half of the exterior of each bag is taken to be initially impermeable. The forward half of the outer circumferential boundary is made impermeable to model the presence of a lead foil liner. The outer part of the forward face of each increment is made impermeable to reflect the impediment due to a salt bag. All the other surfaces of the bag, including the centercore tube, are represented as initially permeable.

Each increment is represented as having a basepad which extends over part of the rear surface of each bag as well as the rear face of each centercore tube. Accordingly, the calculation will reflect an initial thermal stimulus, by the basepad, to both the centercore charge and the main charge. The rates of discharge of the two basepads are assumed to be identical functions of time in this example, a condition which is unlikely to be achieved in practice, and are specified according to the predetermined data contained in Table 4.1 in the section entitled data to describe reactivity of bag substrate 1.

The real initial thermal stimulus created by the discharge of the products of combustion of a primer located in the breechblock is not represented. The initial stimulus in the present calculation is taken to be due to the reaction of the basepads in accordance with the prespecified discharge data.

Subsequently, the spreading of a convective flame through both the centercore igniters and the main charges is modeled as part of the macroscopic two-phase flow.

Because the increments have a smaller diameter than the tube, annular ullage is initially present. The space between the outside of the charge and the tube wall varies from 0.837 cm at the rear to 0.511 cm at the mouth of the chamber.

Axial ullage is also present. We depict the charge as having a standoff of 2.54 cm from the spindle face and an initial separation of 1.0 cm between the increments. The initial separation between the front of the charge and the base of the projectile is therefore 16.68 cm.

Physically compromised data in the previous example were noted to include the following:[2]

(1) Neglect of bag thickness.
(2) Neglect of reactivity and impermeability of the centercore tube.
(3) Representation of the centercore igniter charge as uniformly distributed within the centercore tube.
(4) Use of the same thermodynamic data for the black powder and the main charge.
(5) Use of an extremely low ignition temperature for the black powder, namely 300°K versus the value of 742°K reported by Lenchitz and Hayes.[25]

All of these compromises have been retained in the present example as a matter of convenience. The major aspect of the code extension is the ability to treat more than one increment, and our example is selected accordingly. Of the five areas of compromise, only the fifth is actually thought to be necessary with the current code version, although we do not offer proof of this statement in the present work. With regard to the fifth item, the low ignition temperature of black powder, we note that the real process of flamespreading through black powder is almost certainly outside the physical scope of the present model due to our neglect of the thermal stimulus associated with the discharge of hot molten salts. The use of a reduced ignition temperature for the black powder may be interpreted as an ad hoc compensation for the thermal stimulus induced by molten salts which are transported in mechanical equilibrium with the macroscopic flow of the gas.

The thermochemical data for the M30A1 propellant are as used in a previous study by Horst.[6] The burning rate for the black powder is due to Rose and Hardt.[26]

The present computational example is based on the static mesh allocation mode. A fixed complement of 16 axial mesh points and 7 radial mesh points is assigned to the fully two-dimensional representation of the propelling charge. Equal numbers of points are assigned to each of the two increments. The centercore igniter charges and the regions of ullage contiguous with the increment boundaries are all represented as quasi-one-dimensional. There are a total of six lumped parameter regions, four located at the corners of the chamber and one located at each end of the ullage between the bags. A total of 171 mesh points is therefore in use during the fully two-dimensional part of the solution.

---

[25] *Lenchitz, C. and Hayes, E.*
"An Analysis of Black Powder Ignition and Performance. Ignition Properties of Black Powder, Phase I"
Proc. 16th JANNAF Combustion Meeting. *1979*

[26] *Rose, J. E. and Hardt, A. P.*
"Black Powder--A Modern Commentary--1979"
Proc. 10th Symposium on Explosives and Pyrotechnics, Franklin Research Center, Phila., PA Feb. 14-16. *1979*

The pressure tolerance factor is specified as 0.1 with the significance that a transformation of the problem to a quasi-two-dimensional representation will occur following the completion of flamespreading and total rupture of both of the bags when the difference between the values of pressure at the centerline and the tube wall does not exceed 10% of the value at the tube wall at any axial station in the chamber.

The fully two-dimensional part of the calculation required 313 steps, the transition to a quasi-two-dimensional representation occurring at 2.08 msec. The continuation of the solution to muzzle exit of the projectile required an additional 295 steps. The entire calculation required 152 CPU seconds when performed in double precision on an ITEL AS-6 processor and 72 CPU seconds when performed in single precision on a CYBER 7600 processor. The double precision word length on the ITEL processor is 64 bits, whereas the single precision word length on the CYBER 7600 is 60 bits.

We conclude with some comments on differences in the data format with respect to the previous version of the code.

Variable scheduling of the logout is available, and the present calculation effects a variation in the logout interval from 0.2 msec to 1.0 msec when the transformation to a quasi-two-dimensional representation occurs.

The main charges and the centercore igniter charges are not explicitly labeled as such. Tables of data are entered for each variety of propellant present in the charge. The description of each bag or increment permits designation of any type of propellant as the main charge or the centercore charge.

The description of each bag supports both rear and forward basepads extending over the ends of the centercore tube. Permeability of the ends of the centercore tube to the efflux of the solid-phase is admitted and each bag can be represented as strong. A strong bag is taken never to dilate beyond its initial diameter and the transformation to a quasi-two-dimensional representation is made without reference to the rupture of the bag. The description of the bag geometry includes a specification of the thickness.

With respect to the properties of the projectile, we note a provision to specify the presence of filler elements. This feature supports the modeling of Navy case charges as described elsewhere.[24]

4.2 Discussion of the Solution

We turn now to the details of the numerical solution as represented in Figures 4.2 through 4.29. Figure 4.2 depicts the path of flamespreading through the two-increment charge. Figures 4.3 through 4.15 are isometric views of the pressure field at various times. Figures 4.16 and 4.17 depict the gas-phase density at two times. Figures 4.18 through 4.23 illustrate the gas-phase velocity field at various times, and Figures 4.24 through 4.29 provide the same information for the solid-phase at the same set of times.

The physical sequence of events in the simulation is as follows. The initial quiescent state is disturbed by the simultaneous venting of the products of combustion of the two basepads. The products of the first basepad are vented partly into the rear of the first increment and partly into the rear axial ullage. The products vented into the first increment flow partly into the main charge and partly into the centercore igniter. Because of the low ignition temperature specified for the centercore ignition charge, flamespreading occurs first through the centercore and subsequently through the main charge. The products of combustion of the centercore igniter flow axially through the centercore, promoting flamespread through the igniter, and also radially, promoting flamespread through the main charge.

At the same time, the products of combustion of the second basepad flow partly into the second increment and partly into the axial ullage which separates the two increments. Whereas the gas vented into the rear axial ullage can only travel radially, that vented into the ullage between the bags flows partly radially and partly axially. The axial flow is rearward into the forward face of the first increment.

Accordingly, the ignition stimulus applied to the first increment is very nearly symmetrical. Flamespreading through the second increment, on the other hand, is promoted mainly by the action of a single basepad. However, products of combustion also flow around the charge. Due to the impermeability of the forward part of the outer circumferential surface of each increment, gas flowing around the charge tends to be channeled towards the mouth of the chamber. As the mouth of the chamber becomes pressurized, gas flows into the forward face of the second increment, providing a rearward convection similar to that which occurs in the first increment but of lesser intensity.

The convection of the gas not only heats the propellant; it also induces motion through the mechanism of drag. The action of the rear basepad is to accelerate the propellant in the first increment towards the projectile. Since the propellant is packed, the gas-dynamic forces imparted near the region where the basepad venting occurs are

transmitted by intergranular stresses, resulting in overall motion of the charge prior to the passage of the convective flame. The second basepad induces a similar forward acceleration of the second increment and a rearward acceleration of the first increment which tends to oppose the thrust of the first basepad.

It should be noted that it is not only the mechanical influences of the two basepads which tend to cancel one another; the convections induced by the pair also tend to cancel one another so that the thermal stimulus to the first increment is in fact reduced near its midpoint by the combined action of the pair.

Other forces than those due directly to the venting of the basepad are at play in respect to the motion of the main charge increments. The rapid flamespread through the centercore igniter produces a radial convection which thrusts the propellant outwards towards the tube wall. On the other hand, the gas flowing through the outer radial ullage encounters portions of the exterior surface which are impermeable. On such sections the external gas pressure may exceed that inside the bag. Due to its flexibility, the bag is incapable of supporting such a differential, and the force is transmitted into the solid-phase, resulting in an inward compression of the propellant.

The path of flamespreading through the main charge and the centercore increments is illustrated in Figure 4.2. This figure is a Lagrangian map in the sense that the locus of the ignition front, as revealed by contours of ignition delay, is referred to the original configuration of the charge. Ignition of the first increment is seen to be nearly symmetrical about its midpoint due to the combined action of the two basepads. The relative importance of the centercore near the midpoint is revealed by the flattening of the ignition delay contours into lines of relatively uniform radius. Symmetry is also observed with respect to the second basepad since it has nearly the same effect on the first increment as it does on the second for that period of time prior to the arrival of information concerning the action of the first basepad. A slight deviation from symmetry is also present at very early times near the second basepad. This deviation is due to the fact that the basepad is physically located on the surface of the second increment. Products vented rearward are mixed with the ambient air prior to penetrating into the first increment.

Figure 4.3 illustrates the pressure field at 0.2 msec. The elevations near the centerline are due to the venting of the basepads. Penetration into the centercore and main charges is also seen. The elevation near the tube wall is due to the stagnation of the radially flowing gas which is now beginning to turn the outer corners of the increments and to flow around the outside of the charge.

Figures 4.4, 4.5 and 4.6 show the progression of the pressure field in time. By 0.8 msec, Figure 4.6, the pressurization of the outer annular ullage is well advanced. An excursion in the pressure field is seen over that part of the circumferential boundary of each increment which is impermeable and still unruptured. Further progression is seen in Figures 4.7, 4.8 and 4.9 as the main propellant beds are progressively ignited. The excursion at the outer circumferential boundary of the first increment has disappeared by 1.4 msec due to rupture of the bag following ignition of the propellant. The pressure field is seen to become increasingly one-dimensional in nature. Its continuing radial equilibration is illustrated in Figures 4.10, 4.11 and 4.12.

Shortly after 2.0 msec, the conditions for transformation to a quasi-two-dimensional representation are satisfied. Figures 4.13 and 4.14 illustrate the pressure field at 2.077 msec according to both the fully two-dimensional and quasi-two-dimensional representations. Figure 4.15 presents the pressure field slightly later. It is evident that a smooth ignition event has been produced.

The level of structure supported by the code during the two-dimensional part of the solution is illustrated in Figures 4.16 and 4.17 which present the distributions of gas-phase density at 1.0 and 2.0 msec. Comparing Figures 4.12 and 4.17, it may be seen that although the pressure has equilibrated substantially in the radial direction by 2.0 msec, significant differences still exist between the values of density, and hence of temperature, in the mixture and in the surrounding ullage. These differences in density are not lost in the transformation to a quasi-two-dimensional representation although radial gradients within the mixture itself cease to be represented at that time.

Figures 4.18 through 4.29 illustrate the velocity fields of each of the phases at various times during flamespreading. In these figures the velocity is represented by a directed line segment rooted at the center of each mesh element and with magnitude scaled so that no line segment passes through its respective mesh element boundary. Accordingly, the scale factors change from figure to figure.

These figures also depict quite clearly the deformation of the boundaries of the propelling charge increments. However, in contrast to the previous version of the code, the interior mesh is not required to move with the solid-phase so that no information is conveyed concerning the compaction of the interior as was previously the case. Of particular interest is the deformation of the inner boundary of the increments. It shows the results of the competition between the outward thrust due to the centercore and the inward thrust due to the gas in the outer annular ullage superimposed on the axial compressions induced by the basepads.

Table 4.1 Input Data for Computational Example

155mm M203E1 Charge M199 Cannon M483A1 Projectile		
	CONTROL PARAMETERS	
NPRINT	(0 = no print, 1 = print)	1
NSUMRY	(0 = no summary tables, 1 = yes)	1
NPLOT	(0 = no isometric carpet plots, 1 = plot)	0
NVHL	(0 = hidden lines deleted, 1 = retained)	0
NPLCON	(0 = no contour plots, 1 = plot)	0
NPLFLO	(0 = no flow plots, 1 = plot)	0
NPLFLM	(0 = no flamespread plot, 1 = plot)	0
NDSKW	(0 = no disc save, 1 = disc save)	1
NDSKR	(0 = no disc start, >0 = disc start at step NDSKR)	0

ISOMETRICALLY PLOTTED QUANTITIES (1 = YES, 0 = NO)

Mesh 1 Porosity 0 Granular stress 0 Pressure 1
Density 0 Gas axial velocity 0 Solid axial velocity 0
Gas radial velocity 0 Solid radial velocity 0 Gas temperature 0
Particle surface temperature 0

CONTOUR PLOTTED QUANTITIES (1 = YES, 0 = NO)

Mesh 0 Porosity 0 Granular stress 0 Pressure 1
Density 0 Gas axial velocity 0 Solid axial velocity 0
Gas radial velocity 0 Solid radial velocity 0 Gas temperature 0
Particle surface temperature 0

Scale factor for plotting (-)	0.65
Length of z-axis in CALCOMP plots (in)	25.01
Length of r-axis (in)	4.01
Length of ordinate axis (in)	5.00

Table 4.1 (continued)

LOGOUT PARAMETERS

Parameters Prior to Q-2-D Transformation	
Number of steps before logout N.B. A negative entry for the above datum implies that variable logout scheduling is intended.	1000
Time increment before logout (msec)	0.2000
Parameters After Q-2-D Transformation	
Number of steps before logout	1000
Time increment before logout (msec)	1.0000
Summary Table Parameters	
Number of pressure summary stations	2
Time increment for pressure summary storage (msec)	0.200

TERMINATION PARAMETERS

Maximum number of steps before termination	1000
Maximum integration time (msec)	1.0000
Maximum projectile travel (cm)	520.7

CHARGE REPRESENTATION PARAMETERS

Number of propellants in charge	2
Number of bags in charge	2
Mesh allocation mode (0 = static, 1 = dynamic)	0
Maximum number of storage points for dynamic mesh allocation	0
Number of mesh points in axial direction	16
Number of mesh points in radial direction	7
Number of iterations to determine initial mesh	200
Safety factor for C-F-L criterion	1.1000
Maximum fractional displacement for convergence of initial mesh distribution	0.100D-04
Over-relaxation factor for determination of initial mesh distribution	1.600
Pressure tolerance factor for reduction to quasi-two-dimensional representation (-)	0.100
Axial spatial resolution factor (-)	0.100
Radial spatial resolution factor (-)	0.100

Table 4.1 (continued)

AMBIENT CONDITIONS

Initial temperature (°K)	294.4
Initial pressure (MPa)	0.1014
Initial ratio of specific heats (-)	1.40000
Initial molecular weight (gm/gmol)	29.00000
Charge standoff (cm)	0.0

PROPERTIES OF PROPELLANT TYPE 1

SOLID-PHASE CONSTITUTIVE DATA

Settling porosity of granular bed (-)	0.0
Speed of compression wave (m/sec)	152.4
Speed of expansion wave (m/sec)	1270.0
Density of solid phase (gm/cc)	1.5830
Thermal conductivity (J/cm-sec-°K)	0.0016
Thermal diffusivity (cm^2/sec)	0.0006

GAS-PHASE CONSTITUTIVE DATA

Ratio of specific heats (-)	1.24300
Molecular weight (gm/gmol)	23.360
Covolume (cc/gm)	1.030

SOLID-PHASE COMBUSTION CHARACTERISTICS

Ignition temperature (°K)	444.4
Chemical energy (J/gm)	4384.

Max Pressure (MPa)	Burn Rate Additive Constant (cm/sec)	Pre-Exponent (cm/sec-MPa^n)	Exponent (-)
68.95	0.0	0.41170	0.63370
689.50	0.0	0.22180	0.78640

Table 4.1 (continued)

GRAIN GEOMETRY

External diameter (cm)	1.060
Length (cm)	2.408
Diameter of perforations (cm)	0.086
Number of perforations (-)	7.
Form (0 = cylinder, 1 = sphere)	0

PROPERTIES OF PROPELLANT TYPE 2

SOLID-PHASE CONSTITUTIVE DATA

Settling porosity of granular bed (-)	0.40000
Speed of compression wave (m/sec)	442.0
Speed of expansion wave (m/sec)	1270.0
Density of solid-phase (gm/cc)	1.7990
Thermal conductivity (J/cm-sec-°K)	0.0016
Thermal diffusivity (cm^2/sec)	0.0006

GAS-PHASE CONSTITUTIVE DATA

Ratio of specific heats (-)	1.24300
Molecular weight (gm/gmol)	23.360
Covolume (cc/gm)	1.030

SOLID-PHASE COMBUSTION CHARACTERISTICS

Ignition temperature (°K)	300.0
Chemical energy (J/gm)	2489.

Max Pressure (MPa)	Burn Rate Additive Constant (cm/sec)	Pre-Exponent (cm/sec-MPa^n)	Exponent (-)
0.52	0.0	2.50800	0.46200
690.00	0.0	2.00700	0.13300

Table 4.1 (continued)

GRAIN GEOMETRY

External diameter (cm)	0.300
Length (cm)	0.0
Diameter of perforations (cm)	0.0
Number of perforations (-)	0.
Form (0 = cylinder, 1 = sphere)	1

PROPERTIES OF BAG NUMBER 1

Main charge propellant type	1
Centercore igniter propellant type	2
Rear basepad reactivity data	1
Forward basepad reactivity data	0
Rear of centercore permits solid efflux (1 = yes, 0 = no)	0
Front of centercore permits solid efflux (1 = yes, 0 = no)	0
Strong bag option (1 = yes, 0 = no)	0
Mass of main charge (kg)	5.9310
Initial porosity of main charge (-)	0.0
Mass of centercore charge (kg)	0.0567
Initial porosity of centercore charge (-)	0.0

CONFIGURATION OF REAR OF BAG

Axial Position (cm)	Radial Position (cm)	Thickness (cm)	Flow Res. Data	Reactivity Data	No. Pts Pre-assigned	Data (0=D,1=N)
2.540	1.270	0.0	0	1	0	0
2.540	3.387	0.0	0	0	0	0
2.540	7.620	0.0	0	0	0	0

CONFIGURATION OF FRONT OF BAG

Axial Position (cm)	Radial Position (cm)	Thickness (cm)	Flow Res. Data	Reactivity Data	No. Pts. Pre-assigned	Data (0=D,1=N)
40.640	1.270	0.0	0	0	0	0
40.640	3.387	0.0	1	0	0	0
40.640	7.620	0.0	0	0	0	0

Table 4.1 (continued)

CONFIGURATION OF INSIDE OF BAG

Axial Position (cm)	Radial Position (cm)	Thickness (cm)	Flow Res. Data	Reactivity Data	No. Pts Pre-assigned	Data (0=D,1=N)
2.540	1.270	0.0	0	0	0	0
40.640	1.270	0.0	0	0	0	0

CONFIGURATION OF OUTSIDE OF BAG

Axial Position (cm)	Radial Position (cm)	Thickness (cm)	Flow Res. Data	Reactivity Data	No. Pts Pre-assigned	Data (0=D,1=N)
2.540	7.620	0.0	0	0	0	0
21.590	7.620	0.0	1	0	0	0
40.640	7.620	0.0	0	0	0	0

PROPERTIES OF BAG NUMBER 2

Main charge propellant type	1
Centercore igniter propellant type	2
Rear basepad reactivity data	1
Forward basepad reactivity data	0
Rear of centercore permits solid efflux (1 = yes, 0 = no)	0
Front of centercore permits solid efflux (1 = yes, 0 = no)	0
Strong bag option (1 = yes, 0 = no)	0
Mass of main charge (kg)	5.9310
Initial porosity of main charge (-)	0.0
Mass of centercore charge (kg)	0.0567
Initial porosity of centercore charge (-)	0.0

Table 4.1 (continued)

CONFIGURATION OF REAR OF BAG

Axial Position (cm)	Radial Position (cm)	Thickness (cm)	Flow Res. Data	Reactivity Data	No. Pts Pre-assigned	Data (0=D,1=N)
41.640	1.270	0.0	0	1	0	0
41.640	3.387	0.0	0	0	0	0
41.640	7.620	0.0	0	0	0	0

CONFIGURATION OF FRONT OF BAG

Axial Position (cm)	Radial Position (cm)	Thickness (cm)	Flow Res. Data	Reactivity Data	No. Pts Pre-assigned	Data (0=D,1=N)
79.740	1.270	0.0	0	0	0	0
79.740	3.387	0.0	1	0	0	0
79.740	7.620	0.0	0	0	0	0

CONFIGURATION OF INSIDE OF BAG

Axial Position (cm)	Radial Position (cm)	Thickness (cm)	Flow Res. Data	Reactivity Data	No. Pts Pre-assigned	Data (0=D,1=N)
41.640	1.270	0.0	0	0	0	0
79.740	1.270	0.0	0	0	0	0

CONFIGURATION OF OUTSIDE OF BAG

Axial Position (cm)	Radial Position (cm)	Thickness (cm)	Flow Res. Data	Reactivity Data	No. Pts Pre-assigned	Data (0=D,1=N)
41.640	7.620	0.0	0	0	0	0
60.690	7.620	0.0	1	0	0	0
79.740	7.620	0.0	0	0	0	0

CONFIGURATION OF BREECH

Axial Position (cm)	Radial Position (cm)
0.0	0.0
0.0	7.061
-3.454	8.484

Table 4.1 (continued)

CONFIGURATION OF PROJECTILE BASE

Axial Position (cm)	Radial Position (cm)
87.380	0.0
87.380	7.137
96.420	7.849

CONFIGURATION OF INSIDE BOUNDARY

Axial Position (cm)	Radial Position (cm)
0.0	0.0
87.380	0.0

CONFIGURATION OF OUTSIDE BOUNDARY

Axial Position (cm)	Radial Position (cm)
-3.454	8.484
92.460	8.052
96.420	7.849

PROPERTIES OF PROJECTILE

Projectile mass (kg)	46.720
Number of entries in bore resistance table	7
Resistance law number	0
N.B. If <1 or >3, value will default to 2 internally	
Number of filler elements	0

BORE RESISTANCE DATA

Projectile Travel (cm)	Resistive Pressure (MPa)
0.0	1.720
1.016	23.100
2.540	34.100
3.937	25.000
5.207	22.400
11.430	17.200
520.700	10.300

Table 4.1 (continued)

BAG FLOW RESISTANCE DATA

Type	Initial Friction Factor(-)	Rupture Stress(MPa)	Rupture Interval(msec)
1	1000.000	0.101	0.0

DATA TO DESCRIBE REACTIVITY OF BAG SUBSTRATE 1

Energy released during decomposition (J/gm)	2489.
Density of decomposing solid-phase (gm/cc)	1.6000
Ratio of specific heats (-)	1.2430
Molecular weight (gm/gmol)	23.3600

BAG SUBSTRATE DISCHARGE CHARACTERISTICS

Time(msec)	Rate of Discharge(gm/cm^2-sec)
0.0	2.620
0.100	26.200
30.000	26.200

LOCATION OF POINTS FOR PRESSURE SUMMARY TABLE

Axial Location(cm)	Wall(0) or Axis(1)
0.010	0
87.370	0

2D2P - Two-Dimensional, Two-Phase Flow
Q1D2P - Quasi-One-Dimensional, Two-Phase Flow
Q1D1P - Quasi-One-Dimensional, Single-Phase Flow
LP - Lumped Parameter, Single-Phase Flow

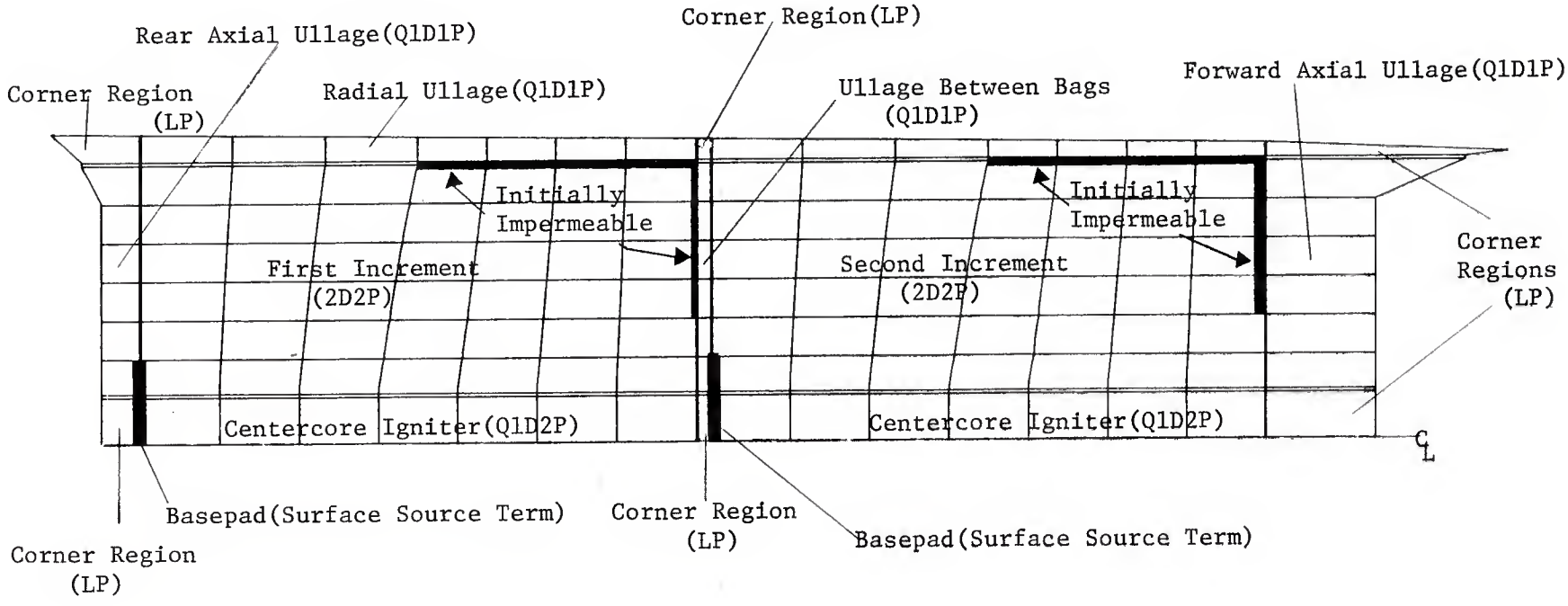

Figure 4.1 Representation of Computational Example

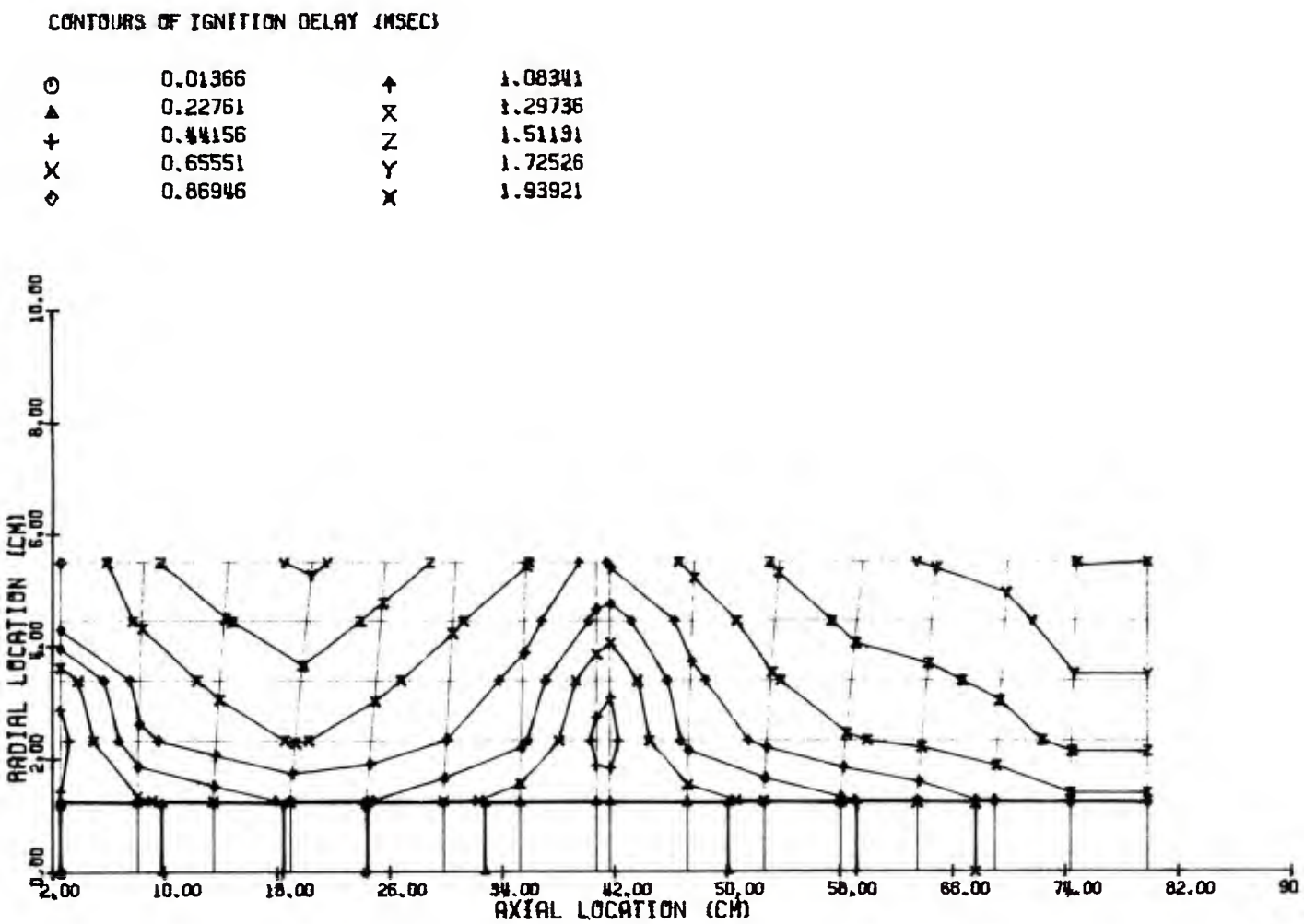

Figure 4.2 Contours of Ignition Delay

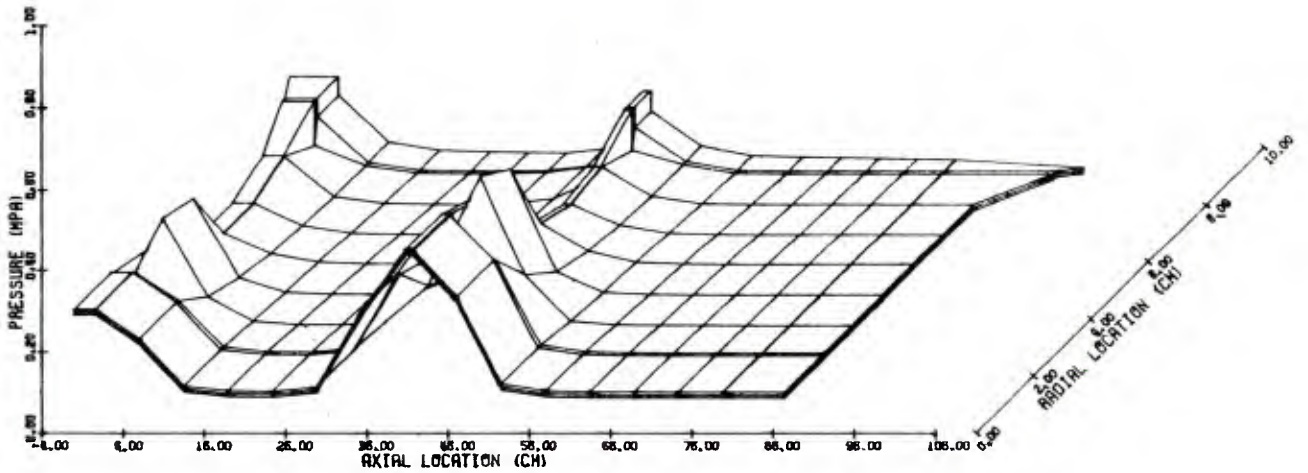

Figure 4.3 Pressure at 0.2 msec

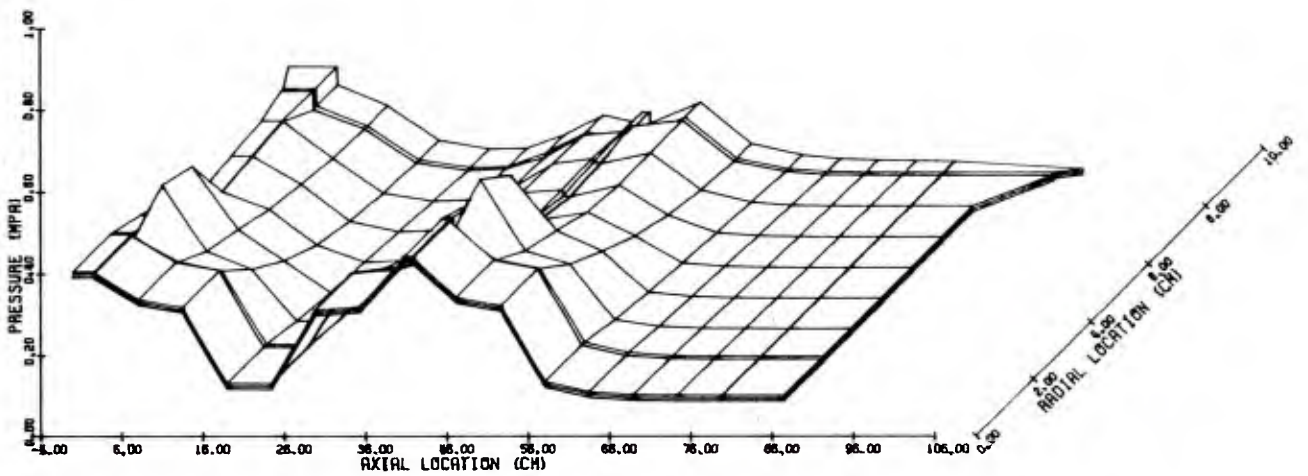

Figure 4.4 Pressure at 0.4 msec

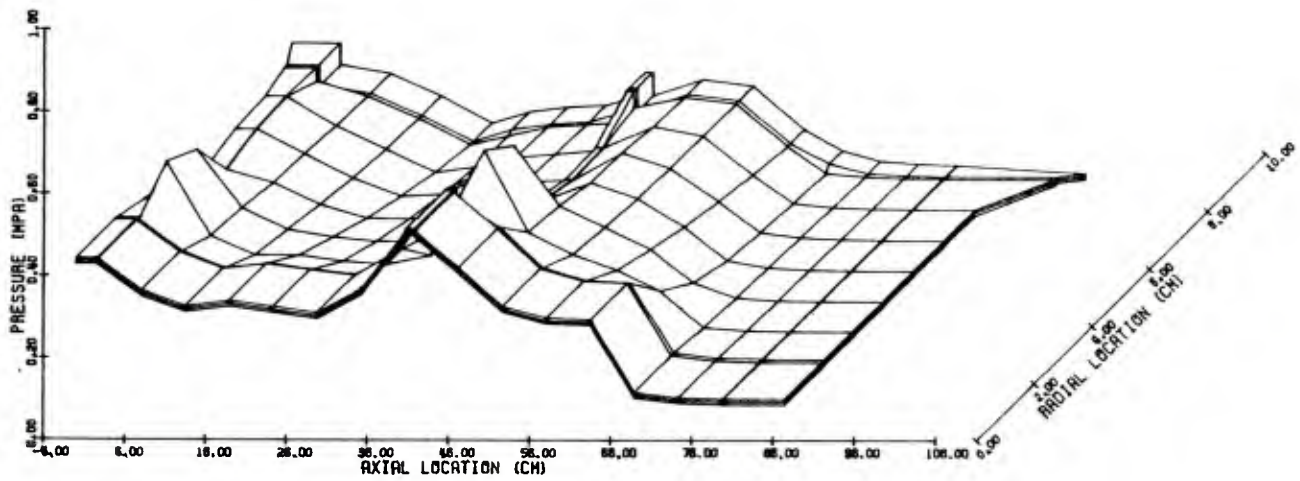

Figure 4.5 Pressure at 0.6 msec

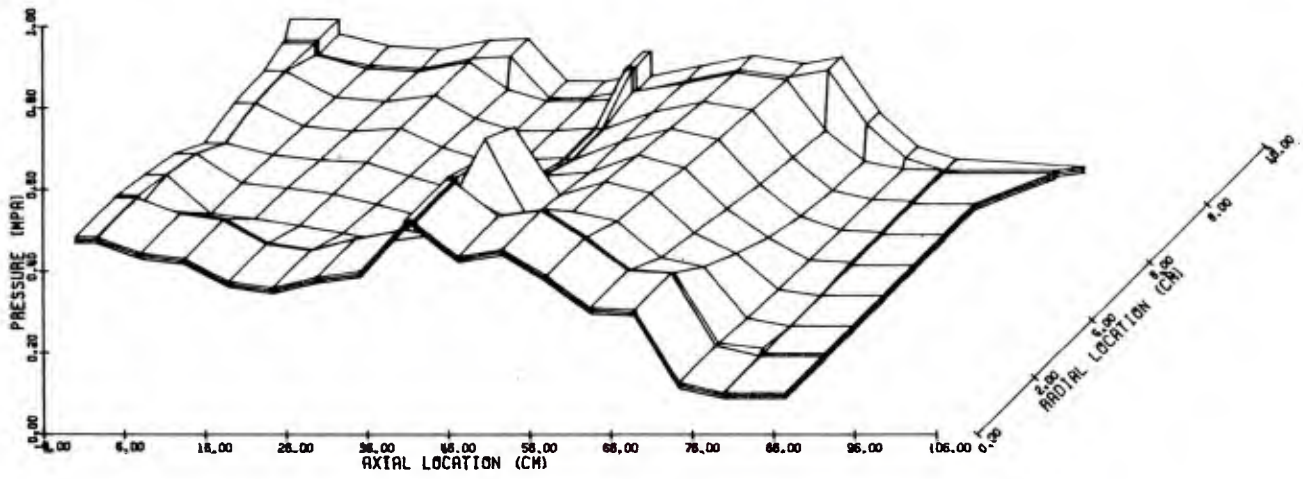

Figure 4.6 Pressure at 0.8 msec

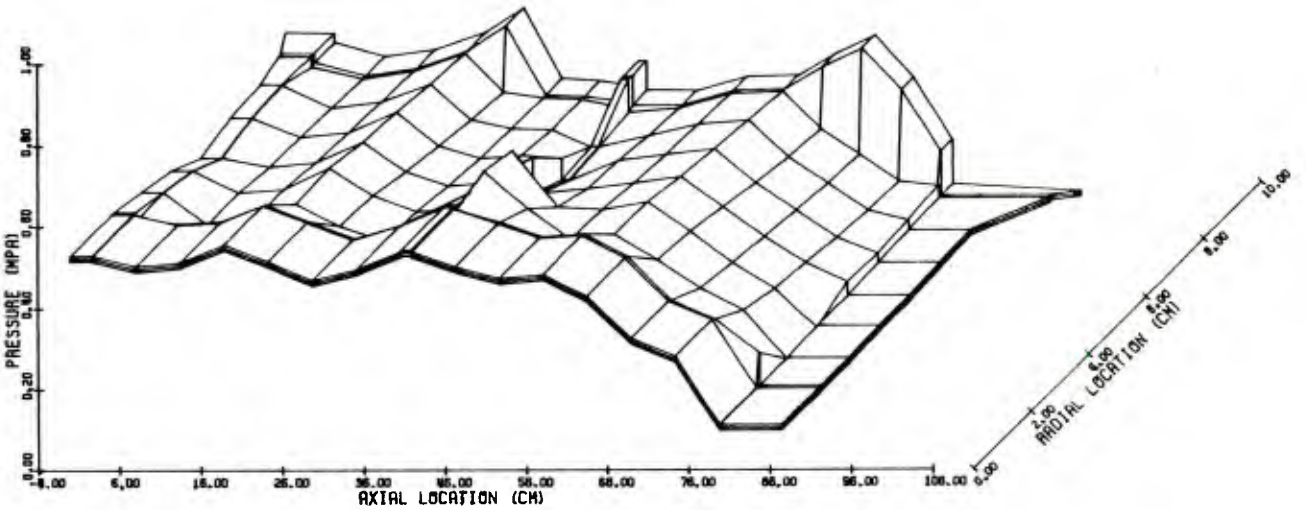

Figure 4.7 Pressure at 1.0 msec

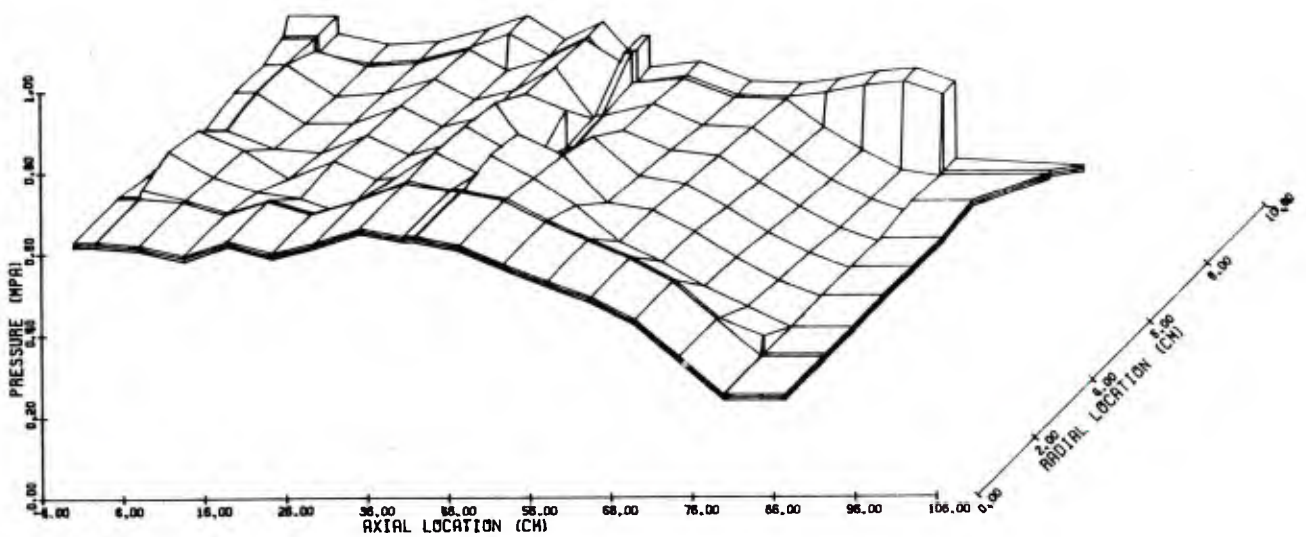

Figure 4.8 Pressure at 1.2 msec

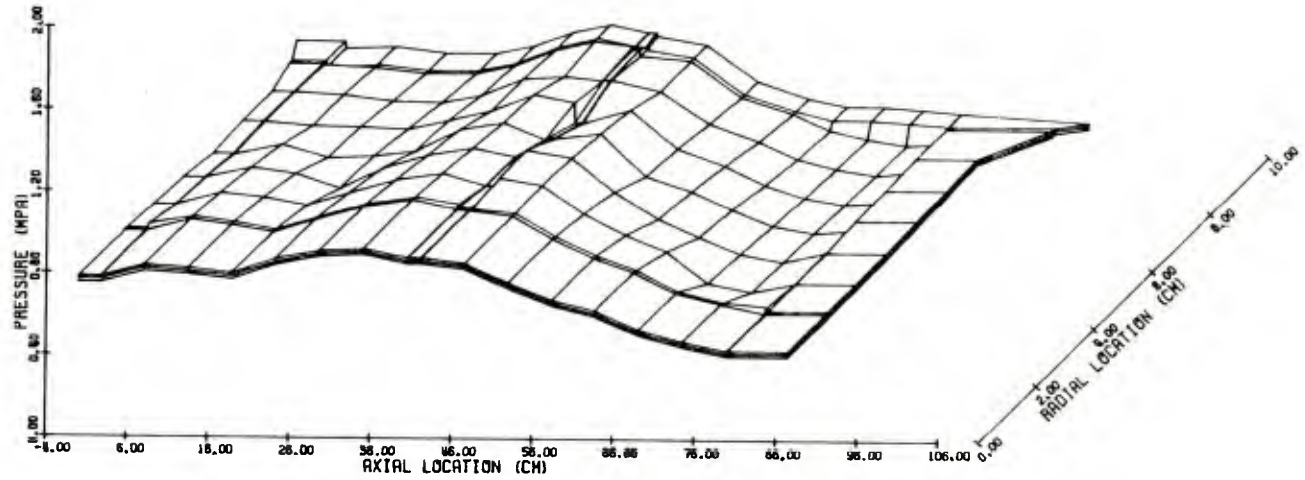

Figure 4.9 Pressure at 1.4 msec

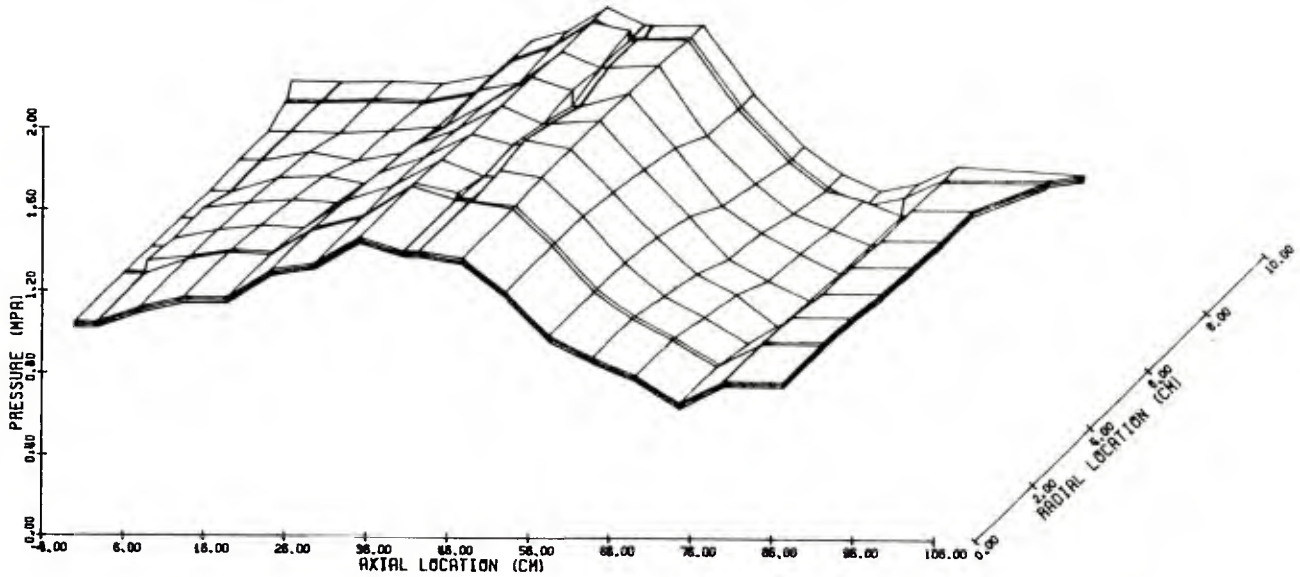

Figure 4.10 Pressure at 1.6 msec

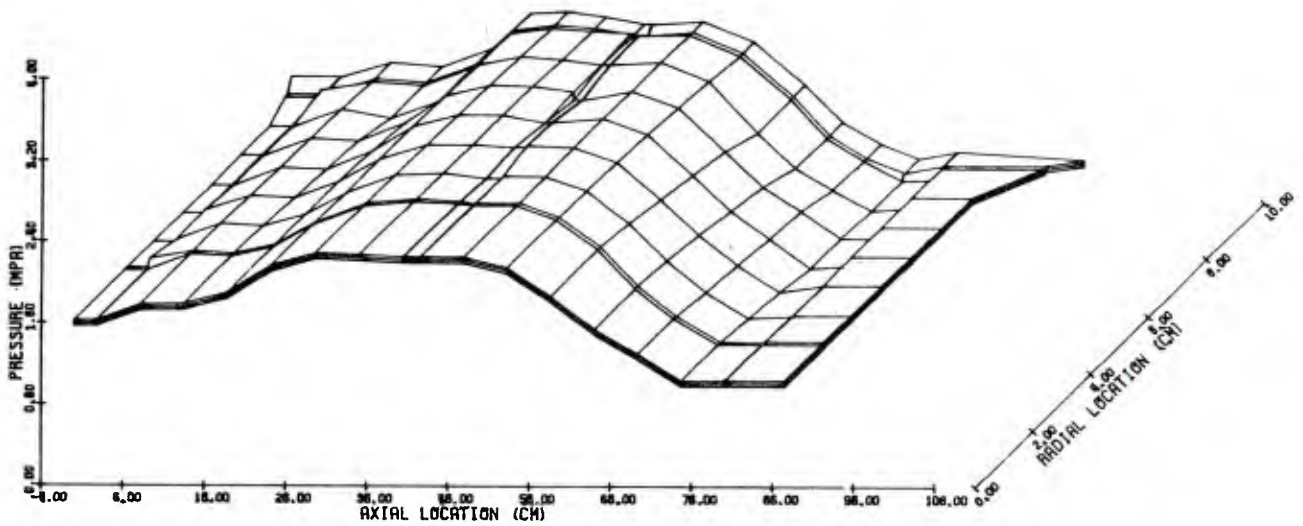

Figure 4.11 Pressure at 1.8 msec

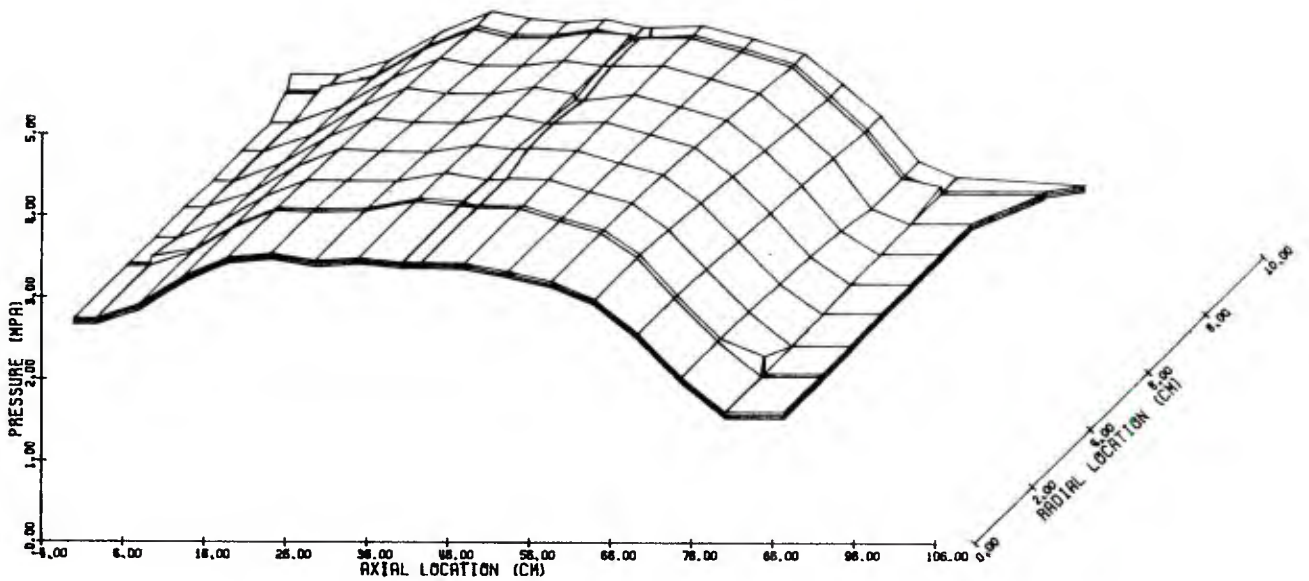

Figure 4.12 Pressure at 2.0 msec

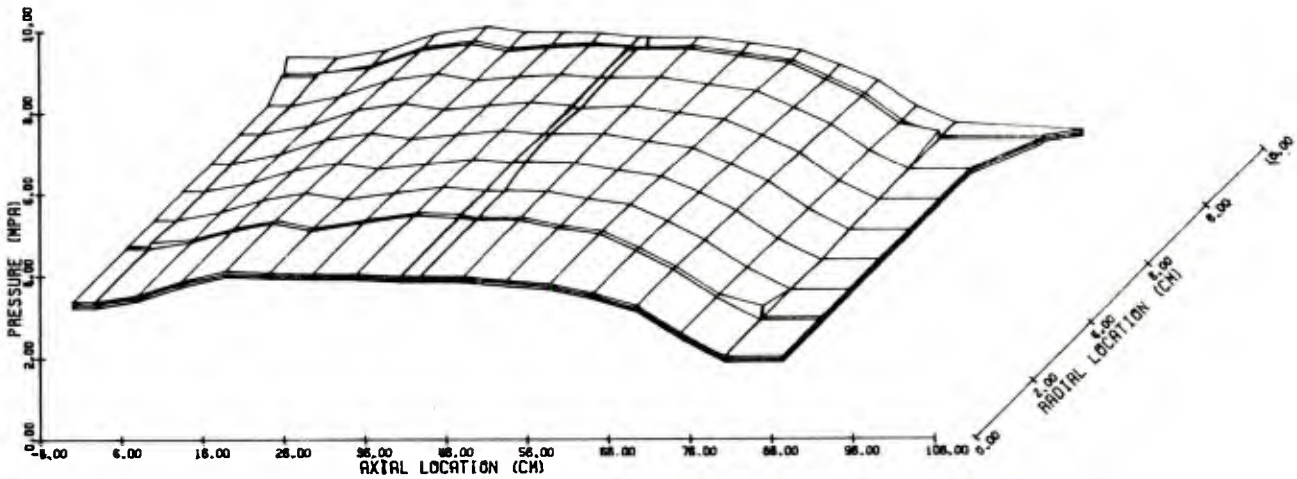

Figure 4.13 Pressure at 2.077 msec

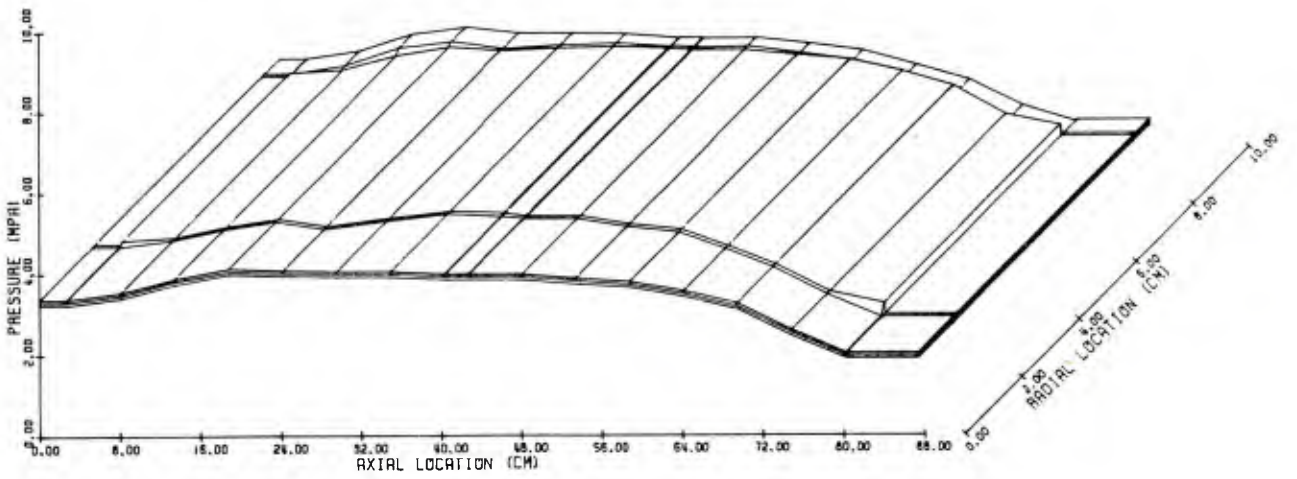

Figure 4.14 Pressure at 2.077 msec Following Transformation to Quasi-Two-Dimensional Representation

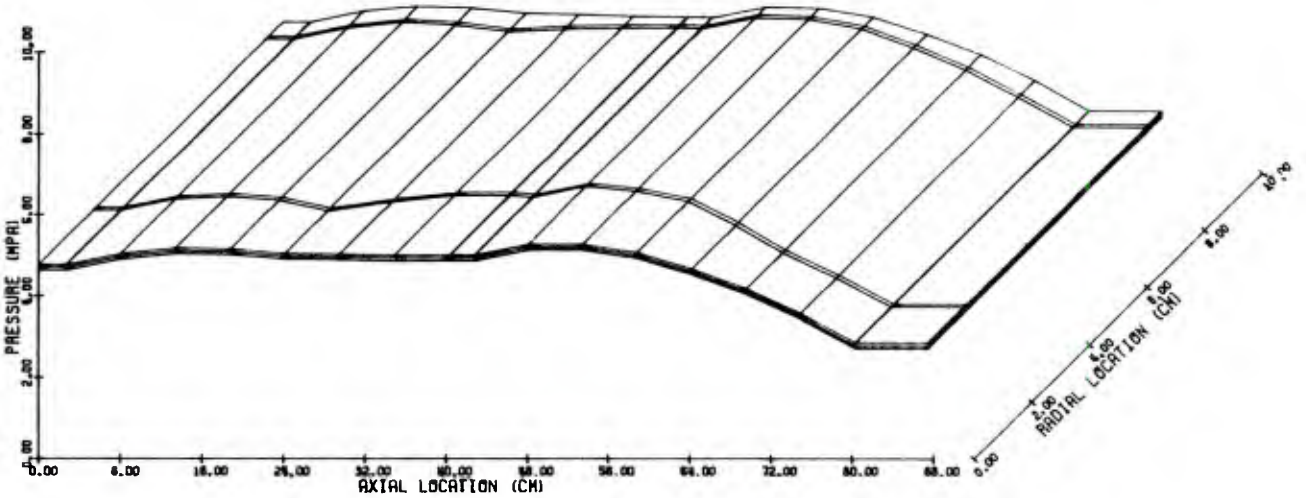

Figure 4.15 Pressure at 2.2 msec

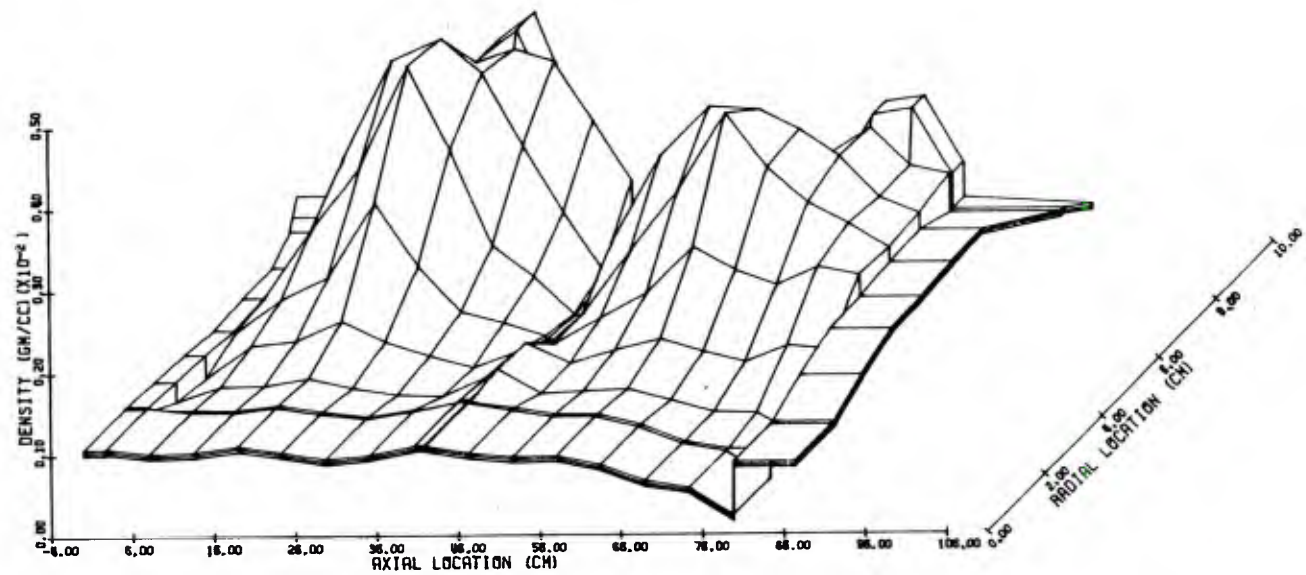

Figure 4.16 Density at 1.0 msec

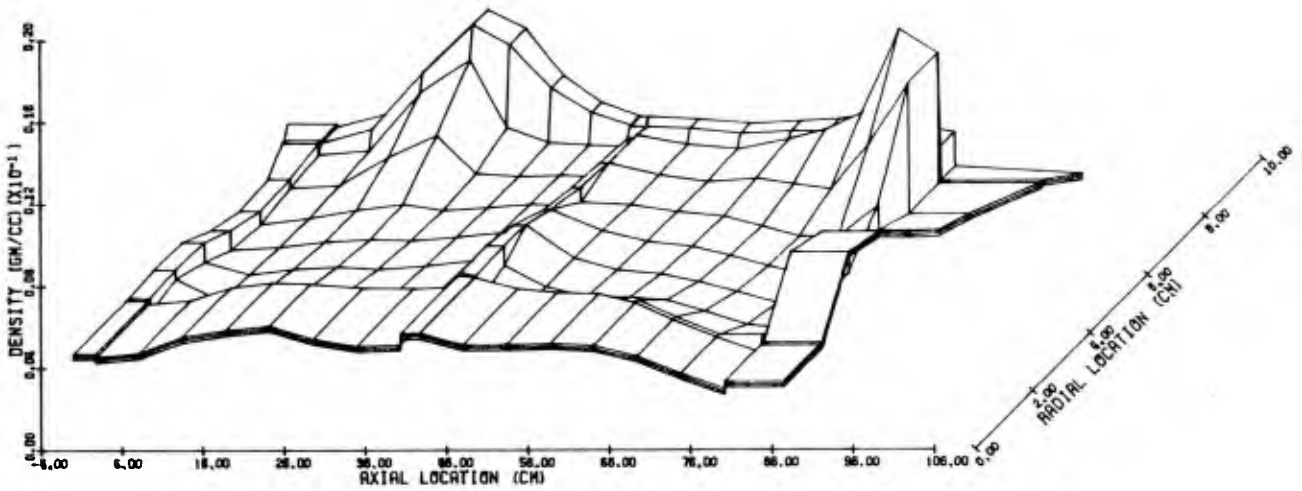

Figure 4.17 Density at 2.0 msec

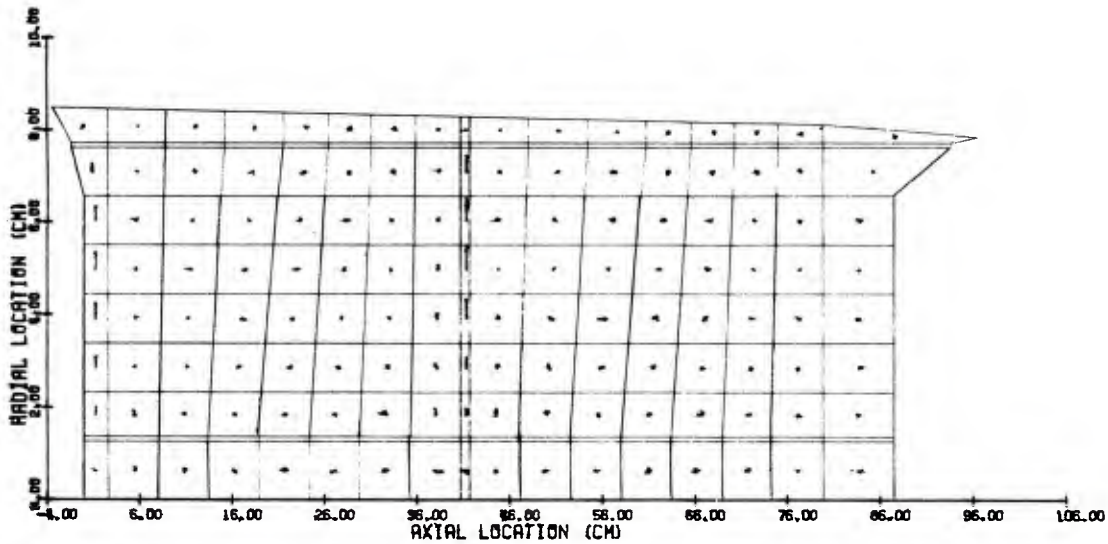

Figure 4.18 Velocity Field of Gas-Phase at 0.2 msec

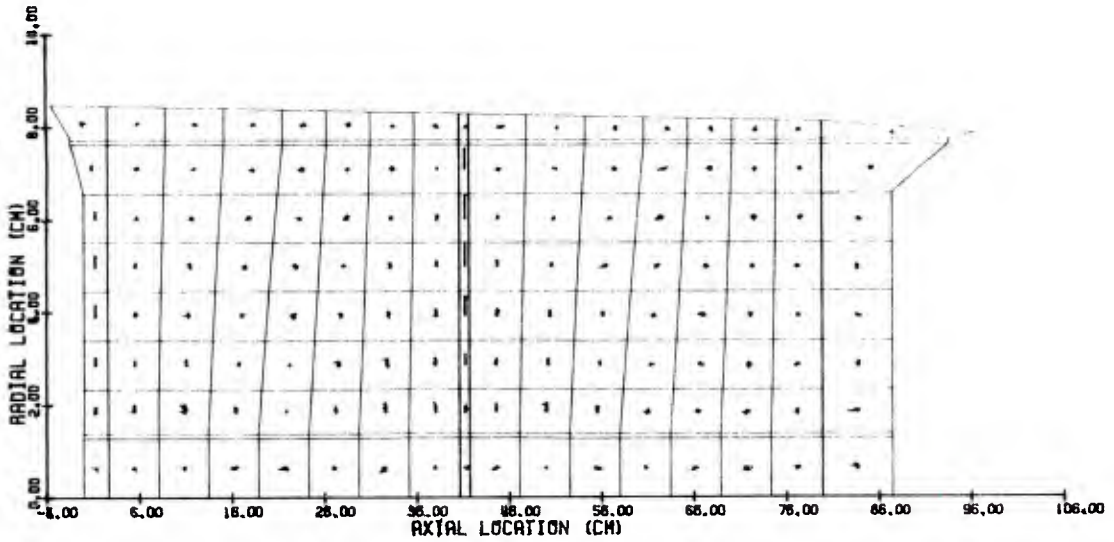

Figure 4.19 Velocity Field of Gas-Phase at 0.4 msec

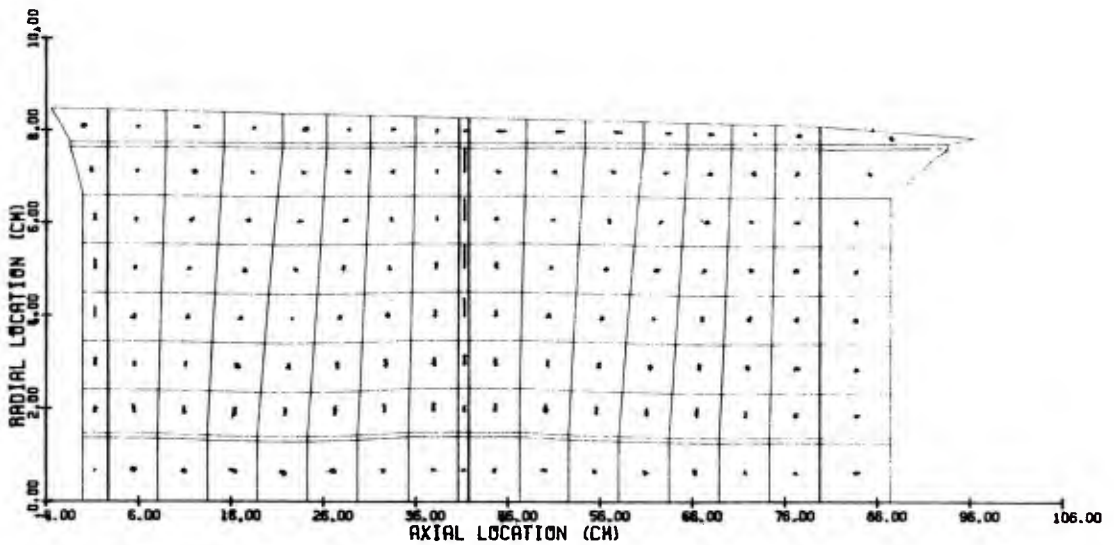

Figure 4.20 Velocity Field of Gas-Phase at 0.8 msec

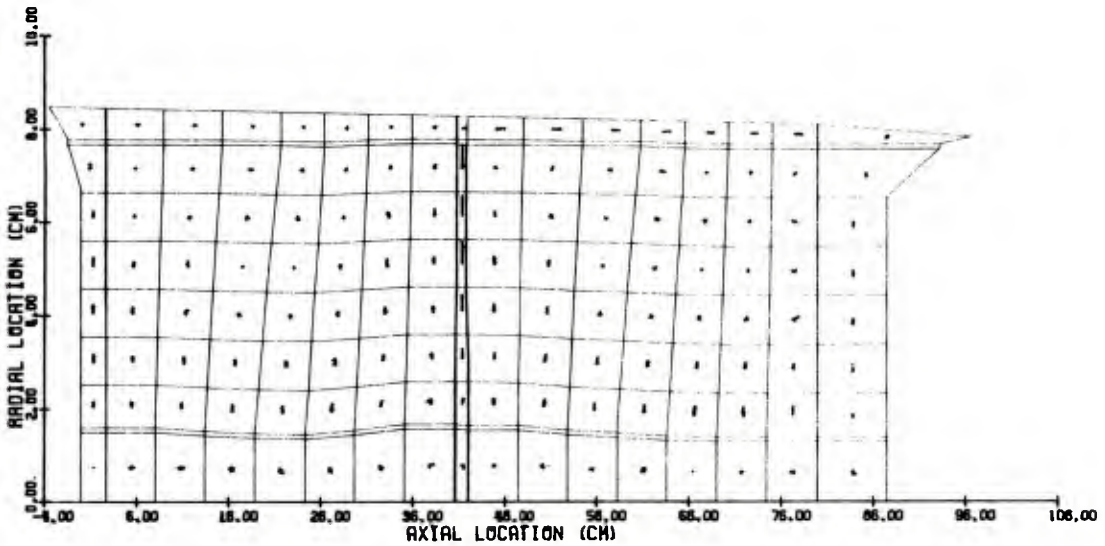

Figure 4.21 Velocity Field of Gas-Phase at 1.2 msec

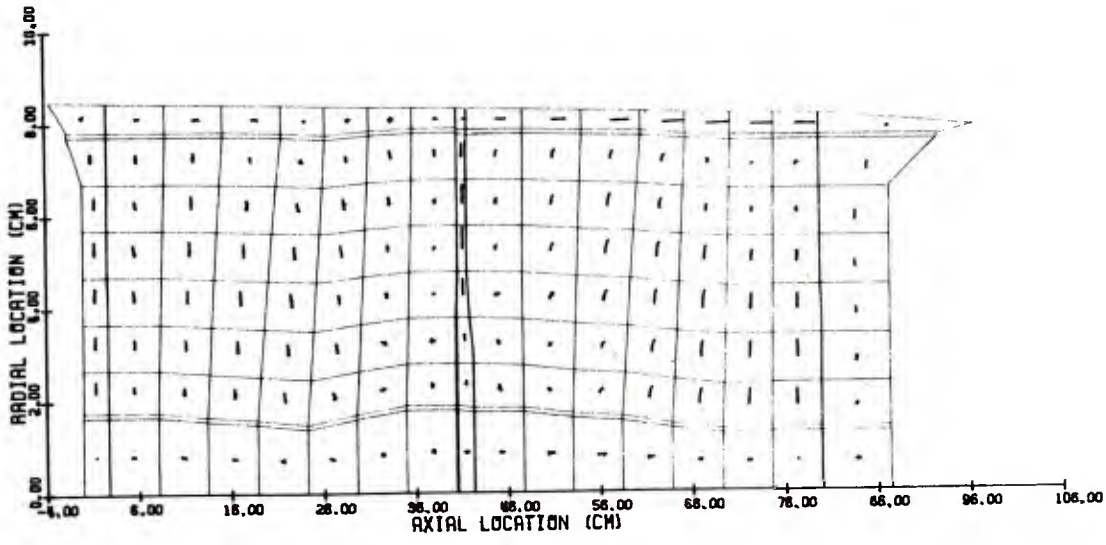

Figure 4.22 Velocity Field of Gas-Phase at 1.6 msec

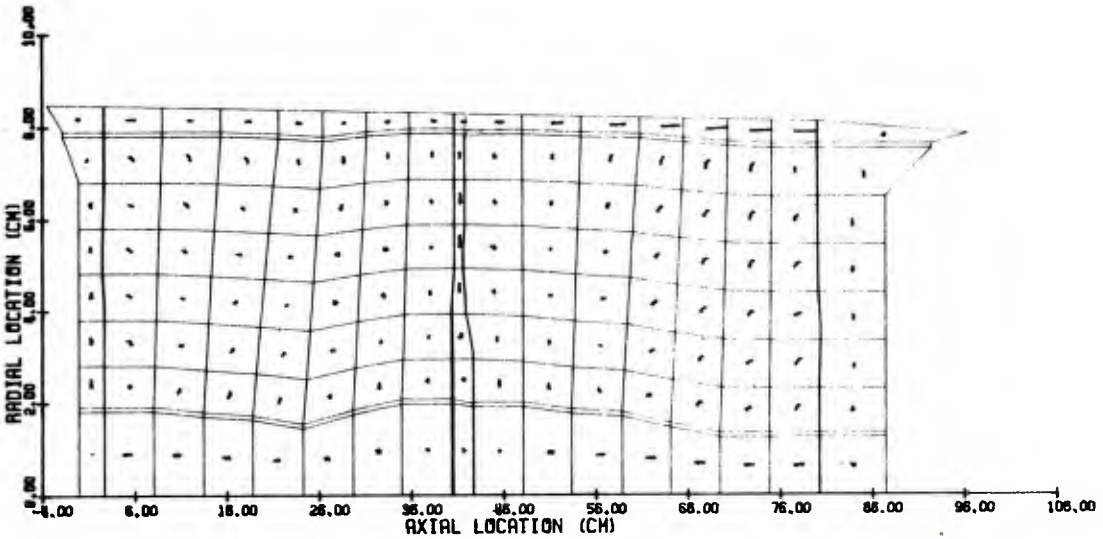

Figure 4.23 Velocity Field of Gas-Phase at 2.0 msec

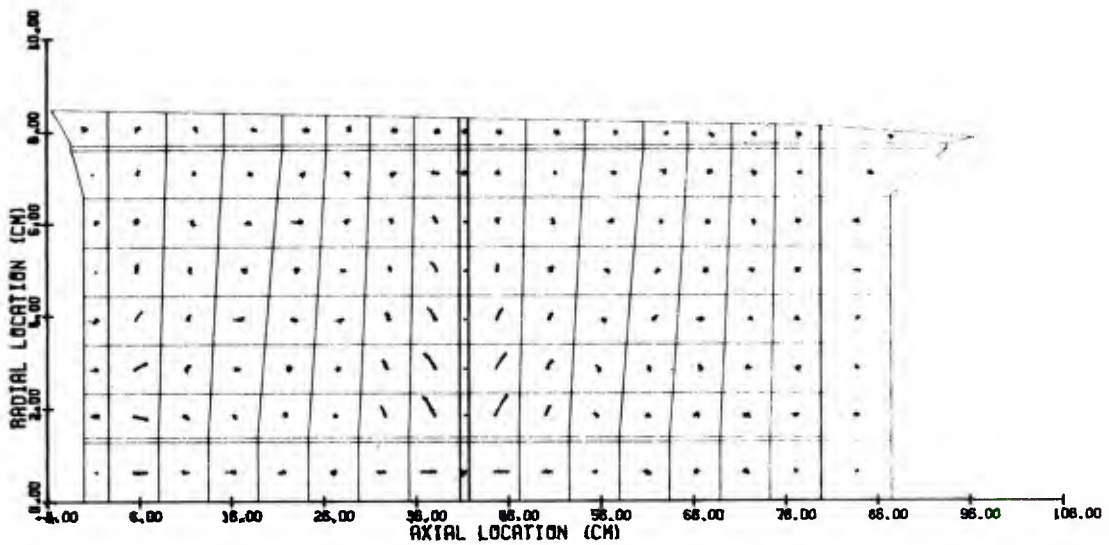

Figure 4.24 Velocity Field of Solid-Phase at 0.2 msec

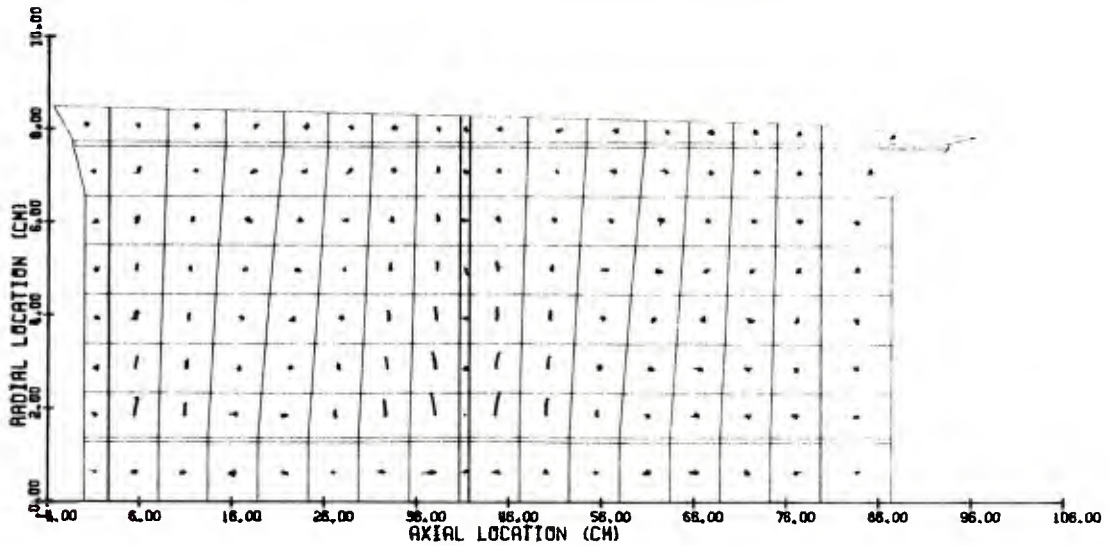

Figure 4.25 Velocity Field of Solid-Phase at 0.4 msec

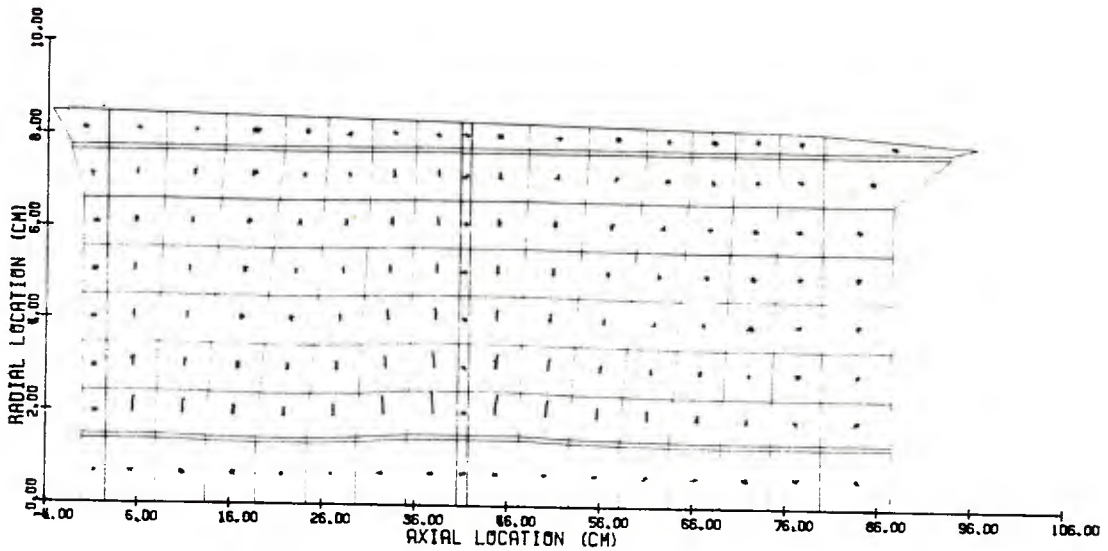

Figure 4.26 Velocity Field of Solid-Phase at 0.8 msec

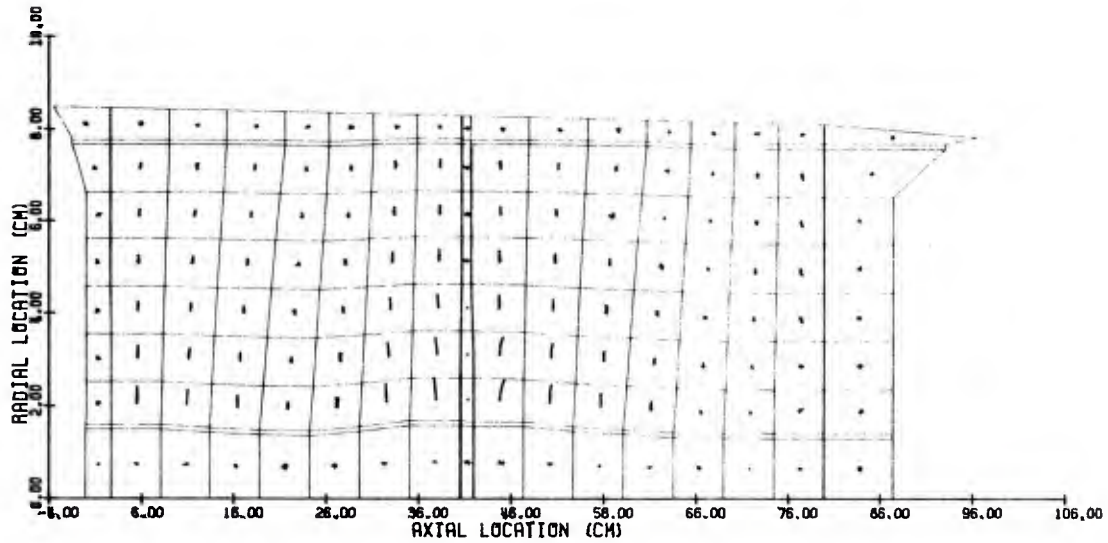

Figure 4.27 Velocity Field of Solid-Phase at 1.2 msec

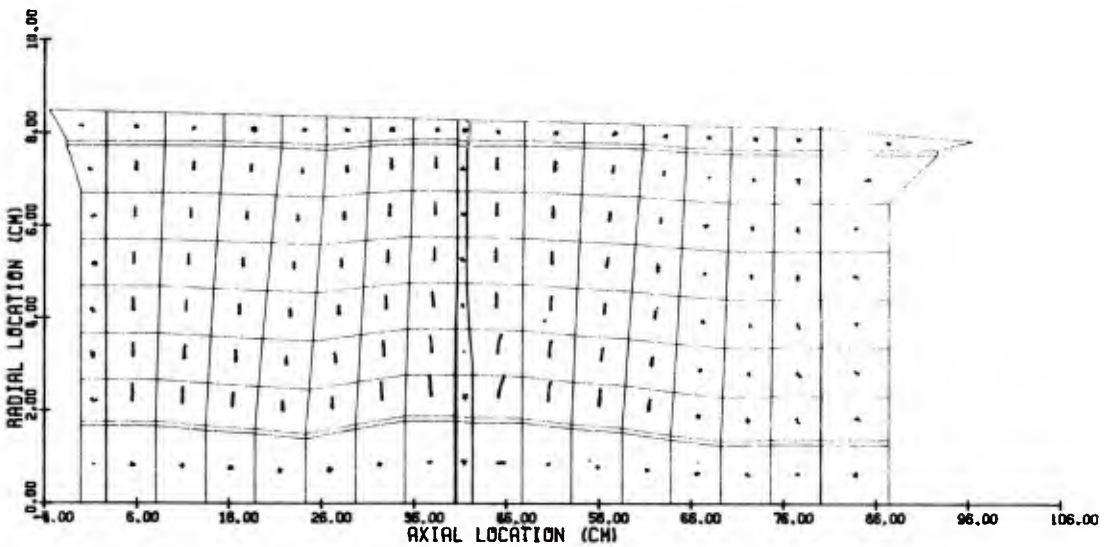

Figure 4.28 Velocity Field of Solid-Phase at 1.6 msec

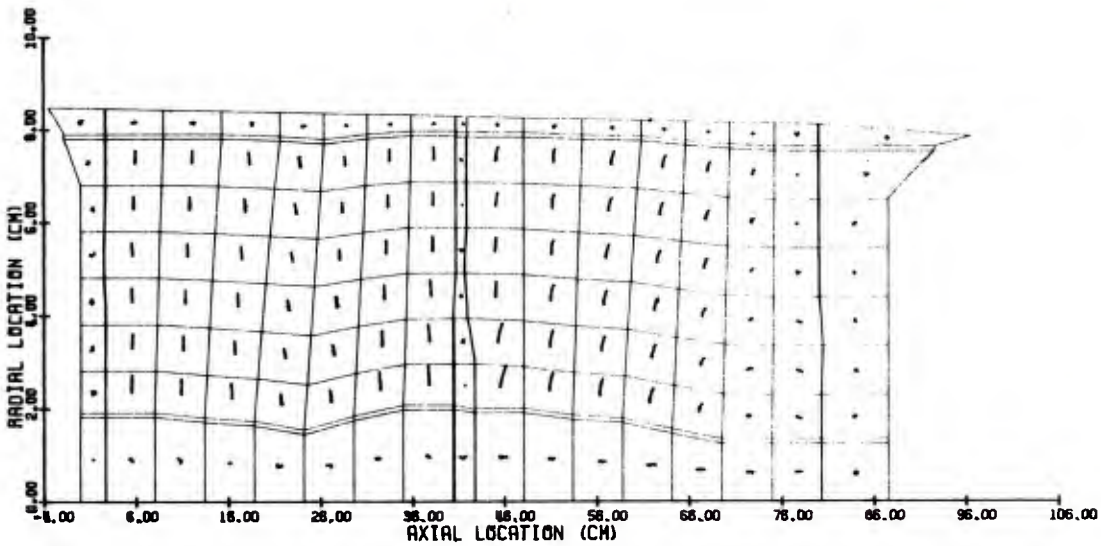

Figure 4.29 Velocity Field of Solid-Phase at 2.0 msec

ACKNOWLEDGMENT

Technical cognizance for the subject contract has been provided by Mr. A. W. Horst, Jr., US Army Armament Research and Development Command, Ballistic Research Laboratory, Aberdeen Proving Ground, Maryland.

REFERENCES

1. Gough, P. S.
"Two Dimensional Convective Flamespreading in Packed Beds of Granular Propellant"
Ballistic Research Laboratory Report ARBRL-CR-00404 July 1979 (ADA 075326)

2. Gough, P. S.
"A Two-Dimensional Model of the Interior Ballistics of Bagged Artillery Charges"
Ballistic Research Laboratory Report ARBRL-CR-00452 April 1981 (ADA 100751)

3. Horst, A. W., Smith, T. C. and Mitchell, S. E.
"Key Design Parameters in Controlling Gun-Environment Pressure-Wave Phenomena--Theory versus Experiment"
Proc. 13th JANNAF Combustion Meeting 1976

4. Horst, A. W. and Gough, P. S.
"Influence of Propellant Packaging on Performance of Navy Case Gun Ammunition"
J. Ballistics, v. 1, n. 3. 1977

5. Gough, P. S.
"Theoretical Study of Two-Phase Flow Associated with Granular Bag Charges"
Final Report, Contract DAAK11-77-C-0028 1978

6. Horst, A. W. and Gough, P. S.
"Modeling Ignition and Flamespread Phenomena in Bagged Artillery Charges"
Ballistic Research Laboratory Technical Report ARBRL-TR-02263 (ADA 091790) 1980

7. Gough, P. S.
"The Flow of a Compressible Gas Through an Aggregate of Mobile, Reacting Particles"
Ph.D. Thesis, McGill University 1974

8. Gough, P. S. and Zwarts, F. J.
"Modeling Heterogeneous Two-Phase Reacting Flow"
AIAA J v. 17, n. 1, pp. 17-25 1979

9. Gough, P. S.
"On the Closure and Character of the Balance Equations for Heterogeneous Two-Phase Flow"
Dynamics and Modelling of Reactive Systems, Academic Press 1980

10. Ishii, M.
"Thermo-Fluid Dynamic Theory of Two-Phase Flow"
Eyrolles, Paris 1975

11. Saffman, P. G.
"On the Boundary Condition at the Surface of a Porous Medium"
Stud. Appl. Math. vol. L, no. 2, p. 93 June 1971

12. Williams, F. A.
"The Role of Black Powder in Propelling Charges"
Picatinny Arsenal Technical Report 4770 1975

13. Gough, P. S.
"The NOVA Code: A User's Manual"
Final Report, Task I, Contract N00174-79-C-0082 1979

14. Krier, H., Shimpi, S. A. and Adams, M. J.
"Interior Ballistic Predictions Using Data from Closed and Variable Volume Simulators"
Univ. of Illinois at Urbana-Champaign
TR-AAE-73-6 1973

15. Horst, A.
Private Communication

16. Ergun, S.
"Fluid Flow Through Packed Columns"
Chem. Eng. Progr. v. 48, p. 89 1952

17. Anderssen, K. E. B.
"Pressure Drop in Ideal Fluidization"
Chem. Eng. Sci. v. 15, pp. 276-297. 1961

18. Gelperin, N. I. and Einstein, V. G.
"Heat Transfer in Fluidized Beds"
Fluidization, edited by Davidson, J. F. and Harrison, D. Academic Press, NY 1971

19. Thompson, J. F., Thames, F. C. and Mastin, C. W.
"Automatic Numerical Generation of Body-Fitted Curvilinear Coordinate System for Field Containing Any Number of Arbitrary Two-Dimensional Bodies"
J. Comp. Phys. 15, pp. 299-319 1974

20. Roache, P. J.
"Computational Fluid Dynamics"
Hermosa Publishers 1972

21. MacCormack, R. W.
"The Effect of Viscosity in Hypervelocity Impact Cratering"
AIAA Paper No. 69-354 1969

22. Moretti, G.
"Calculation of the Three-Dimensional, Supersonic, Inviscid, Steady Flow Past an Arrow-Winged Airframe"
POLY-AE/AM Report No. 76-8 1976

23. Richtmyer, R. D. and Morton, K. W.
"Difference Methods for Initial Value Problems"
Interscience 1967

24. Gough, P. S.
"Extensions to NOVA Flamespread Modeling Capacity"
Final Report for Task I, Contract N00174-80-C-0316
PGA-TR-81-2 April 1981

25. Lenchitz, C. and Hayes, E.
"An Analysis of Black Powder Ignition and Performance. Ignition Properties of Black Powder, Phase I"
Proc. 16th JANNAF Combustion Meeting 1979

26. Rose, J. E. and Hardt, A. P.
"Black Powder --A Modern Commentary--1979"
Proc. 10th Symposium on Explosives and Pyrotechnics, Franklin Research Center, Phila., PA. Feb. 14-16 1979

APPENDIX A

TDNOVA - Structure and Use

The purpose of this Appendix is to provide sufficient information to enable the reader to make use of the code TDNOVA. To that end we provide, in three successive subsections, an overview of the code macrostructure, a brief discussion of the storage arrays and the principal storage pointers, and a complete description of the code input and output files.

It should be noted that the discussion of this Appendix addresses all pertinent details of the code revisions performed for the Navy to enable simulations to be made of case charge ammunition. The corresponding model revisions have not been described in the main body of this report. The interested reader will find relevant modeling details in the appropriate Navy reports.[13, 24]

CODE MACROSTRUCTURE

TDNOVA is written in the FORTRAN IV language. Because it was developed on a 32 bit word machine (ITEL AS-6), all computations are performed in double precision. Thus, users of the code who employ a machine in which the standard word length is 60 or more bits, such as the CYBER 7600, may wish to convert the code to single precision as a measure of economy.

The code macrostructure is illustrated schematically in Figure A.1. The main program TDMAIN is essentially a dummy routine. It executes a call to INPUT, to read and print the problem data, to SETUP, to initialize the problem variables, and then transfers complete control of the calculations to subroutine TDXC, which is, in fact, the principal executive routine. The code version at BRL, following the return from TDXC, also executes a call to a BRL routine called RECAP, whose purpose is to plot data accumulated in the summary tables during the evolution of the solution.

Users who wish to reduce the overall code storage may perform successive overlays onto INPUT and SETUP since these subroutines are each called just once.

The next level of code structure is defined by the principal linkages to the executive TDXC. TDXC is supported by the output routine LOGOUT which is called intermittently to prepare tables of state variables at various times. LOGOUT also stores the solution on disc, if desired, and executes optional calls to PLOTRZ which is responsible for the preparation of graphic representations of the solution. PLOTRZ may be seen to be supported by subroutines PLTLOD, PLTFLO, CONTR, and SEE. Additional output processing is performed by subroutine SUMTAB, which prepares tables of summary data, as desired. These, however, are only printed at the conclusion of the run. It is these data which are further processed by the BRL routine RECAP.

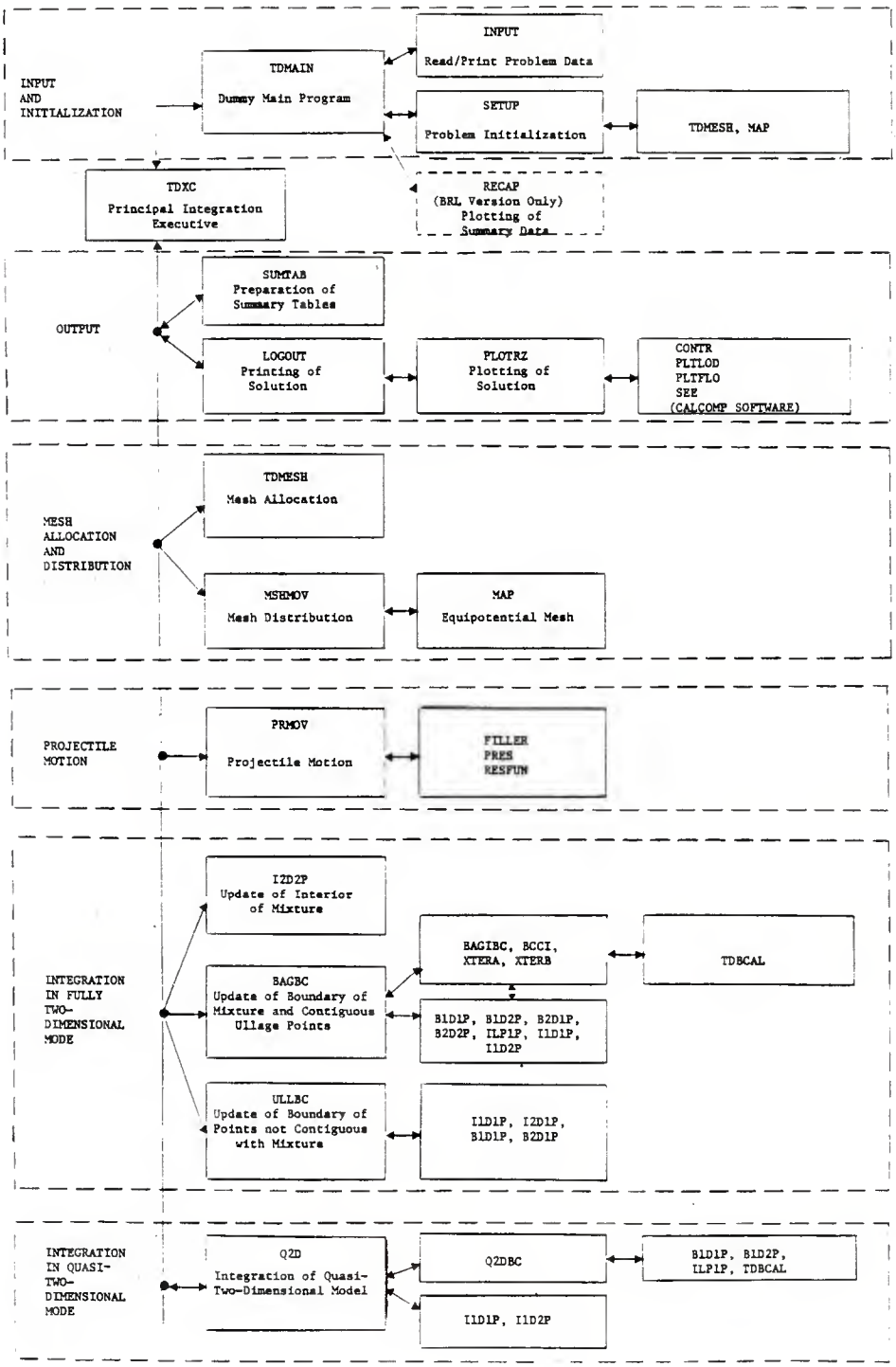

Figure A.1 Schematic Illustration of TDNOVA Macrostructure
(Only principal linkages and routines are shown. See Table A.1)

TDXC is supported by TDMESH and MSHMOV, which respectively allocate storage to the various computational regions and assure that the two-dimensional regions have boundary-fitted equipotential meshes.

The integration at all points interior to the mixture is performed by I2D2P. Subroutine ULLBC executes calls to I2D1P to update the solution in the interior of all fully two-dimensional regions of ullage and also performs the update of all ullage boundary points which are not contiguous with the mixture. In the latter capacity, it is supported by the routines B1D1P, I1D1P and B2D1P.

Subroutine BAGBC is called by TDXC to effect the update of all points on the boundary of the mixture as well as those points in the ullage which are contiguous with the mixture. For this purpose, mesh points in a region of quasi-one-dimensional ullage adjacent to the bag are regarded as contiguous with the mixture.

When only one bag is present, BAGBC is responsible for the implementation of all the conditions of physical compatibility at the bag boundaries contiguous with quasi-one-dimensional ullage. It is supported by the routines I1D1P, I1D2P which update points in the interior of adjacent quasi-one-dimensional regions, by B1D1P, B1D2P, and B2D2P which provide trial update values for contiguous boundary points, and by ILP1P which updates lumped parameter ullage regions. The conditions of physical compatibility at points contiguous with two-dimensional ullage are implemented by XTERA and XTERB which are called from BAGBC.

When two or more bags are present, BAGBC calls BAGIBC to enforce the conditions of physical compatibility at the bag-to-bag interfaces. BAGIBC itself treats those points which are not situated on the bag corners and calls BCCI to update the solution at the corner points. As with BAGBC, the update at the bag-to-bag boundary points is performed simultaneously with that at the contiguous ullage points.

Subroutines I2D2P, ULLBC and BAGBC are called only until the flow has evolved to such a point as to be amenable to a quasi-two-dimensional analysis.* Subsequently, TDXC is supported entirely by the routine Q2D which acts as the integration executive for the quasi-two-dimensional representation. Q2D enforces the conditions of physical compatibility between regions and is supported by the subroutines I1D1P, I1D2P at the interior mesh points. At the boundaries Q2D is supported by Q2DBC which in turn makes use of B1D1P, B1D2P and ILP1P.

We also note that TDXC is cycled twice per complete integration step since each step is composed of a predictor and a corrector level as discussed further in the next section when we consider the structure of the storage arrays.

---

*It should be noted that, in contrast to the previous version of the code, transformation to a quasi-two-dimensional analysis occurs only in the static mesh allocation mode.

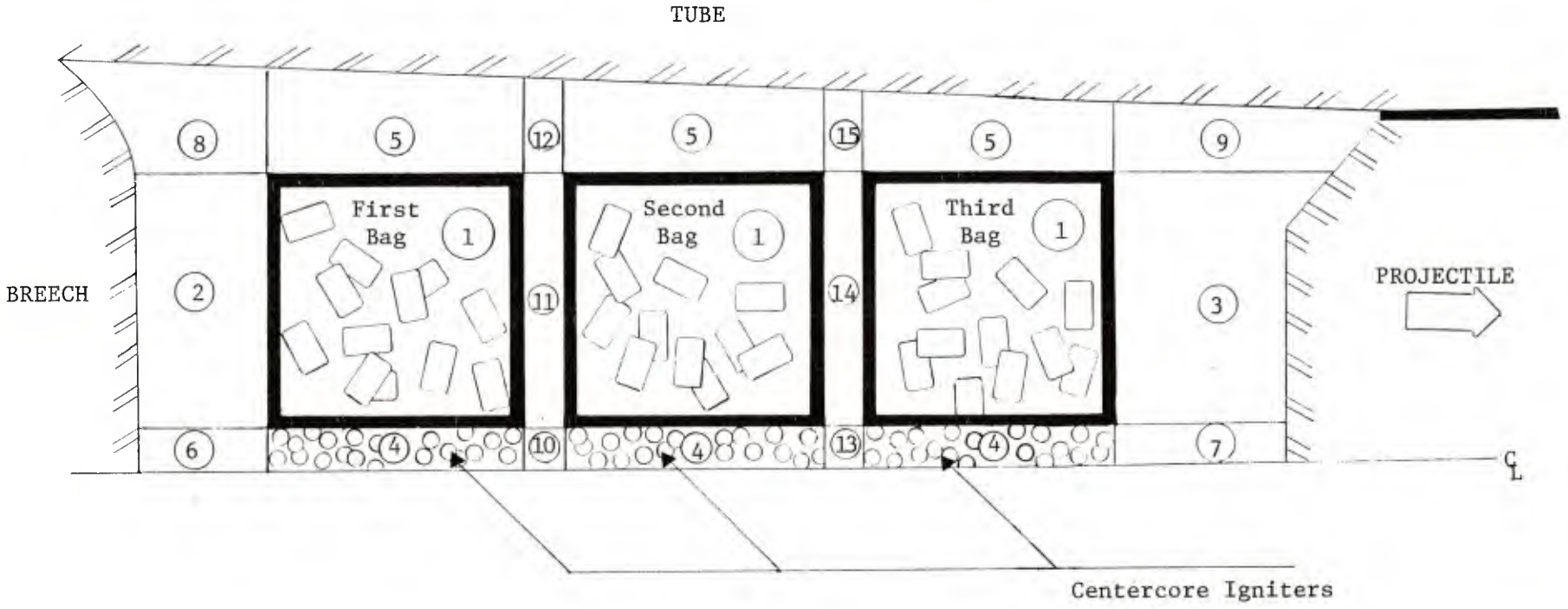

Figure A.2 Nomenclature for Region Labelling in TDNOVA Illustrated for Problem Involving Three Bags

TDNOVA does contain other routines than those which we have mentioned explicitly in this section. A complete summary of the various routines and their linkages to one another is contained in Table A.1. Following the entry for TDMAIN, all the routines are described in alphabetic order. Not shown in Table A.1 are the linkages to standard FORTRAN functions and to the standard CALCOMP software package. The use of the latter may be system-dependent, particularly with regard to the plot initialization and termination routines.

DATA STORAGE

Table A.2 provides a summary of all the program variables stored in common blocks. Variables which are purely local to a given subroutine or function are not described in Table A.2.

The purpose of the present discussion is to provide a description of the principal pointers and to explain the manner in which the state variables are stored.

Each integration step consists of two levels, a predictor and a corrector. The counter NDT, initialized to zero, is bumped by unity on each predictor and each corrector level. The switch INT = MOD(NDT+1,2) is equal to 1 on a predictor level and 0 on a corrector level. At each level the variables NI, NF, NP are used to construct pointers to current, future and past storage, and they cyclically run through the values 1, 2, 3.

If the total number of propellant bags is denoted by NBAGS, then a total of NRG = 9 + 3*(NBAGS - 1) computational regions are defined. A case involving 3 bags for which NRG = 15 is illustrated in Figure A.2. Each region I has attributes NDZ(I), the total number of axial mesh points; NDR(I), the total number of radial mesh points; MODL(I), an indicator of the type of flow equations to be used; and NRBIAS(I), used to construct storage pointers, as described below. The indicator MODL(I) has the following set of values.

MODL(I)	Type of Flow in Region I
1	Lumped Parameter One-Phase (LP1P)
2	Quasi-One-Dimensional One-Phase (1D1P) (Axially directed)
3	Quasi-One-Dimensional One-Phase (1D1P) (Radially directed)
4	Two-Dimensional One-Phase (2D1P)
5	Quasi-One-Dimensional Two-Phase (1D2P)
6	Two-Dimensional Two-Phase (2D2P)

The parenthetical acronyms for each type of region are also present in the names of subroutines dedicated to the integration of each type of region with the further distinguishing characteristic of an initial letter I or B according as the routine pertains to interior or boundary mesh points. The distinction between cases MODL(I) = 2 and 3 is purely formal in the present version of the code.

The state variables are stored in singly indexed arrays. Accordingly, the values pertaining to a given mesh point at a given level of a given time step are located by construction of a suitable pointer.

In order to retain as many of the existing code storage conventions as possible, we have used the previous region labels for those regions which do not lie between successive bags. Thus, as may be seen in Figure A.1, we refer to the propelling charge as region 1 even when several different bags are present. Similarly, regions 4 and 5 extend the length of the entire charge. But these regions--1, 4 and 5--may be interrupted by new regions--10, 11, and 12, for example--when several bags are present.

In our subsequent discussion of the storage pointer construction, we will consider first the case when one bag is present, and then we will note the additional considerations which must be taken into account when two or more bags are present.

As in our previous report,[2] we consider, as an example, the gas-phase density, which is stored in the array RHO(J).

The array RHO contains values of density in the following order. First, the NDZ(1) values pertaining to the line $\eta = 0$ in region 1 (the mixture) are stored. These are followed by successive blocks of NDZ(1) values corresponding to successive increments of the coordinate η. There are, of course, a total of NDR(1) such blocks. Then there are loaded NDZ(2) values corresponding to the line $\eta = 0$ for region 2 and so on through region NRG. It should be noted that NDZ and NDR are each equal to at least one for any type of region. A lumped parameter region has NDZ = NDR = 1.

Following the last value for region NRG, there are loaded NDZ(1) values for the line $\eta = 0$ in region 1 corresponding to the next level of integration. Three such integration level blocks are defined.

The quantity NRBIAS(I) is defined as

$$\text{NRBIAS(I)} = \begin{cases} \sum_{J=1}^{I-1} \text{NDZ(J)*NDR(J)} & \text{for I > 1} \\ 0 & \text{for I = 1} \end{cases}$$

and the total number of mesh points is given by

$$\text{NPTOT} = \sum_{J=1}^{NRG} \text{NDZ(J)*NDR(J)}$$

We also define the quantity

NIBIAS = (NI - 1)*NPTOT

and an analogous definition is given for NPBIAS, NFBIAS which are used to construct pointers to NP- and NF- integration levels, respectively.

Now, let $\rho^{NI}_{IJ,K}$ be the value of ρ at the ζ-mesh point I, the η-mesh point J, in region K, at level NI, then

$$\rho^{NI}_{IJ,K} = \text{RHO(NIBIAS + NRBIAS(K) + (J - 1)*NDZ(K) + I)}$$

This pattern is followed for all the independent state variables. However, for dependent state variables, such as the internal energy, only current storage is maintained. Thus, pointers for the array E are constructed similarly to those for RHO, but the quantities NIBIAS, NPBIAS, NFBIAS are not used.

In the preceding discussion, it has been assumed that only one bag was present. In fact, when several bags are present, only minor revisions to the construction of the storage pointer are required and then only for regions 1, 4 and 5.

Let I_L identify a ζ-mesh point which lies in the L-th bag and let I_L take the value 1 at the left boundary of the bag and the value NSDZ(L) at the right boundary. Define the bias

$$\text{NSBIAS(L)} = \begin{cases} \sum_{J=1}^{L-1} \text{NSDZ(J)} & \text{for L > 1} \\ 0 & \text{for L = 1} \end{cases}$$

Then, with I_L understood to be particularized to the L-th bag, as described above, we have

$$\rho^{NI}_{I_L J,K} = \text{RHO}(\text{NIBIAS} + \text{NRBIAS}(K) + (J - 1)*\text{NDZ}(K) + \text{NSBIAS}(L) + I_L)$$

It should be emphasized that NDZ(K) is used to construct the pointer and not NSDZ(K).

INPUT AND OUTPUT FILES

TDNOVA is structured to run only one problem. It does not support parametric input, nor does it search for a new data set following problem termination. A given problem, however, may be stored on disc at various points during the solution, as part of the logout procedure. Subsequently, the problem may be restarted from disc at any intermediate point at which logout has been performed. The structure of the input files is described fully in Table A.3 and requires no additional comment here.

We conclude with a description of the output files. Logout may be obtained at multiples of an inputted number of integration steps and at multiples of an inputted increment of time. The logout associated with such intermediate points of the solution consists of printed text, disc storage and plotting, all in accordance with user-selectable options.

When printed logout is requested, it is furnished as a table of the current storage of the state variables in the order of storage described in the preceding section. Thus, the table proceeds to list the state variables region by region. Within each region, the state variables are tabulated in successive blocks of constant η (which may be thought of as approximately constant radius). For region 1, however, when several bags are present, we print all data for the first bag, followed by all data for the second bag, and so on. The tabulated quantities are, in order: Region number as described in Figure A.2, mesh axial coordinate, mesh radial coordinate, gas-phase pressure, intergranular stress, gas-phase axial velocity, gas-phase radial velocity, solid-phase axial velocity, solid-phase radial velocity, porosity, gas-phase density, gas-phase temperature, solid-phase surface temperature, and, for points on the boundary of the bag, indicators as to whether the bag is permeable and/or ruptured.

As an option, any of the state variables may be plotted as an isometric view of the surface $\phi(z,r)$ where ϕ is a state variable.

Hidden lines are normally deleted, but may be retained as an option. Further information concerning the solution may be had by requesting contour plots of the same surfaces. The isometric and contour plotting options are, however, fully independent of one another. An additional option is the preparation of flowfield plots in which the velocity fields of the gas- and solid-phases are represented, separately, as vector fields superimposed on the computational mesh.

A plot of the ignition delay, essentially a contour representation, may also be had. This is prepared just once, at the conclusion of the run. It should be noted that this map is constructed by reference to the initial configuration of the propelling charge.

In addition to the intermediate logout one may request certain summary data. These are accumulated during the run and are printed following the completion of the calculation. A table of summarized interior ballistic data is printed which contains, in order: Time, breech pressure, base pressure and space mean pressure, mass fraction of unburnt propellant, mass fraction of unburnt centercore charge, projectile travel, velocity and acceleration. The pressures are all centerline quantities. Optionally, these summary data may be followed by pressure histories at user-selectable locations for comparison with experimental pressure gage records. These values of pressure may be obtained at any axial location on either the tube or the centerline. The tabulation of these histories is followed by a tabulation of the histories of pressure difference formed by subtracting the last pressure history from each of the others.

Table A.1 Summary of TDNOVA Routines and Linkages

TDMAIN	Purpose: Dummy main program. Calls INPUT to read and print data, SETUP to initialize problem and then calls TDXC, which is the principal executive routine, to integrate the solution. The BRL version also executes an optional call to RECAP to plot the summary data. Calls: INPUT, (RECAP), SETUP, TDXC Called by: None
AP	Purpose: Function to compute rate of propagation of intergranular disturbances as a function of porosity and direction of loading. Calls: SIGL Called by: B1D2P, B2D2P, I1D2P, I2D2P
AREA	Purpose: Function to compute area of quadrilateral defined by four mesh points. Calls: None Called by: BAGBC, Q2DBC, SETUP, SUMTAB, TDMESH, XSECT
BAGBC	Purpose: Subroutine to enforce physical boundary conditions at all mesh points on the boundary of the mixture as well as contiguous points in the ullage. Calls: AREA, BAGIBC, BCS1, B1D1P, B1D2P, B2D2P, CALFLO, CALPRM, DIS, EPTOR, ILP1P, I1D1P, I1D2P, NAYBOR, PRTOE, XTERA, XTERB Called by: TDXC
BAGIBC	Purpose: Subroutine to enforce physical boundary conditions at bag-to-bag interfaces and in intervening region of ullage. Calls: BCCI, BCS1, BCS2, B2D2P, CALFLO, CALPRM, DISBAG, I1D1P, TANLOS, TDBCAL, XTERA Called by: BAGBC

BCCI

Purpose: Subroutine to enforce physical boundary conditions at corners of bag-to-bag interfaces and in regions of ullage adjacent to relevant sides.

Calls: BCS1, BCS2, B1D1P, B1D2P, B2D2P, CALFLO, DIS, DISBAG, ILP1P, LOGOUT, SUMTAB, TDBCAL, XTERB

Called by: BAGIBC

BCS1

Purpose Subroutine to make solid-phase state variables compatible with prescribed value of normal velocity or of intergranular stress.

Calls: None

Called by: BAGBC, BAGIBC, BCCI, BCS2, Q2DBC

BCS2

Purpose: Subroutine to make solid-phase state variables on each side of a mixture-to-mixture interface compatible with each other.

Calls: BCS1

Called by: BAGIBC, BCCI, Q2DBC

BLKDAT

Purpose: Block data initialization

Calls: None

Called by: None

B1D1P

Purpose: Subroutine to perform trial update of boundary point of a quasi-one-dimensional single-phase region.

Calls: PSI

Called by: BAGBC, BCCI, Q2DBC, ULLBC, XTERB

B1D2P

Purpose: Subroutine to perform trial update of boundary point of a quasi-one-dimensional two-phase region.

Calls: AP, CDB, DP, PROPER, PSI, QP, RDOT, SIGL

Called by: BAGBC, BCCI, Q2DBC, XTERB

B2D1P

Purpose: Subroutine to perform trial update of boundary point of a two-dimensional, single-phase region.

Calls: LOGOUT, PSI

Called by: ULLBC, XTERA, XTERB

B2D2P

Purpose: Subroutine to perform trial update of boundary point of a two-dimensional, two-phase region.

Calls: AP, CDB, DP, LOGOUT, PROPER, PSI, QP, RDOT

Called by: BAGBC, BAGIBC, BCCI

CALFLO

Purpose: Subroutine to calculate rate of reaction of bag substrate at a given point.

Calls: None

Called by: BAGBC, BAGIBC, BCCI, Q2D, Q2DBC, XTERB

CALPRM

Purpose: Subroutine to compute friction factor associated with bag flow resistance at a given mesh point.

Calls: None

Called by: BAGBC, BAGIBC, LOGOUT

CDB

Purpose: Function to compute friction factor associated with flow resistance through granular bed.

Calls: None

Called by: B1D2P, B2D2P, I1D2P, I2D2P, Q2D

CONTR

Purpose: Subroutine to prepare contour plots of a given state variable.

Calls: None

Called by: PLOTRZ

DIS

Purpose: Function to compute algebraic distance from a given mesh point to a given external boundary element along either a line of constant radius (external boundary given as breech or projectile) or constant axial location (external boundary given as centerline or tube).

Calls: None

Called by: BAGBC, BCCI, MSHMOV, PLTLOD, PRMOV, Q2D, Q2DBC, SETUP, TDMESH, TDXC, ULLBC, XSECT, XTERB

DISBAG

Purpose: Function to compute distance from a given mesh point to either front or rear boundary of a given bag. The distance is computed along a line of constant radius.

Calls: None

Called by: BAGIBC, BCCI, PLTLOD, SETUP, TDMESH, ULLBC, XSECT, XTERB

DP

Purpose: Function to compute ratio of volume to surface area of a propellant grain as a function of surface regression.

Calls: PERF19, SPLIND

Called by: B1D2P, B2D2P, I1D2P, I2D2P, Q2D

EPTOR

Purpose: Function to compute density of gas as a function of internal energy and pressure.

Calls: None

Called by: BAGBC, Q2DBC, SETUP, TDBCAL, TDXC, XTERA, XTERB

FILLER

Purpose: Subroutine to update motion of compactible case closure elements.

Calls: None

Called by: PRMOV, SETUP

FIT

Purpose: Subroutine which replaces NIN equally spaced data by NOUT equally spaced data using a cubic spline interpolation.

Calls: SPLINE

Called by: PLOTRZ

ILP1P

Purpose: Subroutine to update state of a lumped parameter, single-phase region.

Calls: PSI

Called by: BAGBC, BCCI, Q2DBC

INPUT

Purpose: Subroutine to read and print input data used to define problem. See Table A.3 for discussion of input data.

Calls: None

Called by: TDMAIN

I1D1P

Purpose: Subroutine to update state of quasi-one-dimensional, single-phase flow at a given interior mesh point.

Calls: PSI

Called by: BAGBC, BAGIBC, Q2D, ULLBC

I1D2P

Purpose: Subroutine to update state of a quasi-one-dimensional, two-phase region at a given interior mesh point.

Calls: AP, CDB, DP, PROPER, PSI, QP, RDOT, SIGL

Called by: BAGBC, Q2D

I2D1P

Purpose: Subroutine to update state of a two-dimensional, single-phase region at all interior mesh points.

Calls: LOGOUT, PSI

Called by: ULLBC

I2D2P

Purpose: Subroutine to update state of a two-dimensional, two-phase region at all interior mesh points.

Calls: AP, CDB, DP, LOGOUT, PROPER, PSI, QP, RDOT

Called by: TDXC

LOGOUT

Purpose: Subroutine to print tables of flow-field distributions and execute disc storage, plotting, as required.

Calls: CALPRM, PLOTRZ

Called by: BCCI, B2D1P, B2D2P, I2D1P, I2D2P, SETUP TDBCAL, TDMESH, TDXC

MAP

Purpose: Subroutine to establish mesh within a two-dimensional domain to satisfy coupled elliptic equations subject to either Dirichlet or Neumann boundary conditions.

Calls: None

Called by: MSHMOV, SETUP

MSHMOV

Purpose: Subroutine to define boundary distributions of mesh points for all two-dimensional computational regions and, following the definition of the internal distribution by MAP, to set the mesh point velocities.

Calls: DIS, MAP, SIDE

Called by: TDMESH, TDXC

NAYBOR

Purpose: Subroutine to compute region and mesh pointers as required by BAGBC.

Calls: None

Called by: BAGBC, XSECT, XTERA

PERF19

Purpose: Subroutine to compute surface area and volume of a nineteen-perforation propellant grain following slivering.

Calls: None

Called by: DP

PLOTRZ

Purpose: Principal plotting executive for preparation of CALCOMP plots of state variables (isometric, contour, flowfield) and ignition delay.

Calls: CONTR, FIT, PLTFLO, PLTLOD, SEE

Called by: LOGOUT, TDXC

PLTFLO

Purpose: Subroutine to prepare CALCOMP flow-field plots.

Calls: PLTLOD

Called by: PLOTRZ

PLTLOD

Purpose: Subroutine to transfer data from computational arrays into plotting arrays.

Calls: DIS, DISBAG

Called by: PLOTRZ, PLTFLO

PRES

Purpose: Function to compute gas pressure or intergranular stress or sum of both at a specified boundary location.

Calls: SIDE

Called by: PRMOV, SUMTAB, TDMESH

PRMOV

Purpose: Subroutine to update motion of projectile.

Calls: DIS, FILLER, PRES, RESFUN

Called by: TDXC

PROPER

Purpose: Subroutine to move vector properties of solid phase into scalar arrays.

Calls: None

Called by: B1D2P, B2D2P, I1D2P, I2D2P, Q2D, SETUP, TDMESH, TDXC

PRTOE

Purpose: Function to compute internal energy of gas as a function of pressure and density.

Calls: None

Called by: BAGBC, Q2DBC, TDBCAL, TDMESH, TDXC, XTERA, XTERB

PSI

Purpose: Function to compute rate of discharge of externally injected ignition stimulus at a given point and time.

Calls: None

Called by: B1D1P, B1D2P, B2D1P, B2D2P, ILP1P, I1D1P, I1D2P, I2D1P, I2D2P

QP

Purpose: Function to compute interphase heat transfer coefficient and update solid phase surface temperature according to cubic profile approximation.

Calls: VIS

Called by: B1D2P, B2D2P, I1D2P, I2D2P

Q2D

Purpose: Subroutine to effect update of solution through one integration step (predictor or corrector) at interior mesh points when a quasi-two-dimensional representation of the propelling charge is in effect.

Calls: CALFLO, CDB, DIS, DP, I1D1P, I1D2P, PROPER, Q2DBC

Called by: TDXC

Q2DBC

Purpose: Subroutine to effect update of solution at boundary mesh points when a quasi-two-dimensional representation of the propelling charge is in effect.

Calls: AREA, BCS1, BCS2, B1D1P, B1D2P, CALFLO, DIS, EPTOR, ILP1P, PRTOE, TDBCAL

Called by: Q2D

RDOT

Purpose: Function to compute rate of surface regression of solid phase as a function of ambient pressure.

Calls: SPLIND

Called by: B1D2P, B2D2P, I1D2P, I2D2P

RESFUN

Purpose: Function to compute bore resistance exerted on projectile due to interference of rotating band with tube rifling.

Calls: None

Called by: PRMOV

SEE

Purpose: Subroutine to assess visibility of given line segment in preparation of isometric views of state variables at a given time.

Calls: None

Called by: PLOTRZ

SETUP

Purpose: Subroutine to perform initialization of all state variables and internally set constants.

Calls: AREA, DIS, DISBAG, EPTOR, FILLER, LOGOUT MAP, PROPER, SUMTAB, TDMESH, XSECT

Called by: TDMAIN

SIDE

Purpose: Subroutine to compute pointers to mesh storage along a given side of a given computational region.

Calls: None

Called by: MSHMOV, PRES, TDMESH, TDXC, ULLBC

SIGL

Purpose: Function to compute intergranular stress as a function of porosity on nominal loading curve.

Calls: None

Called by: AP, B1D2P, I1D2P, TDXC

SPLIND

Purpose: Subroutine to prepare table of values of second derivatives for double precision cubic spline interpolation.

Calls: None

Called by: DP, RDOT

SPLINE

Purpose: Subroutine to prepare table of values of second derivatives for single precision cubic spline interpolation.

Calls: None

Called by: FIT

SUMTAB

Purpose: Subroutine to compile and print tables of summary data.

Calls: AREA, PRES

Called by: BCCI, SETUP, TDBCAL, TDXC

TANLOS

Purpose: Subroutine to compute loss of tangential momentum experienced by gas entering mixture from ullage.

Calls: None

Called by: BAGIBC

TDBCAL

Purpose: Subroutine to determine physically compatible boundary values of state variables of gas-phase at a mutually connecting interface or region of lumped properties in the direction of the fluxes.

Calls: EPTOR, LOGOUT, PRTOE, SUMTAB

Called by: BAGIBC, BCCI, Q2DBC, ULLBC, XTERB

TDMESH

Purpose: Subroutine to administer region representations and perform mesh point allocations.

Calls: AREA, DIS, DISBAG, LOGOUT, MSHMOV, PRES, PROPER, PRTOE, SIDE

Called by: SETUP, TDXC

TDXC

Purpose: Subroutine to control overall update and logout procedures. TDXC is the principal executive routine of TDNOVA.

Calls: BAGBC, DIS, EPTOR, I2D2P, LOGOUT, MSHMOV, PLOTRZ, PRMOV, PROPER, PRTOE, Q2D, SIDE, SIGL, SUMTAB, TDMESH, ULLBC, XSECT

Called by: TDMAIN

ULLBC

Purpose: Subroutine to control update of all ullage mesh points other than those contiguous with the mixture.

Calls: B1D1P, B2D1P, DIS, DISBAG, I1D1P, I2D1P, SIDE, TDBCAL

Called by: TDXC

VIS

Purpose: Function to compute gas viscosity as a function of temperature.

Calls: None

Called by: QP

XSECT

Purpose: Subroutine to compute cross-sectional flow area of quasi-one-dimensional regions and volume of lumped parameter regions.

Calls: AREA, DIS, DISBAG, NAYBOR

Called by: SETUP, TDXC

XTERA

Purpose: Subroutine to impose physical boundary conditions at a point on the side of the bag adjacent to a fully two-dimensional region of ullage.

Calls: B2D1P, EPTOR, NAYBOR, PRTOE

Called by: BAGBC, BAGIBC

XTERB

Purpose: Subroutine to update solution at a corner of the bag which is bounded by a fully two-dimensional flow on one or both sides.

Calls: B1D1P, B1D2P, B2D1P, CALFLO, DIS, DISBAG, EPTOR, PRTOE, TDBCAL

Called by: BAGBC, BCCI

Table A.2 Glossary of FORTRAN Variables Contained in Common Blocks

Variable	Common Block	Definition
ALFAP	C02	Thermal diffusivity of solid phase, α_p
ANPR	C58	Array of radial components of normal to bag boundary used to define motion of corners by extrapolation.
ANPU	C58	Array of normal velocities of bag boundary used to define motion of corners by extrapolation.
ANPZ	C58	Array of axial components of normal to bag boundary used to define motion of corners by extrapolation.
AP1	C02	Rate of propagation of intergranular disturbances in solid phase, at settling porosity, under conditions of loading a_1.
AP2	C02	Rate of propagation of intergranular disturbances in solid phase, under conditions of unloading, a_2.
AP3	C11	$a_1 \varepsilon_o$
AXC	C34	Array containing cross-sectional areas of quasi-one-dimensional regions and volumes of lumped parameter regions.
BITS	C39	$\zeta_z^2 + \zeta_r^2$ if $\tau - \zeta$ characteristic and $\eta_z^2 + \eta_r^2$ if $\tau - \eta$ characteristic.
BV	C02	Covolume of products of combustion of propellant, b.
CFLON	C39	$\partial \dot{m} / \partial u_n$
CHSO	C14	Charge standoff distance.
CP	C02	Specific heat at constant pressure of products of combustion of propellant, c_p.
CPBC	C54	Array of specific heats at constant pressure of reactive components of bag.

Variable	Common Block	Definition
CPE	C54	Array of internal energies of gas at boundaries of one-dimensional regions terminated by lumped parameter region.
CPF	C11	$0.4Pr^{-2/3}\gamma R_g/(\gamma - 1)$
CPIG	C51	Specific heat at constant pressure of igniter described by tabular input.
CPSS	C53	Specific heat at constant pressure of surface source term.
CPSSS	C57	Array of specific heats of surface sources used for TDBCAL interface.
CV	C02	Specific heat at constant volume of products of combustion of propellant, c_v.
CVBC	C54	Array of specific heats at constant volume of reactive components of bag.
CVE	C54	Array of internal energies of gas at boundaries of one-dimensional regions terminated by lumped parameter region.
CVIG	C51	Specific heat at constant volume of igniter described by tabular input.
CVSS	C53	Specific heat at constant volume of surface source term.
CVSSS	C57	Array of specific heats of surface sources used for TDBCAL interface.
D	C01	Array containing values of d, solid-phase surface regression.
DATFL	SUMCOM	Array inactive.
DATIB	SUMCOM	Array of summarized interior ballistic data as required by BRL routine RECAP.

Variable	Common Block	Definition
DATPR	SUMCOM	Array of pressure histories as required by BRL routine RECAP.
DATR	C37	Plot buffer array.
DATV	C37	Plot buffer array.
DATX	C18	Array used to construct plots.
DATY	C18	Array used to construct plots.
DATZ	C37	Plot buffer array.
DB	C34	Computational mesh increment along boundary.
DEFF	C11	Effective particle diameter, D_p.
DGADM	C57	Derivative of ratio of specific heats with respect to mass flux for region with lumped properties in direction of flux.
DGMDM	C57	Derivative of molecular weight with respect to mass flux for region with lumped properties in direction of flux.
DMDU	C57	Derivative of mass flux with respect to normal velocity at continuum boundary.
DN	C34	Computational mesh increment normal to boundary.
DPDM	C57	Derivative of pressure with respect to mass flux for region with lumped properties in direction of flux.
DPDU	C57	Derivative of pressure with respect to normal velocity at continuum boundary.
DPERF	C02	Initial diameter of grain perforation, d_o.
DR	C36	$\Delta\eta$

Variable	Common Block	Definition
DRDM	C57	Derivative of density with respect to mass flux for region with lumped properties in direction of flux.
DRDP	C57	Derivative of density with respect to pressure at boundary of continuum region.
DRFLO	C46	Estimate of η-variation of gas-phase velocity at corner of two-dimensional region.
DSDEPS	C60	Derivative of intergranular stress with respect to porosity at the boundary of a continuum region.
DSDUS	C60	Derivative of intergranular stress with respect to solid-phase normal velocity at the boundary of a continuum region.
DT	C09	Time step, $\Delta\tau$.
DTLOG	C05	Time increment for logout.
DTLOGI	C48	Time increments for logout before and after transition to quasi-two-dimensional flow.
DTLOGM	C48	Array of times at which variably scheduled logout parameters are changed.
DTLOGV	C48	Variable schedule of logout intervals.
DTMAX	C05	Maximum time step consistent with C-F-L condition.
DTSUM	C16	Time increment for storage in summary tables.
DUTDM	C57	Derivative of tangential velocity with respect to normal mass flux for region with lumped properties in direction of flux.

Variable	Common Block	Definition
DZ	C36	$\Delta\zeta$
DZFLO	C46	Estimate of ζ-variation of gas-phase velocity at corner of two-dimensional region.
E	C01	Array containing current values of e, gas-phase internal energy.
ECH	C02	Chemical energy released during combustion of solid-phase, e_p.
EDDSIG	C44	$\partial\varepsilon/\partial\sigma$ in quasi-one-dimensional two-phase flow.
EIG	C02	Chemical energy released by externally injected ignition stimulus, e_{IG}.
EPDSIG	C36	$\partial\varepsilon/\partial\sigma$ in two-dimensional two-phase flow.
EPS	C01	Array containing values of porosity.
EPSO	C02	Initial porosity of solid phase.
ER	C30	$(1 - \varepsilon_o)/\varepsilon_o$
ERCT	C25	Array of values of chemical energy released by reactive substrates of bag.
ES	C57	Array of internal energies of surface sources used for TDBCAL interface.
ESS	C27	Local value of ESSIG.
ESSBC	C44	Energy of basepad at boundary of centerline.
ESSIG	C27	Array of values of chemical energy released by bag reactive substrates.
ETAS	C34	Mesh transformation coefficient, ζ_s, for quasi-one-dimensional regions.

Variable	Common Block	Definition
EØ	C02	Settling porosity of solid phase, ε_o.
EØR	C11	$1/\varepsilon_o$
E1	C30	$1/(1 + 0.02(1 - \varepsilon_o)/\varepsilon_o)$
FAC	C20	Scale factor used in plotting.
FBRES	C26	Array of values of bore resistance.
FEL	FILL	Array of initial resistances to motion of compactible filler elements used in case charges.
FLO	C57	Coefficient to describe pressure loss associated with mass transfer of gas-phase.
FLOIG	C27	Array of values of rate of reactivity of bag substrates.
FLOLOS	C56	Array of pressure loss coefficients.
FLOLP	C41	Array of values of $\dot{m}$ for transfer between quasi-one-dimensional and lumped parameter regions.
FLOLPC	C41	Array of values of $\partial\dot{m}/\partial u$ for transfers between quasi-one-dimensional and lumped parameter regions.
FLON	C34	Rate of mass flow normal to boundary, positive exiting mixture.
FLORCT	C25	Array of values of rate of bag reactivity.
FLOS	C57	Array of surface source terms used for TDBCAL interface.
FLOSBC	C44	Rate of reactivity of basepad at boundary of centercore.
FLOSS	C27	Local value of FLOIG.
FR	C42	Plotting parameter.

Variable	Common Block	Definition
FRES	FILL	Inactive.
FS	C20	Length of axis corresponding to state variable being plotted.
FZ	C42	Plotting parameter.
G	C04	Constant used to reconcile units, g_o.
GAFAC1	C53	Derivative of ratio of specific heats with respect to transverse mass flux entering one-dimensional flow.
GAM	C02	Ratio of specific heats of products of combustion of propellant, γ.
GAMIG	C62	Ratio of specific heats of igniter described in tabular form.
GAMLP	C54	Derivative of ratio of specific heats with respect to mass flux entering lumped parameter region.
GAMM	C01	Array of ratio of specific heats at computational mesh points.
GAMRCT	C51	Array of ratio of specific heats of reactive components of bag.
GAMØ	C02	Initial ratio of specific heats of ambient gas.
GAM1	C02	$\gamma - 1$
GLEN	C02	Initial length of a grain, L_o.
GMFAC1	C53	Derivative of molecular weight with respect to transverse mass flux entering one-dimensional flow.
GMLSSS	C57	Array of molecular weights of surface source terms used for TDBCAL interface.

Variable	Common Block	Definition
GMOL	C02	Molecular weight of products of combustion of propellant, M_w.
GMOLBC	C54	Array of molecular weights of reactive components of bag.
GMOLE	C54	Array of molecular weights of gas at boundaries of one-dimensional regions terminated by lumped parameter region.
GMOLIG	C51	Molecular weight of igniter described by tabular input.
GMOLL	C01	Array of molecular weights at computational mesh points.
GMOLLP	C54	Derivative of molecular weight with respect to mass flux entering lumped parameter region.
GMOLRC	C51	Array of molecular weights of reactive components of bag.
GMOLSS	C53	Array of molecular weights of surface source terms as used for TDBCAL interface.
GMOLØ	C02	Initial molecular weight of ambient gas.
H	C01	Array containing values of state variable H used in cubic profile solution of solid-phase surface temperature.
HIDEDR	C42	Plotting parameter.
HIDEDZ	C42	Plotting parameter.
I	C35	Counter used to enumerate side and corners of a two-dimensional region during update of boundary values.
IBRES	FILL	Index to determine functional dependence of bore resistance on projectile velocity.

Variable	Common Block	Definition
IBST	SUMCOM	Storage counter for interior ballistic summary data.
IBTABL	SUMCOM	Switch to indicate whether or not summarized interior ballistic data have been prepared.
ICA	C17	Switch used in hidden line algorithm.
ICB	C17	Switch used in hidden line algorithm.
ICL	C17	Switch used in hidden line algorithm.
IHL	C17	Counter used in hidden line algorithm.
INDIMR	C07	Number of mesh points allocated to η-coordinate in representation of propelling charge.
INDIMZ	C07	Number of mesh points allocated to ζ-coordinate in representation of propelling charge.
INT	C07	Switch used to indicate whether step is predictor or corrector.
INTRL	C29	Array of switches used to indicate whether a given mesh point lies on an internal boundary.
IPLTV	C13	Array of switches used to determine whether or not to create isometric plots of various state variables during logout.
ISWP	C17	Counter used in hidden line algorithm.
ITYP	C31	Pointer to type of solid phase (propellant or centercore) under consideration.

Variable	Common Block	Definition
J	C35	Loop counter enumerating points on a side of a two-dimensional region.
JDB	C35	Storage increment in direction tangential to boundary.
JDN	C35	Storage increment in direction normal to boundary.
JF	C35	Pointer to future storage level of a point on the boundary of a two-dimensional region.
JP	C35	Pointer to past storage level of a point on the boundary of a two-dimensional region.
JPLTV	C13	Array of switches used to determine whether or not to create contour plots of various state variables during logout.
JPRP	C52	Pointer to propellant property arrays.
JRCT	C25	Number of entries in tables of bag reactivity rates.
JRP	C03	Number of entries in array RPHI.
JTP	C03	Number of entries in array TPHI.
JZP	C03	Number of entries in array ZPHI.
J1	C35	Loop delimiter used in update of side of boundary.
J2	C35	Loop delimiter used in update of side of boundary.
J3	C35	Storage increment along side of two-dimensional region.
J4	C35	Pointer to current storage level of a point on the boundary of a two-dimensional region.

Variable	Common Block	Definition
KDIMR	C42	Number of radial points in plot field.
KDIMRM	C42	KDIMR - 1
KDIMZ	C42	Number of axial points in plot field.
KDIMZM	C42	KDIMZ - 1
KDR	C38	Array of values of NDR, a subset.
KDZ	C38	Array of values of NDZ, a subset.
KFL	SUMCOM	Inactive.
KP	C02	Thermal conductivity of solid-phase, k_p.
KPR	SUMCOM	Counter for pressure history tables.
KPT	C55	Array of mesh point storage addresses.
KPTF	C55	Array of mesh point storage addresses biased to NF-level.
KPTHID	C42	Number of points in plot field.
KPTI	C55	Array of mesh point storage addresses biased to NI-level.
KPTP	C55	Array of mesh point storage addresses biased to NP-level.
KREG	C55	Array of pointers to computational regions.
KSDZ	C38	Array of numbers of axial mesh points allocated to successive bag increments and intervening ullage as required for plot interface.
LOC	C16	Array of switches indicating whether stations for pressure history summaries are on tube or centerline.
MAPIT	C15	Maximum allowable number of iterations for convergence of SOR algorithm for equipotential mesh.

Variable	Common Block	Definition
MBASIG	C47	Array of pointers to reactivity data bases to describe rear base pads of successive bag increments.
MCCORE	C47	Array of pointers to propellant properties to describe centercore charge for successive bag increments.
MEL	FILL	Array of masses of case closure elements.
MFLOWF	C59	Switch used to indicate whether front end of centercore tube is permeable to solid-phase for successive bag increments.
MFLOWR	C59	Switch used to indicate whether rear end of centercore tube is permeable to solid-phase for successive bag increments.
MFORIG	C59	Array of pointers to reactivity data bases to describe forward base pads of successive bag increments.
MODL	C29	Array of values indicating type of flow in each region.
MPRP	C47	Array of pointers to propellant properties to describe main charge for successive bag increments.
MSTRNG	C47	Array of switches to indicate whether strong bag option applies to successive bag increments.
NABRB	C35	Pointer to mesh point adjacent to side η = constant at corner of mixture.
NABRBF	C41	Pointer to future storage level of side η = constant at corner of mixture.
NABRC	C35	Pointer to mesh point adjacent to corner of mixture, in corner region of physical domain.

Variable	Common Block	Definition
NABRCF	C41	Pointer to future storage level of point of physical corner region adjacent to corner of mixture.
NABRN	C35	Pointer to mesh point adjacent to first point on a given side of a two-dimensional region.
NABRND	C35	Storage increment between points adjacent to a given side of a two-dimensional region.
NABRNF	C41	Pointer to future storage level of mesh point adjacent to boundary of two-dimensional region. Pertains to ζ = constant side of corner of mixture.
NAY	SUMCOM	Inactive.
NBAGS	C47	Number of bags of propellant used to define charge.
NBASIG	C25	Pointer to reactivity data set associated with end of centercore.
NBH1	C17	Counter used in hidden line algorithm.
NBH2	C17	Counter used in hidden line algorithm.
NBH11	C17	Counter used in hidden line algorithm.
NBRES	C26	Number of entries in bore resistance arrays.
NBY	C14	Array containing number of points used to specify bag boundaries initially.
NBYE	C22	Array of number of entries in tables of points used to define external boundaries.

Variable	Common Block	Definition
NCCORE	C25	Switch to determine whether or not a centercore ignition charge is present.
NCHAR	C35	Switch used to indicate whether characteristic is $\tau - \zeta$ or $\tau - \eta$.
NCHOK	C55	Array of switches to indicate whether mass transfer is choked.
NCYCL	C35	Switch used to indicate whether characteristic direction has been altered in call to B2D2P.
NDATA	FILL	Array of counters for files of constitutive data pertaining to case closure elements.
NDIM	SUMCOM	Inactive.
NDIMR	C35	Number of η-mesh points in a region.
NDIMRM	C35	NDIMR - 1
NDIMZ	C35	Number of ζ-mesh points in a region.
NDIMZM	C35	NDIMZ - 1
NDR	C29	Array of values of η-mesh points allocated to regions.
NDSKR	C06	Switch used to determine whether or not solution is to be initialized by disc read.
NDSKW	C06	Switch used to determine whether or not solutions are to be stored on disc during logout.
NDT	C07	Counter, initialized to zero, bumped by unity on each predictor and each corrector level of each integration step.
NDTSKP	C32	Switch used to bypass tests of C-F-L criterion four steps out of five.

Variable	Common Block	Definition
NDZ	C29	Array of values of number of ζ-mesh points allocated to regions.
NEL	FILL	Number of case closure elements.
NEL1	FILL	NEL + 1
NEW	C17	Counter used in hidden line algorithm.
NF	C07	Pointer to future storage.
NFBIAS	C12	Quantity used to construct pointer to future storage location in state variable arrays.
NFLAM	SUMCOM	Inactive.
NFORM	C50	Array of switches to indicate whether propellant species consists of cylinders or spheres.
NFORMI	C50	Scalar value of NFORM.
NH	C17	Number of points on horizon of visibility in isometric plotting.
NI	C07	Pointer to current storage.
NIBIAS	C12	Quantity used to construct pointer to current storage location in state variable arrays.
NLAST	FILL	Pointer to first case closure element currently bounded by a space on the right-hand side.
NLAST1	FILL	NLAST + 1
NMPT	C23	Maximum number of mesh points to be used in dynamic allocation mode.
NMSH	C23	Switch used to determine strategy for mesh allocation.

Variable	Common Block	Definition
NOC	C17	Switch used in hidden line algorithm.
NOKE	C61	Switch used to indicate form of kinetic energy contributed to heating of gas transferred to region with lumped properties in direction of transfer.
NOR	C14	Array of switches indicating whether initial mesh in mixture satisfies Dirichlet or Neumann boundary conditions.
NP	C07	Pointer to past storage.
NPBIAS	C12	Quantity used to contruct pointer to past storage location in state variable arrays.
NPERF	C02	Total number of perforations in a grain, N.
NPERM	C24	Array of pointers to bag permeability data sets.
NPLCON	C06	Switch used to determine whether or not contour plots are required on logout.
NPLFLM	C06	Switch used to determine whether flame-spread map is to be plotted at conclusion of run.
NPLFLO	C06	Switch used to determine whether or not flow field plots are required on logout.
NPLOT	C06	Switch used to determine whether or not isometric plots are required on logout.
NPRINT	C06	Switch used to determine whether or not printed output is required on logout.
NPRM	C25	Number of bag permeability data sets.

Variable	Common Block	Definition
NPROP	SUMCOM	Number of propellants to be considered in summary plotting.
NPRPS	C47	Number of propellant species in charge.
NPT	C35	Total number of mesh points in a region.
NPTABL	SUMCOM	Switch used to indicate whether or not pressure histories have been tabulated.
NPTBY	C14	Array indicating numbers of points pre-allocated to various segments of boundaries of bag.
NPTOL	C29	Switch used to indicate whether or not quasi-two-dimensional analysis is in effect.
NPTOT	C07	Total number of mesh points allocated at any time.
NRBIAS	C29	Array of values used to construct storage pointers.
NRCT	C25	Number of bag reactivity data sets.
NREACT	C24	Array of pointers to bag reactivity data sets.
NREGB	C35	At a corner of the mixture, NREGB points to the region adjacent to the η = constant side.
NREGC	C35	At a corner of the mixture, NREGC points to a corner region of the physical domain.
NREGN	C35	Pointer to region adjacent to boundary point of two-dimensional region. At a corner, NREGN points to the ζ = constant side.
NRG	C49	Total number of computational regions.

Variable	Common Block	Definition
NSBIAS	C49	Array of pointer biases to distinguish mesh storage for successive bag increments.
NSDZ	C49	Number of axial mesh points allocated to successive bag increments.
NSTEP	C06	Number of integration steps for logout.
NSTEPI	C48	Number of integration steps after which logout is to occur.
NSTEPM	C48	Array of integration steps at which variably scheduled logout parameters are changed.
NSTEPV	C48	Variable schedule of logout step cycles.
NSTOP	C06	Number of integration steps for termination of solution.
NSUBSK	C27	Array of pointers to bag permeability data sets.
NSUBSM	C27	Array of pointers to bag reactivity data sets.
NSUM	C16	Number of stations at which pressure histories are to be summarized.
NSUMRY	C06	Switch used to determine whether or not summary tables are to be prepared for printing at the conclusion of the run.
NTABIG	C25	Switch to determine whether or not an externally injected ignition stimulus is present.
NTB	C21	Array of number of entries in burn rate tables.
NTYPE	FILL	Switch used to indicate constitutive nature of case closure element.

Variable	Common Block	Definition
NVHL	C20	Switch used to determine whether or not to delete hidden lines from isometric plots.
NZPT	SUMCOM	Counter to describe number of stations at which pressure histories are to be plotted.
OD	C02	Initial diameter of grain, D_o.
OREL	C15	Overrelaxation factor used to establish equipotential mesh.
P	C01	Array containing values of p, gas-phase pressure.
PBIT	FILL	Force on projectile base, or first case closure element, due to gas pressure and intergranular stress.
PDUN	C36	$\partial p/\partial u_n$
PERM	C27	Array of values of bag friction factor.
PFAC1	C39	$\partial p/\partial \dot{m}$ for quasi-one-dimensional region.
PFAC2	C41	Array of values of $\partial p/\partial u_T$ for boundaries of quasi-one-dimensional regions.
PFACLP	C41	$\partial p/\partial \dot{m}$ for lumped parameter region.
PHI	C03	Array of values used to describe rate of injection of external ignition stimulus, ψ.
PI	C04	π
PR	C04	Prandtl number, Pr.
PR3	C04	$Pr^{1/3}$
PRM	C25	Array of values of initial bag friction factor.

Variable	Common Block	Definition
PRMASS	C26	Projectile mass.
PST	C02	Initial pressure of gas phase.
PTOL	C23	Fractional pressure difference below which quasi-two-dimensional solution is implemented.
QEDSIG	C56	Array of derivatives of porosity with respect to intergranular stress.
QEDVP	C56	Array of derivatives of porosity with respect to transverse solid-phase velocity of quasi-one-dimensional flow.
QFLON	C45	Array of values of transverse mass fluxes used in quasi-two-dimensional analysis.
QGAFAC	C45	Array of derivatives of ratio of specific heats with respect to mass flux.
QGMFAC	C45	Array of derivatives of molecular weight with respect to mass flux.
QPFAC1	C45	Array of values of $\partial p/\partial \dot{m}$ used in quasi-two-dimensional analysis.
QRFAC1	C45	Array of values of $\partial \rho/\partial \dot{m}$ used in quasi-two-dimensional analysis.
QSDUP	C56	Array of derivatives of intergranular stress with respect to solid-phase velocity.
QSDVP	C56	Array of derivatives of intergranular stress with respect to transverse velocity of solid-phase in quasi-one-dimensional flow.
QUFAC1	C45	Array of values of $\partial u/\partial \dot{m}$ used in quasi-two-dimensional analysis.
R	C04	Universal gas constant, R.
RBY	C14	Array of radial coordinates of points on boundaries of bag.
RBYE	C22	Array of values of radial coordinate of points on external boundaries.

Variable	Common Block	Definition
RESEL	FILL	Array of stresses used to define constitutive properties of case closure elements.
RFAC1	C39	$\partial\rho/\partial\dot{m}$ for quasi-one-dimensional region.
RFAC2	C41	Array of values of $\partial\rho/\partial u_T$ for quasi-one dimensional region.
RFACLP	C41	$\partial\rho/\partial\dot{m}$ for lumped parameter region.
RFRAC	C23	Radial spatial resolution factor.
RG	C04	Gas constant for products of combustion of solid-phase, R_G.
RHO	C01	Array containing values of ρ, gas-phase density.
RHODP	C36	$\partial\rho/\partial p$
RHOIG	C27	Array of densities of solid-phase associated with reactivity of bag material. Index runs over computational mesh.
RHOP	C02	Solid-phase density, ρ_p.
RHORCT	C25	Array of densities of solid-phase associated with reactivity of bag material.
RM	C01	Array containing values of r_m, radial component of mesh point.
RMO	C43	Array of initial values of r_m.
ROZR	C39	η_r if $\tau - \zeta$ characteristic and ζ_r if $\tau - \eta$ characteristic.
ROZZ	C39	η_z if $\tau - \zeta$ characteristic and ζ_z if $\tau - \eta$ characteristic.

Variable	Common Block	Definition
RPHI	C03	Array of radial positions used to describe externally injected ignition stimulus.
RRA	C39	r_η
RS	C20	Length of r-axis in plots.
RUPINT	C25	Array of values of interval over which bag rupture is completed once rupture strength is exceeded.
RUPSTR	C25	Array of values of bag rupture strength.
RUPT	C27	Array of values of time at which bag rupture is complete locally.
RZA	C39	r_ζ
SAFE	C05	Safety factor used to divide time step allowable by C-F-L criterion.
SDUPN	C36	$\partial\sigma/\partial\hat{u}_{p_n}$
SDVP	C44	$\partial\sigma/\partial V_{p_n}$ where σ is in a quasi-one-dimensional region and V_{p_n} is normal component of velocity of contiguous region.
SGB	C36	Equal to ±1 depending on side of region at which boundary point is located.
SGN	C36	Equal to ±1 depending on side of region at which boundary point is located.
SIG	C01	Array containing values of σ, intergranular stress (N.B. This is a partial stress).
SIGLC	C11	$\rho_p a_1^2 \varepsilon_o^2 / g_o$

Variable	Common Block	Definition
SQUDOT	C11	$[(u - u_p)^2 + (v - v_p)^2]^{1/2}$
SSK	C27	Local value of PERM.
TBN	C21	Array of values of burn rate exponents.
TB1	C21	Array of values of burn rate additive constants.
TB2	C21	Array of values of burn rate pre-exponential coefficients.
TDR	C36	$2\Delta\eta$
TDZ	C36	$2\Delta\zeta$
TEMST	C02	Initial temperature of gas phase.
THCK	C01	Thickness of bag material at each computational mesh point.
THK	C24	Array used to imput initial thickness of bag material.
TIG	C02	Ignition temperature of solid-phase, T_{ig}.
TIME	C02	Time, τ.
TIMIG	C43	Array of values of time at which ignition occurs.
TITLE	C08	Array containing problem title.
TKPP	C11	$3k_p^2$
TMAXP	C21	Array of values of maximum pressure for which burn rate coefficients are to be used.
TMAXSM	C33	Pending time for data storage in summary table.
TOL	C15	Maximum allowable fractional displacement of mesh to satisfy equipotential equations.

Variable	Common Block	Definition
TP	C01	Array containing current values of T_p, solid-phase surface temperature.
TPHI	C03	Array of times used to describe externally injected ignition stimulus.
TRCT	C25	Array of values of times used to define rate of bag reactivity.
TSTOP	C05	Time for termination of solution.
U	C01	Array containing values of u, axial component of gas-phase velocity.
UDUN	C36	$\partial u/\partial \hat{u}_n$
UDUT	C36	$\partial u/\partial \hat{u}_t$
UDOTN	C41	Array of values of $\hat{u}_n$ (not in physical units).
UFAC1	C39	$\partial u_T/\partial \dot{m}$ for quasi-one-dimensional region.
UMR	C01	Radial velocity component of computational mesh.
UMZ	C01	Axial velocity component of computational mesh.
UN	C34	Gas-phase velocity component normal to boundary (not in physical units).
UOLD	C41	Array of trial boundary values of u_T in quasi-one-dimensional regions.
UP	C01	Array containing values of u_p, axial component of solid-phase velocity.
UPDOTN	C41	Array of values of $\hat{u}_{p_n}$ (not in physical units).
UPN	C36	Component of solid-phase velocity normal to boundary (not in physical units).

Variable	Common Block	Definition
UPR	C01	Array containing values of v_p, radial component of solid-phase velocity.
UPT	C36	Component of solid-phase velocity tangential to boundary (not in physical units).
UR	C01	Array containing values of v, radial component of gas-phase velocity.
URDUN	C36	$\partial v/\partial \hat{u}_n$
URDUT	C36	$\partial v/\partial \hat{u}_t$
UT	C34	Gas-phase velocity component parallel to boundary (not in physical units).
UTC	C40	Coefficient to convert $\hat{u}_n$ into physical units.
V	C34	Array containing current local state variables at boundary point in mixture.
VE	C34	Current local value of e at boundary point in mixture.
VFRA	C40	$1 + \frac{f_s \overline{\Delta\tau}}{\varepsilon\rho \lvert u - u_p \rvert}$ where $\overline{\Delta\tau} = \Delta\tau$ on predictor level and $\overline{\Delta\tau} = \Delta\tau/2$ on corrector level.
VPR	C26	Projectile velocity.
VPRDOT	C26	Projectile acceleration.
VRM	C34	Current local value of r_m at boundary point in mixture.
VUM	C34	Mesh velocity in quasi-one-dimensional region.
XA	C17	Coordinate of endpoint of segment to be plotted isometrically.

Variable	Common Block	Definition
XALFAP	C28	Array of values of ALFAP.
XAP1	C28	Array of values of AP1.
XAP2	C28	Array of values of AP2.
XAP3	C28	Array of values of AP3.
XB	C17	Coordinate of endpoint of segment to be plotted isometrically.
XBV	C28	Array of covolumes for propellant species.
XCHWT	C28	Array of values of initial mass of solid phase in successive bag increments.
XCP	C51	Array of specific heats at constant pressure for propellant species.
XCV	C51	Array of specific heats at constant volume for propellant species.
XDPERF	C28	Array of values of DPERF.
XDTA	C34	Rate of change of cross-sectional area or of volume.
XDTU	C34	Rate of change of gas-phase velocity at boundary of quasi-one-dimensional region.
XDTUP	C44	$\partial u_p / \partial t$ in quasi-one-dimensional two-phase flow.
XE	C57	Array of internal energies used for TDBCAL interface.
XECH	C28	Array of values of ECH, internal energies of propellant species.

Variable	Common Block	Definition
XEL	FILL	Array of positions of case closure elements.
XEP	C60	Array of porosities used for BCS1, BCS2 interfaces.
XEPSO	C28	Array of values of EPSO.
XER	C30	Array of values of ER.
XEO	C28	Array of values of EO.
XEOR	C28	Array of values of EOR.
XE1	C30	Array of values of E1.
XGA	C57	Array of ratios of specific heats used for TDBCAL interface.
XGAM	C28	Array of ratios of specific heats for propellant species.
XGLEN	C28	Array of values of GLEN.
XGM	C57	Array of molecular weights used for TDBCAL interface.
XGMOL	C28	Array of molecular weights of propellant species.
XH	C19	Array of abscissae of visibility horizon in hidden line algorithm.
XI	FILL	Array of positions of case closure elements.
XID	FILL	Array of velocities of case closure elements.
XIDD	FILL	Array of accelerations of case closure elements.
XK	C57	Array of bag pressure loss terms used for TDBCAL interface.

Variable	Common Block	Definition
XKP	C28	Array of values of KP.
XM	C57	Array of mass fluxes used for TDBCAL interface.
XNPERF	C28	Array of values of NPERF.
XOD	C28	Array of values of OD.
XP	C57	Array of pressures used for TDBCAL interface.
XPR	C26	Projectile displacement.
XR	C57	Array of densities used for TDBCAL interface.
XRHOP	C28	Array of values of RHOP.
XSIG	C60	Array of intergranular stresses used for BCS1, BCS2 interface.
XSIGLC	C28	Array of values of SIGLC.
XTIG	C28	Array of values of TIG.
XTKPP	C28	Array of values of TKPP.
XU	C57	Array of gas-phase velocities used for TDBCAL interface.
XUP	C57	Array of boundary velocities used for TDBCAL interface.
XUS	C60	Array of solid-phase velocities used for BCS1, BCS2 interfaces.
XUT	C57	Array of transverse velocities used for TDBCAL interface.
XVCP	C53	Specific heat at constant pressure at boundary of two-dimensional region.

Variable	Common Block	Definition
XVCV	C53	Specific heat at constant volume at boundary of two-dimensional region.
XVGMOL	C53	Molecular weight at boundary of two-dimensional region.
XXDTA	C45	Array of rates of changes of cross-sectional area at points adjacent to boundaries of successive bag increments.
XXK	C57	Array of bag friction factors used for TDBCAL interface.
YA	C17	Coordinate of endpoint of segment to be plotted isometrically.
YB	C17	Coordinate of endpoint of segment to be plotted isometrically.
YEL	FILL	Array of compactions used to define constitutive properties of case closure elements.
YH	C19	Array of ordinates of visibility horizon in hidden line algorithm.
ZBPR	SUMCOM	Position of projectile as required for summary plots.
ZBRES	C26	Array of projectile displacements used to define bore resistance.
ZBY	C14	Array of axial coordinates of points on boundaries of bag.
ZBYE	C22	Array of axial coordinates of points on external boundaries.
ZFRAC	C23	Axial spatial resolution factor.
ZM	C01	Array containing values of z_m, axial coordinate of mesh point.

Variable	Common Block	Definition
ZMO	C43	Array of initial values of z_m.
ZORR	C39	ζ_r if $\tau - \zeta$ characteristic and η_r if $\tau - \eta$ characteristic.
ZORZ	C39	ζ_z if $\tau - \zeta$ characteristic and η_z if $\tau - \eta$ characteristic.
ZPHI	C03	Array of axial positions used to describe externally injected ignition stimulus.
ZPT	SUMCOM	Array of positions used to define pressure history summary plots.
ZRA	C39	z_η
ZS	C20	Length of z-axis in plots.
ZSTOP	C05	Projectile displacement for termination of solution.
ZSUM	C16	Array of axial locations of stations at which histories of gas pressure are to be tabulated at conclusion of run.
ZZA	C39	z_ζ

Table A.3 Description of TDNOVA Input Files

File 1: One Card (20A4) Problem Title	
TITLE	- Problem title, up to 80 alphanumeric characters.

File 2: Two Cards (9I5,4X,11I1,4X,11I1/4F10.1) Control Parameters	
NPRINT	0 - Tables of state variables are not printed. 1 - Tables of the state variables are printed on a logout schedule determined by NSTEP and DTLOG as described in File 3.
NSUMRY	0 - No summary tables are produced at the conclusion of the run. 1 - Summary tables are provided of the histories of the conventional interior ballistic variables and, if NSUM (File 3) is greater than zero, of the histories of pressure at selected positions in the tube. 2 - The summary data are not only tabulated at the end of the run, but are also plotted by the BRL plot package (RECAP). This option applies only to the code version at BRL.
NPLOT	0 - No isometric plots produced on logout. 1 - CALCOMP plots of state variables produced on logout. These plots are isometric views of the state variables as selected in accordance with the values of the array IPLTV defined below.
NVHL	0 - Hidden lines are removed from CALCOMP plots. 1 - If not zero, hidden lines are retained and plots are faired with a cubic spline interpolator.
NPLCON	0 - No CALCOMP contour plots produced on logout. 1 - Contour plots will be produced in accordance with the values of JPLTV defined below.
NPLFLO	0 - No CALCOMP plots of flow field on logout. 1 - Plots are produced of the velocity fields of both the gas and solid phases.

NPLFLM
- 0 - No summary plot of flamespreading.
- 1 - A summary plot is produced at the conclusion of the run to illustrate the path of flame-spreading by reference to contours of the ignition boundary at various times.

NDSKW
- 0 - No disc storage on logout.
- 1 - Solution saved on disc (Unit 8) on logout.

NDSKR
- 0 - Initial distributions are constructed from input data.
- >0 - If not zero, initial distributions are read from Unit 8 and correspond to time step equal to NDSKR.

IPLTV(I),I=1,...,11 - If IPLTV(I) = 1, the quantity tabulated below will be plotted as an isometric view. Otherwise, not.

I	QUANTITY PLOTTED IF IPLTV(I)=1
1	Mesh
2	Porosity
3	Granular Stress
4	Pressure
5	Density
6	Gas Axial Velocity
7	Solid Axial Velocity
8	Gas Radial Velocity
9	Solid Radial Velocity
10	Gas Temperature
11	Particle Surface Temperature

JPLTV(I),I=1,...,11 - As per IPLTV but pertaining to the contour plots. It should be noted that if JPLTV(1) is set equal to one, the result is identical to that produced if IPLTV(1) = 1.

FAC - Scale factor for CALCOMP plots. (Begin second card).

ZS - Length of Z-axis in CALCOMP plots (in).

RS - Length of R-axis in CALCOMP plots (in).

FS - Length of ordinate axis in isometric plots (in).

File 3: One Card (I5,F10.0,I5,F10.0,I5,F10.0) Logout Parameters

NSTEPI(1) >0 - Number of integration steps before logout prior to transformation to quasi-two-dimensional analysis.
0 - Logout will occur on every predictor and every corrector step. Disc write is suppressed on the predictor step.
<0 - If |NSTEPI(1)| is not greater than eight, then variably scheduled logout is understood to be required and File 34 is required as defined below.

DTLOGI(1) - Time increment at which logout will occur prior to transformation to quasi-two-dimensional analysis (msec).

NSTEPI(2) >0 - Number of integration steps before logout after transformation to quasi-two-dimensional analysis.
0 - Logout will occur on every predictor and every corrector step. Disc write is suppressed on the predictor step. If NSTEPI(1) is entered as a negative value, both NSTEPI(2) and DTLOGI(2) will be overridden by the variable logout data of File 34.

DTLOGI(2) - Time increment at which logout will occur after transformation to quasi-two-dimensional analysis (msec).

Note: If DTLOGI is less than or equal to zero, logout will occur only in accordance with the value of NSTEPI.

NSUM - Number of stations for storage of pressure summary data, maximum of eight. If NSUM > 0, File 34 is required.

DTSUM - Desired time interval for summary table storage (msec). Automatically increased if table overflow about to occur during execution.

File 4: One Card (I5,2F10.0) Termination Parameters

NSTOP - Number of integration steps before termination. If problem involves a disc start, NSTOP is taken to include all steps up to the point of restart.

TSTOP - Time for termination of solution (msec).

ZSTOP - Projectile displacement for termination of solution (cm).

File 5: Two Cards (7I5/6F10.0) Charge Representation Parameters

NPRPS - Number of types of propellant in charge. Maximum of 10.

NBAGS - Number of bags of propellant. Maximum of 10.

NMSH

0 - The propelling charge is initially represented by means of INDIMZ axial mesh points and INDIMR radial mesh points. The propelling charge will continue to be given a fully two-dimensional representation until the PTOL criterion is satisfied as defined below. Moreover, in this case, the ullage contiguous with each side of the charge will be represented as quasi-one-dimensional for that period in which the charge is treated as two-dimensional. It should be noted that the quasi-two-dimensional analysis applies only in the case NMSH = 0 in the present version of the code.

1 - The treatment of the propelling charge will be the same as in the case when NMSH = 0. However, the mesh will be allocated to the ullage regions dynamically in such a fashion as to constrain the total number of storage points to a value less than or equal to NMPT defined below, and so that no region has an axial mesh spacing less than ZFRAC times the distance between the breech face and the base of the projectile or a radial mesh spacing less than RFRAC times the radius of the bore, where ZFRAC and RFRAC are input quantities as defined below. Thus, in this case, the ullage may be treated as either quasi-one-dimensional or as fully two-dimensional according as its geometry dictates.

NMPT - Maximum number of storage points to be used in dynamic allocation of mesh as occurs when NMSH is equal to one and PTOL criterion has not been satisfied. It should be noted that NMPT is a grand total and includes the points allocated to the propelling charge as well as those to be allocated dynamically to the ullage.

INDIMZ - Number of axial mesh points used to represent the propelling charge in both the fully two-dimensional and quasi-one-dimensional modes. When more than one bag is present, the axial mesh is allocated to the bags on the basis of their initial lengths, the total number being equal to INDIMZ.

INDIMR - Number of radial mesh points used to represent the propelling charge in the fully two-dimensional mode.

MAPIT - Maximum number of iterations to be used in determining initial mesh distribution by successive over-relaxation. See also Files 12-15 for discussion of boundary conditions on initial mesh.

SAFE - Safety factor to be applied to CFL stability criterion. Must be greater than or equal to 1.

TOL - Maximum fractional displacement of mesh coordinates for initial configuration to be accepted as converged.

OREL - Over-relaxation factor. Must be between 1 and 2.

PTOL - Quantity used to determine point in solution at which a quasi-two-dimensional representation of the flow is adequate to complete the solution. The value of PTOL is inspected only after the completion of flamespreading and when bag rupture is complete on the sidewalls. It should be noted that the transition to a quasi-two-dimensional treatment may occur prior to the rupture of the outer sidewall of a given bag if the relevant value of MSTRNG (File 11) has

	been set equal to one. If the maximum value of pressure difference in each cross-section of the tube does not exceed PTOL times the pressure at the centerline, the solution is continued according to a quasi-two-dimensional representation until all radial ullage has disappeared or until burnout occurs and according to a quasi-one-dimensional representation thereafter.
ZFRAC	- Dimensionless quantity used to allocate axial distribution of mesh to individual regions when NMSH is equal to one.
RFRAC	- Dimensionless quantity used to allocate radial distribution of mesh to individual regions when NMSH is equal to one.

File 6: One Card (5F10.0) Ambient Conditions

TEMST	- Initial temperature of both phases (°K).
PST	- Initial pressure of gas phase (MPa).
GAMO	- Ratio of specific heats of ambient gas (-).
GMOLO	- Molecular weight of ambient gas (gm/gm-mol).
CHSO	- Charge standoff distance (cm). This input datum may be used to effect axial translations of the propelling charge and it is understood to be a quantity which is added to the axial coordinate of every point used to define the geometry of the bags. If the description of the bags (see Files 12-15) represents them as already having a standoff with respect to the breech face, then CHSO may be given a negative value provided that this does not result in a rearward translation of such a magnitude as actually to move the charge out of the gun chamber.

Note: Files 7, 8, 9, 10 are repeated, as a group, NPRPS times, once for each of the NPRPS types of propellant present in the charge. The centercore igniter is considered to be a distinct propellant for this purpose, but a basepad, treated as a reactive bag component, is not.

Neither is the centercore tube treated as a distinct propellant. It, like the basepad, is an attribute of the bag.
It should be noted that the subscript used to distinguish the various types of propellant is suppressed in the subsequent discussion.

File 7: One Card (6F10.0) Solid Phase Constitutive Data

XEO - Settling porosity of bed (-).
See the note following the discussion of File 11 concerning default properties of this datum.

XAP1 - Rate of propagation of compressive wave in settled bed (m/sec).

XAP2 - Rate of propagation of unloading wave (m/sec).

XRHOP - Density of solid phase (gm/cc).

XKP - Thermal conductivity of solid phase (J/cm-sec-°K).

XALFAP - Thermal diffusivity of solid phase (cm^2/sec).

File 8: One Card (3F10.0) Gas Phase Constitutive Data

XGAM - Ratio of specific heats (-).

XGMOL - Molecular weight (gm/gm-mol).

XBV - Covolume (cc/gm).

File 9: Two or more Cards (2F10.0,I5/(8F10.0)) Solid Phase Combustion Characteristics

XTIG - Ignition temperature of solid phase (°K).

XECH - Chemical energy released in combustion (J/gm).

NTB - Number of tabular data to define burn rate. Maximum of 10.

TMAXP(1) - Maximum pressure for which corresponding coefficients are applicable in the law RDOT = TB1(1) + TB2(1)*P**TBN(1) where P is pressure and RDOT is regression rate. This quantity starts a new card.

TB1(1) - Burn rate additive constant (cm/sec).

TB2(1) - Burn rate pre-exponential factor (cm/sec-MPa$^{TBN(1)}$).

TBN(1) - Burn rate exponent (-).

.
.
.

TMAXP(NTB) - Maximum pressure for which corresponding coefficients are applicable in the law RDOT = TB1(NTB) + TB2(NTB)*P**TBN(NTB) where P is pressure and RDOT is regression rate.

TB1(NTB) - Burn rate additive constant (cm/sec).

TB2(NTB) - Burn rate pre-exponential factor (cm/sec-MPa$^{TBN(NTB)}$).

TBN(NTB) - Burn rate exponent (-).

Notes: (1) A new card is started for TMAXP(1), TMAXP(3) etc., but not for TMAXP(2), TMAXP(4) etc.
(2) If the pressure exceeds TMAXP(NTB), the corresponding data are used as default values.

File 10: One Card (4F10.0,I5) Grain Geometry

XOD - External diameter (cm).

XGLEN - Length (cm).

XDPERF - Diameter of perforation (cm).

XNPERF - Number of perforations (-).

NFORM 0 - Grain is a cylinder.
1 - Grain is a sphere.

Note: Files 11, 12, 13, 14, 15 are repeated as a group, NBAGS times, once for each of the NBAGS bags of propellant. It should be noted that the subscript used to distinguish the various bags of propellant is suppressed in the subsequent discussion.

File 11: Two Cards (11I5/4F10.0) Description of Bag

NBY(1) - Number of entries in file for tabular description of rear of bag. Maximum of 10.

NBY(2) - Number of entries in file for tabular description of front of bag. Maximum of 10.

NBY(3) - Number of entries in file for tabular description of properties of internal circumferential boundary of bag. Maximum of 10.

NBY(4) - Number of entries in file for tabular description of properties of external circumferential boundary of bag. Maximum of 10.

MPRP - Pointer to file of propellant properties which characterize the main charge contained in the bag. MPRP must be greater than zero and less than or equal to NPRPS (File 5).

MCCORE
0 - A centercore igniter is not considered for the bag in question.
>0 - A centercore igniter is assumed to occupy the region interior to the bag, namely that defined by Files 14 and 19 over the axial extent of the charge. In this case MCCORE is a pointer to a file of propellant properties and is subject to the same restrictions as MPRP.

MBASIG - When MCCORE is not equal to zero, MBASIG is a pointer to a reactivity data set in the same sense as NREACT (File 12) and defines the discharge characteristics of that part of a basepad which overlaps the rear section of the centercore igniter tube.

MFORIG - MFORIG is analogous to MBASIG but refers to the front of the centercore ignition tube.

MFLOWR
0 - The rear boundary of the centercore tube will not admit efflux of the solid-phase.
1 - The solid-phase is permitted to exit the centercore tube.

MFLOWF - MFLOWF is analogous to MFLOWR but refers to the front of the centercore tube.

Note: At a bag-to-bag interface in which MFLOWF and MFLOWR are both set equal to one on their respective sides of the interface, the solid-phase fluxes through the centercore are made mechanically compatible. Accordingly, mass transfer may occur from one tube to its neighbor not only for the gas-phase but also for the solid-phase. However, influx of the solid-phase to the extreme ends of the charge never occurs. Moreover, no account is taken of the influence of solid effluents from the extreme ends of the centercore subsequent to their discharge.

MSTRNG 1 - The conversion to Q-2-D will occur independently of the rupture of the bag outer sidewall. In Q2D no radial sidewall motion will be allowed.

XCHWT(1) - Initial mass of main charge in bag (kg).

XEPSO(1) - Initial porosity of main charge in bag (-).

XCHWT(2) - Initial mass of centercore igniter in bag (kg).

XEPSO(2) - Initial porosity of centercore igniter in bag (-).

Note: The following conventions apply to each pair of values XCHWT and XEPSO for each charge component of each bag.
If XCHWT is entered as zero, a value is computed from XEPSO and is printed following the tabulation of all the input data. If a nonzero value of XCHWT is entered, the value of XEPSO will be replaced by a value which is consistent with the entered value of XCHWT.

The following default procedure applies to the datum XEO (see File 7) for each type of propellant present in the charge as a whole.

If XEO is entered as zero, it will automatically be replaced by the minimum value of XEPSO which occurs among all bags in which the given type of propellant is present, following the preceding tests of consistency of XEPSO with XCHWT. Internally revised values of XEPSO and XEO are printed following the tabulation of all input data.

File 12: NBY(1) Cards (3F10.0,4I5) Properties of Rear of Bag

ZBY(1,1) - Axial location of first point on rear (cm).

RBY(1,1) - Corresponding radial location (cm).

THK(1,1) - Thickness of rear of bag at first point (cm).

NPERM(1,1) - Pointer to data set (File 31) to describe the flow resistance of a section of the bag wall defined by (ZBY(1,1),RBY(1,1)) and (ZBY(2,1),RBY(2,1)). May take any integer value from zero to ten.

NREACT(1,1) - Pointer to data set (File 32) to describe the reactivity of the same segment. May take any integer value from zero to ten.

NPTBY(1,1) - Number of points pre-allocated to interior of a line segment defined by (ZBY(1,1),RBY(1,1)) and (ZBY(2,1),RBY(2,1)).

NOR(1,1)
0 - Dirichlet data will be assumed for the initial distribution of mesh points on the line segment defined by (ZBY(1,1),RBY(1,1)) and (ZBY(2,1),RBY(2,1)).
1 - Neumann data will be assumed for the initial distribution of mesh points on the line segment defined by (ZBY(1,1),RBY(1,1)) and (ZBY(2,1),RBY(2,1)). The mesh will be made orthogonal on the boundary segment.

.
.

ZBY(NBY(1),1) - Axial location of last point on rear (cm).

RBY(NBY(1),1) - Corresponding radial location (cm).

THK(NBY(1),1) - Corresponding thickness (cm).

File 13: NBY(2) Cards (3F10.0,4I5) Properties of Front of Bag

ZBY(1,2) - Axial location of first point on front (cm).

RBY(1,2) - Corresponding radial location (cm).

THK(1,2) - Thickness of front of bag at first point (cm).

NPERM(1,2) - Pointer to data set (File 31) to describe the flow resistance of a section of the bag wall defined by (ZBY(1,2),RBY(1,2)) and (ZBY(2,2),RBY(2,2)). May take any integer value from zero to ten.

NREACT(1,2) - Pointer to data set (File 32) to describe the reactivity of the same segment. May take any integer value from zero to ten.

NPTBY(1,2) - Number of points pre-allocated to interior of line segment defined by (ZBY(1,2),RBY(1,2)) and (ZBY(2,2),RBY(2,2)).

NOR(1,2)
0 - Dirichlet data will be assumed for the initial distribution of mesh points on the line segment defined by (ZBY(1,2),RBY(1,2)) and (ZBY(2,2),RBY(2,2)).
1 - Neumann data will be assumed for the initial distribution of mesh points on the line segment defined by (ZBY(1,2),RBY(1,2)) and (ZBY(2,2),RBY(2,2)). The mesh will be made orthogonal on the boundary segment.

.
.

ZBY(NBY(2),2) - Axial location of last point on front (cm).

RBY(NBY(2),2) - Corresponding radial location (cm).

THK(NBY(2),2) - Corresponding thickness (cm).

File 14: NBY(3) Cards (3F10.0,4I5) Properties of Internal Circumferential Boundary of Bag

---

ZBY(1,3) - Axial location of first point on internal boundary of bag (cm).

RBY(1,3) - Corresponding radial location (cm).

THK(1,3) - Thickness of inside of bag at first point (cm).

NPERM(1,3) - Pointer to data set (File 31) to describe the flow resistance of a section of the bag wall defined by (ZBY(1,3),RBY(1,3)) and (ZBY(2,3),RBY(2,3)). May take any integer value from zero to ten.

NREACT(1,3) - Pointer to data set (File 32) to describe the reactivity of the same segment. May take any integer value from zero to ten.

NPTBY(1,3) - Number of points pre-allocated to interior of line segment defined by (ZBY(1,3),RBY(1,3)) and (ZBY(2,3),RBY(2,3)).

NOR(1,3)
0 - Dirichlet data will be assumed for the initial distribution of mesh points on the line segment defined by (ZBY(1,3),RBY(1,3)) and (ZBY(2,3),RBY(2,3)).
1 - Neumann data will be assumed for the initial distribution of mesh points on the line segment defined by (ZBY(1,3),RBY(1,3)) and (ZBY(2,3),RBY(2,3)). The mesh will be made orthogonal on the boundary segment.

.
.

ZBY(NBY(3),3) - Axial location of last point (cm).

RBY(NBY(3),3) - Corresponding radial location (cm).

THK(NBY(3),3) - Corresponding thickness (cm).

File 15: NBY(4) Cards (3F10.0,4I5) Properties of External Circumferential Boundary of Bag

---

ZBY(1,4) - Axial location of first point on external boundary of bag (cm).

RBY(1,4) - Corresponding radial location (cm).

THK(1,4) - Thickness of outside of bag at first point (cm).

NPERM(1,4) - Pointer to data set (File 31) to describe the flow resistance of a section of the bag wall defined by (ZBY(1,4),RBY(1,4)) and (ZBY(2,4),RBY(2,4)). May take any integer value from zero to ten.

NREACT(1,4) - Pointer to data set (File 32) to describe the reactivity of the same segment. May take any integer value from zero to ten.

NPTBY(1,4) - Number of points pre-allocated to interior of line segment defined by (ZBY(1,4),RBY(1,4)) and (ZBY(2,4),RBY(2,4)).

NOR(1,4)
- 0 - Dirichlet data will be assumed for the initial distribution of mesh points on the line segment defined by (ZBY(1,4),RBY(1,4)) and (ZBY(2,4),RBY(2,4)).
- 1 - Neumann data will be assumed for the initial distribution of mesh points on the line segment defined by (ZBY(1,4),RBY(1,4)) and (ZBY(2,4),RBY(2,4)). The mesh will be made orthogonal on the boundary segment.

.
.

ZBY(NBY(4),4) - Axial location of last point (cm).

RBY(NBY(4),4) - Corresponding radial location (cm).

THK(NBY(4),4) - Corresponding thickness (cm).

Notes on Files 12 through 15:

(1) Note that a new card is started for each value of ZBY(I,K), all I and K.

(2) Values of NPTBY and NOR are only required for the first NBY-1 cards of each boundary set, at most.

(3) Files 12 through 15 must be consistent with each other in the sense that the end points must match to define a continuous closed boundary for the computational domain.

(4) In Files 12 and 13, the first point must correspond to the internal boundary of the domain and the last point must correspond to the external boundary.

(5) In Files 14 and 15, the first point must correspond to the rear and the last must correspond to the front of the bag.

(6) Only endpoints of Files 12 through 15 are treated as explicit corners of the computational domain. All other corners, defined implicitly by the tabular data within a given file, are treated as though they lay on a continuously differentiable curve.

(7) A mesh point is always located at the initial location defined by ZBY(I,K),RBY(I,K), all I and K.

(8) If NPERM is set equal to zero for any line segment, the segment in question is assumed to be fully permeable to the gas phase. A similar convention applies to NREACT for which a zero value implies that the segment in question is nonreactive.

(9) With regard to the initial description of the properties of the bag, it should be noted that a fully independent analysis is not made of the permeability and reactivity of the corners. Instead, values of flow resistance and surface mass generation are established by extrapolation of either the source terms or of the state variables themselves along each side of the bag boundary.

(10) For a given segment of the bag, the designated resistance and reactivity models are applied to all mesh points in the interior of the segment and to the mesh point at the end of the segment, but not to the mesh point at the start of the segment.

(11) It is assumed that if flow resistance and reactivity models are specified, then the initial distribution of boundary point is to be determined by Dirichlet data.

(12) In contrast to the resistance and reactivity pointers, the values of THK are understood to apply only at the given points on each side. Initial distributions along each segment are defined by linear interpolation of the entered values.

(13) When nonzero values of THK are specified, it is understood that the values of ZBY and RBY define the outside of the bag. The values of THK therefore define the extent to which the bag material--cloth, wear-reducing additive, basepad, centercore tube, and flash suppressant--intrude on the volume available to the propellant within the bag. Accordingly, the initial distribution of mesh points on the boundary of each bag will be displaced inwardly from the exterior surface defined by ZBY and RBY.

(14) In the present version of the code, it is assumed that when more than one bag is present, the mesh distributions coincide on the bag-to-bag interfaces. This represents a constraint on the specification of ZBY and RBY on the bag-to-bag interfaces which may be relaxed when future need so warrants.

File 16: One Card (4I5) External (Breech, Tube and Projectile) Boundary File Counters

NBYE(1) - Number of entries in file for tabular description of breech geometry, maximum of fifty.

NBYE(2) - Number of entries in file for tabular description of geometry of projectile base, maximum of fifty.

NBYE(3) - Number of entries in file for tabular description of geometry of internal circumferential boundary of tube (normally centerline). Maximum of fifty.

NBYE(4) - Number of entries in file for tabular description of geometry of external circumferential boundary of tube. Maximum of fifty.

File 17: NBYE(1) Cards (2F10.0) Geometry of Breech

ZBYE(1,1) - Axial location of first point on breech (cm).

RBYE(1,1) - Corresponding radial location (cm).

ZBYE(2,1) - Axial location of second point, starts a new card.

.
.

ZBYE(NBYE(1),1) - Axial location of last point on breech (cm).

RBYE(NBYE(1),1) - Corresponding radial location (cm).

File 18: NBYE(2) Cards (2F10.0) Geometry of Projectile Base

ZBYE(1,2) - Axial location of first point on projectile base (cm).

RBYE(1,2) - Corresponding radial location (cm).

.
.

ZBYE(NBYE(2),2) - Axial location of last point on projectile base (cm).

RBYE(NBYE(2),2) - Corresponding radial location (cm).

File 19: NBYE(3) Cards (2F10.0) Geometry of Internal Circumferential Boundary

ZBYE(1,3) - Axial location of first point on internal boundary (cm).

RBYE(1,3) - Corresponding radial location (cm).

.
.

ZBYE(NBYE(3),3) - Axial location of last point (cm).

RBYE(NBYE(3),3) - Corresponding radial location (cm).

File 20: NBYE(4) Cards (2F10.0) Geometry of External Circumferential Boundary

ZBYE(1,4) - Axial location of first point on external boundary (cm).

RBYE(1,4) - Corresponding radial location (cm).

.
.

ZBYE(NBYE(4),4) - Axial location of last point (cm).

RBYE(NBYE(4),4) - Corresponding radial location (cm).

File 21: One Card (4I5) Igniter Discharge Table Counters and Options

NTABIG
- 0 - A tabular representation of an ignition stimulus viewed as an externally injected source is not considered.
- 1 - An externally injected ignition source is considered. Values of JZP, JRP and JTP must be specified and Files 22, 23, 24, 25 and 26 must be included.

JZP - Number of axial stations in discharge table for case when NTABIG = 1. JZP must not exceed twenty.

JRP - Number of radial stations in discharge table for case when NTABIG = 1. JRP must not exceed eight.

JTP - Number of times levels in discharge table for case when NTABIG = 1. JTP must not exceed twenty.

File 22: One Card (3F10.0) Energy of External Ignition Source

Note: This file is required if and only if NTABIG is equal to one.

EIG - Energy of igniter gas (J/gm).

GAMIG - Ratio of specific heats of igniter gas (-).

GMOLIG - Molecular weight of igniter gas (gm/gmol).

File 23: One to Three Cards (8F10.0) Axial Positions for Discharge Table

Note: This file is required if and only if NTABIG is equal to one.

ZPHI(I),I=1,JZP - Axial positions (cm).

File 24: One Card (8F10.0) Radial Positions for Discharge Table

Note: This file is required if and only if NTABIG is equal to one.

RPHI(I),I=1,JRP - Radial positions (cm).

File 25: One to Three Cards (8F10.0) Time Levels for Discharge Table

Note: This file is required if and only if NTABIG is equal to one.

TPHI(I),I=1,JTP - Time levels (msec).

File 26: JRP*JTP to 3*JRP*JTP Cards (8F10.0) Discharge Table

Note: This file is required if and only if NTABIG is equal to one.

PHI(1,1,1) - First value of rate of discharge per unit volume (gm/cc-sec).

PHI(2,1,1) - Second value.

.
.

PHI(JZP,1,1) - Value at last axial position, first radial position and first time.

PHI(1,2,1) - Value at first axial, second radial position. This entry starts a new card.

.
.

PHI(JZP,JRP,JTP) - Last value.

File 27: One Card (F10.0,3I5) Projectile Mass and Bore Resistance Counter

PRMASS - Projectile mass (kg).

NBRES - Number of entries in tabular description of bore resistance. Must not exceed 10.

IBRES - Type of law for bore resistance.
1 - Resistance given directly by interpolation of tabular data of File 28.
2 - Interpolated value multiplied by $7.2/V^{0.6}$ where V is projectile velocity in ft/sec.
3 - Interpolated value multiplied by (1+.0004414V/1+.005046V) where V is projectile velocity in in/sec.
N.B. If IBRES < 1 or > 3, the value is internally defaulted to 2.

NEL - Number of filler elements to be interposed between the propellant and the projectile base. $0 \leq NEL \leq 10$.
>0 - Files 29 and 30 are required.

File 28: One to Three Cards (8F10.0) Bore Resistance Table

ZBRES(1) - First value of projectile displacement at which bore resistance is specified (cm).

FBRES(1) - Corresponding value of bore resistance (MPa).

.
.

ZBRES(NBRES) - Last value of displacement.

FBRES(NBRES) - Corresponding value of bore resistance.

File 29: NEL Cards (3F10.0,2I5) Filler Element Data

Note: This file is required if and only if NEL is not zero. One card is used to describe each element.

XEL - Position of left hand boundary of element (cm). It is assumed that successive values of XEL increase monotonically.

MEL - Mass of element (kg). If $<10^{-10}$, element is interpreted as a space. MEL must not be less than 10^{-10} for the first element.

FEL - Initial resistance to motion of element (N).

NTYPE - Indicator of constitutive behavior of element.

NTYPE	CONSTITUTIVE RESPONSE
0	Plastic - no deformation when unloading
1	Elastic
2	Rigid
3	Incompressible

NDATA - Number of pairs of entries in stress-strain table for given element. $0 \leq$ NDATA ≤ 10. If NDATA > 0, then File 30 is required for the given element. Note that all files of the type 29 are entered first and that the files of the type 30 follow as a group.

File 30: Zero to Three*NEL Cards (8F10.0) Filler Element Constitutive Data

Note: This file is required only if NEL is greater than zero, the element in question has nonzero mass, and is of either type 0 (plastic) or type 1 (elastic).

YEL(1) - First value of engineering strain (-).

RESEL(1) - Corresponding stress (MPa). Taken positive in compression.

.
.

RESEL(NDATA) - Last value of stress. Should exceed maximum pressure in gun.

Notes: (1) The array YEL must be well-ordered for each element. The values must lie in the interval (0,1).

(2) The array RESEL must have nonzero entries (except possibly for the first) and must be nondecreasing for each element.

File 31: One + NPRM Cards (I5/(3F10.0)) Bag Flow Resistance Data

NPRM - Total number of bag resistance data sets. May take any integer value from zero to ten. The subsequent data of this file are required if and only if NPRM is greater than zero.

PRM(1) - Initial friction factor for normal flux through bag element (-).

RUPSTR(1) - Pressure difference supportable by bag element before rupture commences (MPa).

RUPINT(1) - Time interval over which bag flow resistance decreases to zero in a linear fashion (msec). May have any nonnegative value, including zero.

PRM(2) - (New card).

.

RUPINT(NPRM)

Note: The impediment to gas flow is controlled by the friction factor. However, the motion of the solid-phase at the external circumferential boundary is also influenced by the state of integrity of the bag. Dilation of the bag beyond its initial radius will not occur until it is completely ruptured locally. Thus, by setting PRM = 0 and RUPSTR equal to some large number (or RUPINT equal to some period which exceeds the firing interval), one may characterize a bag segment as impeding the motion of the solid-phase alone.
A similar consideration applies at the internal circumferential boundary which embeds the structural characteristics of the centercore tube. No radial displacement will occur in either the positive or the negative direction until the tube is locally ruptured. The rupture pressure of the tube is assumed to be the same for bursting as for crushing.

File 32: 1+NRCT*(Two or Three) Cards (I5/(I5,4F10.0/(8F10.0)))
Bag Reactivity Data

NRCT - Total number of reactivity data sets. May take any integer value from zero to ten.
The subsequent data of this file are required if and only if NRCT is greater than zero.

JRCT(1) - Number of pairs of data in tabular description of mass generation rate for element type 1. (New card). Maximum of eight.

ERCT(1) - Chemical energy released by reaction of bag material (J/gm). Positive if reaction is exothermic.

RHORCT(1) - Density of solid-phase consumed by reaction of bag (gm/cc).

GAMRCT(1) - Ratio of specific heats of gas created by reaction of bag (-).

GMOLRC(1) - Molecular weight of gas created by reaction of bag (gm/gm-mol).

TRCT(1,1) - Value of time (msec). (New card).

FLORCT(1,1) - Corresponding rate of reaction of bag element (gm/cm^2-sec).

.
.

FLORCT(JRCT(1),1).

JRCT(2) - New card.

.
.

FLORCT(JRCT(NRCT),NRCT).

File 33: Two Cards (8F10.0/8I5) Pressure Summary Table Locations

Note: This file is required if and only if NSUM is not zero. (See File 3).

ZSUM(1) - Axial location of first station (cm).

.
.

ZSUM(NSUM) - Axial location of last station (cm).

LOC(1) 0 - First station is assumed to be on the tube wall.
1 - First station is assumed to be on the centerline of the tube.

.
.

LOC(NSUM) - Location of the last station.

File 34: Two or Three Cards (16I5/(8F10.0)) Variably Scheduled Logout Data

Note: This file is required if and only if NSTEP(1) is less than zero. (See File 3).

NSTEPM(1) - Last integration step at which MSTEPV(1) is used to define logout schedule based on the number of steps.

NSTEPV(1) - Number of integration steps before logout.

.
.

NSTEPM(|NSTEPI(1)|) - Last value of NSTEPM.

NSTEPV(|NSTEPI(1)|) - Last value of NSTEPV.

DTLOGM(1) - Last value of integration time at which DTLOGV(1) is used to define logout schedule based on integration time (msec).

DTLOGV(1) - Time increment before logout (msec).

.
.

DTLOGM(|NSTEPI(1)|) - Last value of DTLOGM.

DTLOGV(|NSTEPI(1)|) - Last value of DTLOGV.

Note: For values of integration step or integration time outside the table range defined by File 34, the final entries are used.

NOMENCLATURE

English Symbols

A	Cross-sectional area of a quasi-one-dimensional flow
a	Rate of propagation of intergranular disturbances
a_1	Value of a for settled bed during compression
a_2	Value of a for unloading or reloading bed when porosity is less than settling porosity
B_1	Burn rate additive constant
B_2	Burn rate pre-exponential factor
b	Covolume of gas phase
c	Speed of sound in gas phase
c_v, c_p	Specific heats at constant volume and constant pressure
D_p	Effective diameter of a grain of propellant
D_o	Initial external diameter of a grain of propellant
d	Total surface regression of a grain of propellant
$\dot{d}$	Rate of surface regression
d_o	Initial diameter of a perforation of a grain of propellant
E	Sum of internal and kinetic energies
e	Internal energy of gas phase
e_p	Chemical energy released in combustion of solid-phase
F_{RES}	Bore resistance
$\vec{f}$	Interphase drag
$\hat{f}_s$	Steady state interphase drag coefficient
g_o	Constant used to reconcile units of measurement
H	Parameter used to deduce propellant surface temperature by cubic profile method

h	Heat transfer coefficient
j	Mass flux
K	Friction factor for pressure drop due to mass flux through permeable section of bag
k	Thermal conductivity
L_o	Initial length of a grain of propellant
M	Projectile mass
M_w	Molecular weight
$\dot{m}$	Mass production per unit volume per unit time due to propellant combustion
$\dot{m}_i, \dot{m}_o$	Mass fluxes to and from a region
$\dot{m}_s$	Mass production per unit surface area per unit time due to reactive substrates of bag
N	Number of perforations of a grain of propellant
Nu_p	Nusselt number based on effective grain diameter
$\vec{n}$	Normal vector
n	Burn rate exponent
Pr	Prandtl number
p	Pressure
q	Heat flux
Re_p	Reynolds number based on effective particle diameter
R_i, R_o	Radii of surfaces of quasi-one-dimensional axial flow across which mass enters and exits, respectively
r	Radial coordinate
S_p	Surface area of a propellant grain
s	Streamwise coordinate in region of quasi-one-dimensional flow
s_p	Surface area of propellant per unit volume

T	Gas temperature
T_p	Surface temperature of solid phase
t	Time
$\vec{u}$	Gas velocity vector, components (u,v)
$\vec{u}_p$	Solid-phase velocity vector, components (u_p, v_p)
u_T	Streamwise velocity component of gas in region of quasi-one-dimensional flow
V_p	Volume of a propellant grain
z	Axial coordinate

Greek Symbols

α_p	Thermal diffusivity of a grain of propellant
γ	Ratio of specific heats
ε	Porosity
ε_o	Settling porosity
ζ	Computational coordinate, corresponds to axial direction
η	Computational coordinate, corresponds to radial direction
θ	Thickness of bag
μ	Viscosity
ρ	Density of gas
ρ_p	Density of solid propellant, a constant
σ	$(1 - \varepsilon)R$
τ	Time coordinate in computational frame
ψ	Rate of production of gas per unit volume due to igniter

Special Symbols and Subscripts

D/Dt	Convective derivative along average gas-phase streamline
D/Dt_p	Convective derivative along average solid-phase streamline
IG,p	The subscript IG is used to denote properties of the igniter and p is used to denote properties of the solid-phase. Gas-phase properties are unsubscripted.

DISTRIBUTION LIST

No. Of Copies	Organization
12	Administrator Defense Technical Info Center ATTN: DTIC-DDA Cameron Station Alexandria, VA 22314
1	Office of the Under Secretary of Defense Research & Engineering ATTN: R. Thorkildsen Washington, DC 20301
1	HQDA/SAUS-OR, D. Hardison Washington, DC 20301
1	HQDA/DAMA-ZA Washington, DC 20310
2	HQDA, DAMA-CSM, A. German E. Lippi Washington, DC 20310
1	HQDA/SARDA Washington, DC 20310
1	Commandant US Army War College ATTN: Library-FF229 Carlisle Barracks, PA 17013
1	Ballistic Missile Defense Advanced Technology Center P. O. Box 1500 Huntsville, AL 35804
1	Chairman DOD Explosives Safety Board Room 856-C Hoffman Bldg. 1 2461 Eisenhower Avenue Alexandria, VA 22331
3	Commander US Army Materiel Development and Readiness Command ATTN: DRCDMD-ST DCRSF-E, Safety Office DRCDE-DW 5001 Eisenhower Avenue Alexandria, VA 22333
14	Commander US Army Armament R&D Command ATTN: DRDAR-TSS DRDAR-TDC D. Gyorog DRDAR-LCA K. Russell A. Moss J. Lannon A. Beardell D. Downs S. Einstein L. Schlosberg S. Westley S. Bernstein P. Kemmy C. Heyman Dover, NJ 07801
9	US Army Armament R&D Command ATTN: DRDAR-SCA, L. Stiefel B. Brodman DRDAR-LCB-I, D. Spring DRDAR-LCE, R. Walker DRDAR-LCU-CT, E. Barrieres R. Davitt DRDAR-LCU-CV C.Mandala E. Moore DRDAR-LCM-E S. Kaplowitz Dover, NJ 07801

DISTRIBUTION LIST

No. Of Copies	Organization
5	Commander US Army Armament R&D Command ATTN: DRDAR-QAR, J. Rutkowski G. Allen J. Donner P. Serao D. Adams Dover, NJ 07801
7	Project Manager Cannon Artillery Weapons System ATTN: DRCPM-CAWS F. Menke (3 Cys) DRCPM-CAWS-WS H. Noble DRCPM-CAWS-SI M. Fisette DRCPM-CAWS-AM R. DeKleine H. Hassmann Dover, NJ 07801
3	Project Manager Munitions Production Base Modernization and Expansion ATTN: DRCPM-PMB, J. Ziegler M. Lohr A. Siklosi Dover, NJ 07801
3	Project Manager Tank Main Armament System ATTN: DRCPM-TMA, D. Appling DRCPM-TMA-105 DRCPM-TMA-120 Dover, NJ 07801
4	Commander US Army Armament R&D Command ATTN: DRDAR-LCW-A M.Salsbury DRDAR-LCS DRDAR-LCU, A. Moss DRDAR-LC, J. Frasier Dover, NJ 07801
5	Commander US Army Armament Materiel Readiness Command ATTN: DRSAR-LEP-L, DRSAR-LC, L. Ambrosini DRSAR-IRC, G. Cowan DRSAR-LEM, W. Fortune, R. Zastrow Rock Island, IL 61299
1	Commander US Army Watervliet Arsenal ATTN: SARWV-RD, R. Thierry Watervliet, NY 12189
1	Director US Army ARRADCOM Benet Weapons Laboratory ATTN: DRDAR-LCB-TL Watervliet, NY 12189
1	Commander US Army Aviation Research and Development Command ATTN: DRDAV-E 4300 Goodfellow Blvd. St. Louis, MO 63120
1	Commander US Army TSARCOM 4300 Goodfellow Blvd. St. Louis, MO 63120
1	Director US Army Air Mobility Research And Development Laboratory Ames Research Center Moffett Field, CA 94035

DISTRIBUTION LIST

No. Of Copies	Organization
1	Commander US Army Communications Research and Development Command ATTN: DRDCO-PPA-SA Fort Monmouth, NJ 07703
1	Commander US Army Electronics Research and Development Command Technical Support Activity ATTN: DELSD-L Fort Monmouth, NJ 07703
1	Commander US Army Harry Diamond Lab. ATTN:DELHD-TA-L 2800 Powder Mill Road Adelphi, MD 20783
2	Commander US Army Missile Command ATTN: DRSMI-R DRSMI-YDL Redstone Arsenal, AL 35898
1	Commander US Army Natick Research and Development Command ATTN: DRDNA-DT, D. Sieling Natick, MA 01762
1	Commander US Army Tank Automotive Research and Development Command ATTN: DRDTA-UL Warren, MI 48090
1	US Army Tank Automotive Materiel Readiness Command ATTN: DRSTA-CG Warren, MI 48090
1	Project Manager Improved TOW Vehicle ATTN: DRCPM-ITV US Army Tank Automotive Research & Development Command Warren, MI 48090
1	Program Manager M1 Abrams Tank System ATTN: DRCPM-GMC-SA, Warren, MI 48090
1	Project Manager Fighting Vehicle Systems ATTN: DRCPM-FVS Warren, MI 48090
1	Director US Army TRADOC Systems Analysis Activity ATTN: ATAA-SL, Tech Lib White Sands Missile Range, NM 88002
1	Project Manager M-60 Tank Development ATTN: DRCPM-M60TD Warren, MI 48090
1	Commander US Army Training & Doctrine Command ATTN: ATCD-MA/ MAJ Williams Fort Monroe, VA 23651
2	Commander US Army Materials and Mechanics Research Center ATTN: DRXMR-ATL Tech Library Watertown, MA 02172

DISTRIBUTION LIST

No. Of Copies	Organization
1	Commander US Army Research Office ATTN: Tech Library P. O. Box 12211 Research Triangle Park, NC 27709
1	Commander US Army Mobility Equipment Research & Development Command ATTN: DRDME-WC Fort Belvoir, VA 22060
1	Commander US Army Logistics Mgmt Ctr Defense Logistics Studies Fort Lee, VA 23801
2	Commandant US Army Infantry School ATTN: Infantry Agency Fort Benning, GA 31905
1	US Army Armor & Engineer Board ATTN: STEBB-AD-S Fort Knox, KY 40121
1	Commandant US Army Aviation School ATTN: Aviation Agency Fort Rucker, AL 36360
1	Commandant Command and General Staff College Fort Leavenworth, KS 66027
1	Commandant US Army Special Warfare School ATTN: Rev & Tng Lit Div Fort Bragg, NC 28307
1	Commandant US Army Engineer School ATTN: ATSE-CD Ft. Belvoir, VA 22060
1	Commander US Army Foreign Science & Technology Center ATTN: DRXST-MC-3 220 Seventh Street, NE Charlottesville, VA 22901
1	President US Army Artillery Board Ft. Sill, OK 73504
2	Commandant US Army Field Artillery School ATTN: ATSF-CO-MW, B. Willis Ft. Sill, OK 73503
3	Commandant US Army Armor School ATTN: ATZK-CD-MS/ M. Falkovitch Armor Agency Fort Knox, KY 40121
1	Chief of Naval Materiel Department of the Navy ATTN: J. Amlie Washington, DC 20360
1	Office of Naval Research ATTN: Code 473, R. S. Miller 800 N. Quincy Street Arlington, VA 22217
2	Commander Naval Sea Systems Command ATTN: SEA-62R2, J. W. Murrin R. Beauregard National Center, Bldg. 2 Room 6E08 Washington, DC 20362
1	Commander Naval Air Systems Command ATTN: NAIR-954-Tech Lib Washington, DC 20360

DISTRIBUTION LIST

No. Of Copies	Organization
1	Strategic Systems Project Office Dept. of the Navy Room 901 ATTN: J. F. Kincaid Washington, DC 20376
1	Assistant Secretary of the Navy (R, E, and S) ATTN: R. Reichenbach Room 5E787 Pentagon Bldg. Washington, DC 20350
1	Naval Research Lab Tech Library Washington, DC 20375
5	Commander Naval Surface Weapons Center ATTN: Code G33, J. L. East D. McClure W. Burrell J. Johndrow Code DX-21 Tech Lib Dahlgren, VA 22448
2	Commander US Naval Surface Weapons Center ATTN: J. P. Consaga C. Gotzmer Indian Head, MD 20640
4	Commander Naval Surface Weapons Center ATTN: S. Jacobs/Code 240 Code 730 K. Kim/Code R-13 R. Bernecker Silver Spring, MD 20910
2	Commanding Officer Naval Underwater Systems Center Energy Conversion Dept. ATTN: CODE 5B331, R. S. Lazar Tech Lib Newport, RI 02840
4	Commander Naval Weapons Center ATTN: Code 388, R. L. Derr C. F. Price T. Boggs Info. Sci. Div. China Lake, CA 93555
2	Superintendent Naval Postgraduate School Dept. of Mechanical Engineering ATTN: A. E. Fuhs Code 1424 Library Monterey, CA 93940
6	Commander Naval Ordnance Station ATTN: P. L. Stang J. Birkett S. Mitchell C. Christensen D. Brooks Tech Library Indian Head, MD 20640
1	AFSC Andrews AFB Washington, DC 20331
1	Program Manager AFOSR Directorate of Aerospace Sciences ATTN: L. H. Caveny Bolling AFB, DC 20332
6	AFRPL (DYSC) ATTN: D. George J. N. Levine B. Goshgarian D. Thrasher N. Vander Hyde Tech Library Edwards AFB, CA 93523

DISTRIBUTION LIST

No. Of Copies	Organization
1	AFFTC ATTN: SSD-Tech LIb Edwards AFB, CA 93523
1	AFATL ATTN: DLYV Eglin AFB, FL 32542
1	AFATL/DLDL ATTN: O. K. Heiney Eglin AFB, FL 32542
1	ADTC ATTN: DLODL Tech Lib Eglin AFB, FL 32542
1	AFFDL ATTN: TST-Lib Wright-Patterson AFB, OH 45433
1	HQ NASA 600 Independence Avenue, SW ATTN: Code JM6, Tech Lib. Washington, DC 20546
1	NASA/Lyndon B. Johnson Space Center ATTN: NHS-22, Library Section Houston, TX 77058
1	Aerodyne Research, Inc. Bedford Research Park ATTN: V. Yousefian Bedford, MA 01730
1	Aerojet Solid Propulsion Co. ATTN: P. Micheli Sacramento, CA 95813
1	AVCO Everett Rsch Lab ATTN: D. Stickler 2385 Revere Beach Parkway Everett, MA 02149
2	Calspan Corporation ATTN: E. B. Fisher Tech Library P. O. Box 400 Buffalo, NY 14225
1	Foster Miller Associates ATTN: A. Erickson 135 Second Avenue Waltham, MA 02154
1	Atlantic Research Corp. ATTN: M. K. King 5390 Cherokee Avenue Alexanria. VA 22314
1	General Applied Sciences Lab ATTN: J. Erdos Merrick & Stewart Avenues Westbury Long Island, NY 11590
1	General Electric Company Armament Systems Dept. ATTN: M. J. Bulman, Room 1311 Lakeside Avenue Burlington, VT 05412
1	Hercules Powder Co. Allegheny Ballistics Laboratory ATTN: R. B. Miller P. O. Box 210 Cumberland, MD 21501
1	Hercules, Inc Bacchus Works ATTN: K. P. McCarty P. O. Box 98 Magna, UT 84044

DISTRIBUTION LIST

No. Of Copies	Organization
1	Hercules, Inc. Eglin Operations AFATL DLDL ATTN: R. L. Simmons Eglin AFB, FL 32542
1	IITRI ATTN: M. J. Klein 10 W. 35th Street Chicago, IL 60616
2	Lawrence Livermore Laboratory ATTN: M. S. L-355, A. Buckingham M. Finger P. O. Box 808 Livermore, CA 94550
1	Olin Corporation Badger Army Ammunition Plant ATTN: R. J. Thiede Baraboo, WI 53913
1	Olin Corporation Smokeless Powder Operations ATTN: R. L. Cook P. O. Box 222 ST. Marks, FL 32355
1	Paul Gough Associates, Inc. ATTN: P. S. Gough P. O. Box 1614 Portsmouth, NH 03801
1	Physics International Company 2700 Merced Street Leandro, CA 94577
1	Princeton Combustion Research Lab., Inc. ATTN: M. Summerfield 1041 US Highway One North Princeton, NJ 08540
1	Pulsepower Systems, Inc. ATTN: L. C. Elmore 815 American Street San Carlos, CA 94070
2	Rockwell International Rocketdyne Division ATTN: BA08 J. E. Flanagan J. Grey 6633 Canoga Avenue Canoga Park, CA 91304
1	Science Applications, INC. ATTN: R. B. Edelman 23146 Cumorah Crest Woodland Hills, CA 91364
1	Scientific Research Assoc., Inc. ATTN: H. McDonald P. O. Box 498 Glastonbury, CT 06033
1	Shock Hydrodynamics, Inc. ATTN: W. H. Andersen 4710-16 Vineland Avenue North Hollywood, CA 91602
3	Thiokol Corporation Huntsville Division ATTN: D. Flanigan R. Glick Tech Library Huntsville, AL 35807
2	Thiokol Corporation Wasatch Division ATTN: J. Peterson Tech Library P. O. Box 524 Brigham City, UT 84302
2	Thiokol Corporation Elkton Division ATTN: R. Biddle Tech Lib. P. O. Box 241 Elkton, MD 21921

DISTRIBUTION LIST

No. Of Copies	Organization
2	United Technologies Chemical Systems Division ATTN: R. Brown Tech Library P. O. Box 358 Sunnyvale, CA 94086
1	Universal Propulsion Company ATTN: H. J. McSpadden Black Canyon Stage 1 Box 1140 Phoenix, AZ 85029
1	Southwest Research Institute Institute Scientists ATTN: Robert E. White 8500 Culebra Road San Antonio, TX 78228
1	Battelle Memorial Institute ATTN: Tech Library 505 King avenue Columbus, OH 43201
1	Brigham Young University Dept. of Chemical Engineering ATTN: M. Beckstead Provo, UT 84601
1	California Institute of Tech 204 Karman Lab Main Stop 301-46 ATTN: F. E. C. Culick 1201 E. California Street Pasadena, CA 91125
1	California Institute of Tech Jet Propulsion Laboratory ATTN: L. D. Strand 4800 Oak Grove Drive Pasadena, CA 91103
1	University of Illinois Dept. of Mech. Eng. ATTN: H. Krier 144 MEB, 1206 W. Green Street Urbana, IL 61801
1	University of Massachusetts Dept. of Mechanical Engineering ATTN: K. Jakus Amherst, MA 01002
1	University of Minnesota Dept. of Mechanical Engineering ATTN: E. Fletcher Minneapolis, MN 55455
1	Case Western Reserve University Division of Aerospace Sciences ATTN: J. Tien Cleveland, OH 44135
3	Georgia Institute of Tech School of Aerospace Eng. ATTN: B. T. Zinn E. Price W. C. Strahle Atlanta, GA 30332
1	Institute of Gas Technology ATTN: D. Gidaspow 3424 S. State Street Chicago, IL 60616
1	Johns Hopkins University Applied Physics Laboratory Chemical Proplsion Information Agency ATTN: T. Christian Johns Hopkins Road Laurel, MD 20707
1	Massachusetts Institute of Tech Dept of Mechanical Engineering ATTN: T. Toong Cambridge, MA 02139

DISTRIBUTION LIST

No. Of Copies	Organization
1	Pennsylvania State University Applied Research Lab ATTN: G. M. Faeth P. O. Box 30 State College, PA 16801
1	Pennsylvania State University Dept. Of Mechanical Engineering ATTN: K. Kuo University Park, PA 16802
1	Purdue University School of Mechanical Engineering ATTN: J. R. Osborn TSPC Chaffee Hall West Lafayette, IN 47906
1	Rensselaer Polytechnic Inst. Department of Mathematics Troy, NY 12181
1	Rutgers University Dept. of Mechanical and Aerospace Engineering ATTN: S. Temkin University Heights Campus New Brunswick, NJ 08903
1	SRI International Propulsion Sciences Division ATTN: Tech Library 333 Ravenswood Avenue Menlo Park, CA 94025
1	Stevens Institute of Technology Davidson Laboratory ATTN: R. McAlevy, III Hoboken, NJ 07030
2	Los Alamos Scientific Lab ATTN: T. D. Butler, MS B216 M. Division, B. Craig P. O. Box 1663 Los Alamos, NM 87545
1	University of Southern California Mechanical Engineering Dept. ATTN: OHE200, M. Gerstein Los Angeles, CA 90007
2	University of Utah Dept. of Chemical Engineering ATTN: A. Baer G. Flandro Salt Lake City, UT 84112
1	Washington State University Dept. of Mechanical Engineering ATTN: C. T. Crowe Pullman, WA 99164

Aberdeen Proving Ground

Dir, USAMSAA
ATTN: DRXSY-D
DRXSY-MP, H. Cohen
Cdr, USATECOM
ATTN: DRSTE-TO-F
STEAP-MT, S. Walton
G. Rice
D. Lacey
C. Herud
Dir, HEL
ATTN: J. Weisz
Dir, USACSL, Bldg. E3516, EA
ATTN: DRDAR-CLB-PA
DRDAR-ACW

USER EVALUATION OF REPORT

Please take a few minutes to answer the questions below; tear out this sheet, fold as indicated, staple or tape closed, and place in the mail. Your comments will provide us with information for improving future reports.

1. BRL Report Number _____

2. Does this report satisfy a need? (Comment on purpose, related project, or other area of interest for which report will be used.)

_____

_____

_____

3. How, specifically, is the report being used? (Information source, design data or procedure, management procedure, source of ideas, etc.) _____

_____

_____

4. Has the information in this report led to any quantitative savings as far as man-hours/contract dollars saved, operating costs avoided, efficiencies achieved, etc.? If so, please elaborate.

_____

_____

5. General Comments (Indicate what you think should be changed to make this report and future reports of this type more responsive to your needs, more usable, improve readability, etc.) _____

_____

_____

_____

6. If you would like to be contacted by the personnel who prepared this report to raise specific questions or discuss the topic, please fill in the following information.

Name: _____

Telephone Number: _____

Organization Address: _____

_____

_____